



TECHNISCHE  
UNIVERSITÄT  
WIEN  
Vienna University of Technology



Diploma Thesis

# “Investigations on LiF as protective layer for lithium metal electrodes”

carried out for the purpose of obtaining the degree of

**Diplom-Ingenieur, Dipl.-Ing./Master of Science, MSc**

under the supervision of

**Ao.Univ.Prof. Dipl.-Ing. Dr.techn. Günter Fafilek**

(E164-04-2 - Forschungsgruppe Elektrochemische Methoden und Korrosion, TU Wien)

**Dr. Alexander Beutl**

(AIT Austrian Institute of Technology, Center for Low-Emission Transport – Electric Drive Technology)

submitted at the Vienna University of Technology,

Faculty of Technical Chemistry

from

**Michael Georg Stadt, BSc**

Falkensteinstraße 5, 4132 Lembach i. M.

Vienna, January 2021

## Affirmation

I declare in lieu of oath, that I wrote this Thesis and performed the associated research myself, using only literature cited in this volume. If text passages from sources are used literally, they are marked as such.

I confirm that this work is original and has not been submitted elsewhere for any examination, nor is currently under consideration for a thesis elsewhere.

Vienna, January 2021

Signature:



Michael Stadt

## Table of contents

1	Acknowledgement.....	4
2	Abbreviations.....	5
3	Abstract.....	6
4	Theoretical background.....	7
4.1	Lithium-ion batteries and Lithium metal batteries .....	7
4.1.1	Lithium-ion batteries.....	7
4.1.2	Lithium metal batteries and their drawbacks.....	11
4.1.3	Solutions for the drawbacks of lithium metal.....	13
4.2	Surface fluorination .....	15
5	Methodology .....	19
5.1	Preparation of a LiF coating on lithium metal .....	19
5.1.1	Polyvinylidene fluoride (PVDF) in dimethylformamide (DMF).....	19
5.1.2	Ammonium hydrogen difluoride (NH <sub>4</sub> HF <sub>2</sub> ) in Dimethyl sulfoxide (DMSO)....	19
5.1.3	Gas-phase reaction with 1,1,1,2-Tetrafluoroethane (R-134a).....	20
5.2	Electrochemical measurements.....	21
5.3	Analytical Methods.....	23
5.3.1	Galvanostatic cycling/ cyclic chronopotentiometry.....	23
5.3.2	Electrochemical impedance spectroscopy EIS .....	27
5.3.3	Measurement of the exchange current $i_0$ .....	29
5.3.4	Other measurements .....	31
6	Results and discussion.....	33
6.1	Characterisation of the LiF coatings.....	33
6.1.1	Polyvinylidene fluoride (PVDF) in dimethyl formamide (DMF).....	33
6.1.2	Ammonium hydrogen difluoride .....	35
6.1.3	Gas-phase reaction with R-134a .....	38
6.1.4	XRD characterisation of the layers .....	39
6.2	Electrochemical investigations .....	40
6.2.1	Pristine lithium reference system .....	41

6.2.1.1	Galvanostatic cycling .....	41
6.2.1.2	Open-circuit-voltage relaxation.....	44
6.2.1.3	Electrochemical impedance spectroscopy .....	45
6.2.2	Comparison of pristine lithium and LiF-coated lithium.....	48
6.2.2.1	Galvanostatic cycling .....	48
6.2.2.2	OCV – relaxation .....	55
6.2.2.3	Electrochemical impedance spectroscopy .....	56
6.2.2.4	Capacity measurements in full cells .....	61
6.2.2.5	Conclusion.....	62
6.2.3	Validation of the destruction of the layer .....	62
6.2.3.1	Stability threshold of the layer.....	64
6.2.3.2	Plating/stripping morphologies .....	67
6.3	Stability under ambient conditions (Photographs, XRD, FT-IR) .....	69
6.3.1	Photographs.....	69
6.3.2	X-Ray diffraction.....	70
6.3.3	FTIR-Spectroscopy .....	71
7	Conclusion .....	73
8	Literature.....	76
9	Appendix.....	80

# 1 Acknowledgement

Firstly, I would like to thank my supervisor Dr. Alexander Beutl for his guidance through each stage of the process. Furthermore, I would like to acknowledge Prof. Dr. Günter Fafilek for inspiring my interest in the development of innovative technologies in the field of electrochemistry and supervision of my Master Thesis. My gratefulness is also to Dr. Arlavinda Rezquita for the support at the first three months of my Thesis.

Another big thanks for my colleagues at the Austrian Institute of Technology for the fruitful discussions about different topics. I would like to acknowledge Mag. Hamid Raad especially for the XRD measurements and Dr. Ningxin Zhang for the many hours we spent at the SEM device.

## 2 Abbreviations

### Chemicals:

DC .....	Diethyl carbonate
DME .....	1,2-Dimethoxyethane
DMF .....	Dimethyl formamide
DMSO .....	Dimethyl sulfoxide
DOL .....	1,3-Dioxolane
EMC .....	Ethyl methyl carbonate
FEC .....	Fluoroethylene carbonate
LFP .....	Lithium iron phosphate
LiPF <sub>6</sub> .....	Lithium hexafluorophosphate
LiTFSI .....	Lithium bis(trifluoromethanesulfonyl)imide
LMO .....	Lithium manganese oxide
NH <sub>4</sub> HF <sub>2</sub> .....	Ammonium hydrogen difluoride
NMC <sub>xyz</sub> .....	Nickel manganese cobalt oxide, whereby x,y and z representing the amount of Ni, Co, Mn (e.g. the formula of NMC622 is LiNi <sub>0.6</sub> Mn <sub>0.2</sub> Co <sub>0.2</sub> O <sub>2</sub> )
PE .....	Polyethylene
PMMA .....	Poly(methyl methacrylate)
PP .....	Polypropylene
PVDF .....	Polyvinylidene fluoride
R-134a .....	1,1,1,2-Tetrafluoroethane
VC .....	Vinylene carbonate

### Other:

CP .....	Chronopotentiometry (same as GC)
GC .....	Galvanostatic cycling (same as CP)
HOMO .....	Highest occupied molecular orbital
LIB .....	Lithium-ion battery
LUMO .....	Lowest unoccupied molecular orbital
OCV .....	Open circuit voltage
SEI .....	Solid electrolyte interphase
SEM .....	Scanning electron microscopy
XRD .....	X-Ray Diffraction

### 3 Abstract

The improvement of lithium-ion batteries is necessary to get a higher specific capacity which is especially needed for the electromobility to ensure higher driving ranges. State of the art batteries offer specific energy densities of about 200 Wh/kg, which can be raised up to 350 Wh/kg with lithium metal as anode material [1]. There are a few challenges upcoming with the usage of lithium metal due to its high reactivity. One approach to increase the chemical and electrochemical stability of lithium metal is a proper coating, for which lithium fluoride is a promising candidate due to its chemical stability and high surface energy.

Different reported coating methods were used to obtain LiF coatings with different morphologies and thicknesses e.g., immersion in a  $\text{NH}_4\text{HF}_2/\text{DMSO}$  solution or gas phase reaction with R-134a. To investigate the influence of LiF on lithium metal, different analytical methods were carried out, focusing on the chemical stability at ambient conditions and electrochemical performance during plating/stripping cycles. The aim of this project is to re-evaluate the impact of LiF coatings on the stability of lithium metal electrodes.

## 4 Theoretical background

### 4.1 Lithium-ion batteries and Lithium metal batteries

#### 4.1.1 Lithium-ion batteries

Nearly all the portable devices nowadays are using Li-ion batteries for energy storage. Therefore, it is very useful to improve the specific capacity, environmental aspects and last but not least the price of them. Due to the inherent limits regarding the specific capacity of current active materials state-of-the-art lithium-ion batteries are reaching their physical limits. Therefore, huge effort is put into the optimisation of the different parts of the LIBs. This thesis focuses on the anode side. For mobile applications like electromobility energy storage with high specific energy and high specific power is needed, to grant long driving ranges. As seen in Figure 1, Li-ion batteries are very promising candidates in this regard.

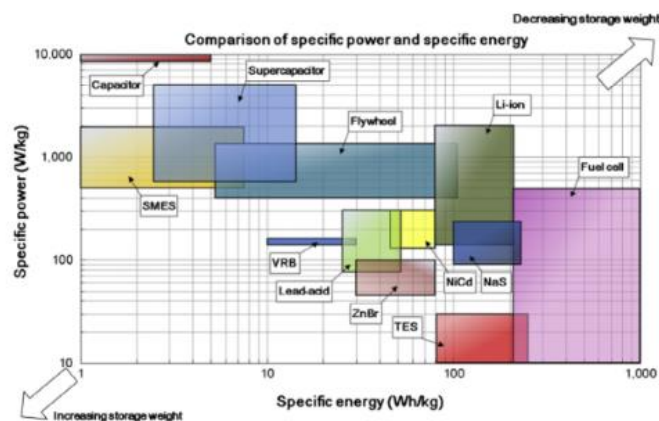


Figure 1: Ragone Plot: Specific energy vs. specific power for different electrical energy storage systems [2].

The lithium-ion battery consists of three main parts: cathode, anode and electrolyte which are displayed schematically in the following Figure 2. The electrodes are spatially separated by a separator to avoid electrical contact between them, which is combined with liquid or solid-state electrolytes to ensure an ionic conductivity between them. The electrodes are placed on thin metal foils, called current collectors. Aluminium is used at the cathode side, while copper is used at the anode side to collect the current from the active materials. Copper offers a potential of 3.38 V (vs Li/Li<sup>+</sup>) which is stable in the 0-2 V operation potential of the anodes. The operation potential at the cathode is around 3.5-4.5 V, where copper will not be stable at all. Therefore aluminium is used because of its formation of a stable Al<sub>2</sub>O<sub>3</sub> layer protecting the metal [3].



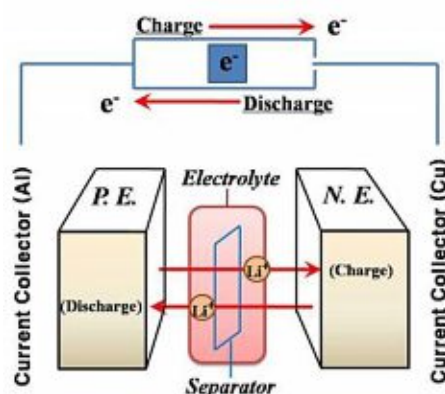


Figure 2: Schematic of a lithium-ion battery [4].

For charging the battery, an external source drives the electrons from the positive electrode to the negative side. Meanwhile  $\text{Li}^+$ -Ions are removed from the negative side, resulting in the oxidation of the remaining active material (e.g.  $\text{Co}^{3+}$  to  $\text{Co}^{4+}$  in  $\text{LiCoO}_2$ ) in the cell displayed above. Due to the applied potential these ions are moving through the electrolyte to the negative electrode. At the negative electrode the positive lithium ions are intercalated into the active material (e.g. graphene layers for graphite), which is reduced to a lower oxidation state. Formally  $\text{C}_6$  is reduced to  $\text{C}_6^-$  during intercalating one  $\text{Li}^+$ -Ion.

In a secondary battery the electrode where the Li-ions are stored in charged state is defined as the anode. Driven by the difference in the chemical potential of lithium in the anode ( $\mu_A$ ) and cathode materials ( $\mu_C$ ), a potential difference is built up between the anode and the cathode which is called the open circuit voltage  $V_{OC}$ . It can be described by the following formula, whereby  $e$  is the elementary charge.

$$V_{OC} = (\mu_A - \mu_C)/e \quad (1) \quad [5]$$

But unfortunately, the voltage obtained from an electrochemical cell is also limited by the electrochemical stability of the electrolyte, i.e. the electrochemical window. If the chemical potential of the negative electrode is higher than the LUMO (lowest unoccupied molecular orbital) of the electrolyte, the electrolyte gets reduced at this electrode. At the positive electrode it works the opposite way, if the HOMO (highest occupied molecular orbital) is higher than the  $\mu_C$  the electrolyte gets oxidised [5].

As a result of the reduction and oxidation of the electrolyte the so called SEI (Solid electrolyte interphase) is formed on the surfaces of the electrodes. It consist mainly of  $\text{LiF}$ ,  $\text{Li}_2\text{O}$  and  $\text{Li}_2\text{CO}_3$  where the exact composition depends on the electrolyte solvent and salt used [6]. This results in a strong change of the chemical potential of lithium in this interphase. At the negative side or the defined anode of the battery, the chemical

potential of lithium is reduced below the level of the LUMO, resulting in a stop of the SEI growth. Almost all common electrolyte systems i.e. mixtures of polar and aprotic solvents and lithium salts like  $\text{LiPF}_6$  or  $\text{LiBF}_4$  suffer from spontaneous reaction with lithium metal. The so formed SEI-layer works as a passivation layer inhibiting this reaction once a layer is formed. So, the lithium metal becomes kinetically, but not thermodynamically stable against the electrolyte [7]. The following Figure 3 displays the energy diagram of an electrochemical cell, whereby the influence of the SEI on the energy levels is displayed.

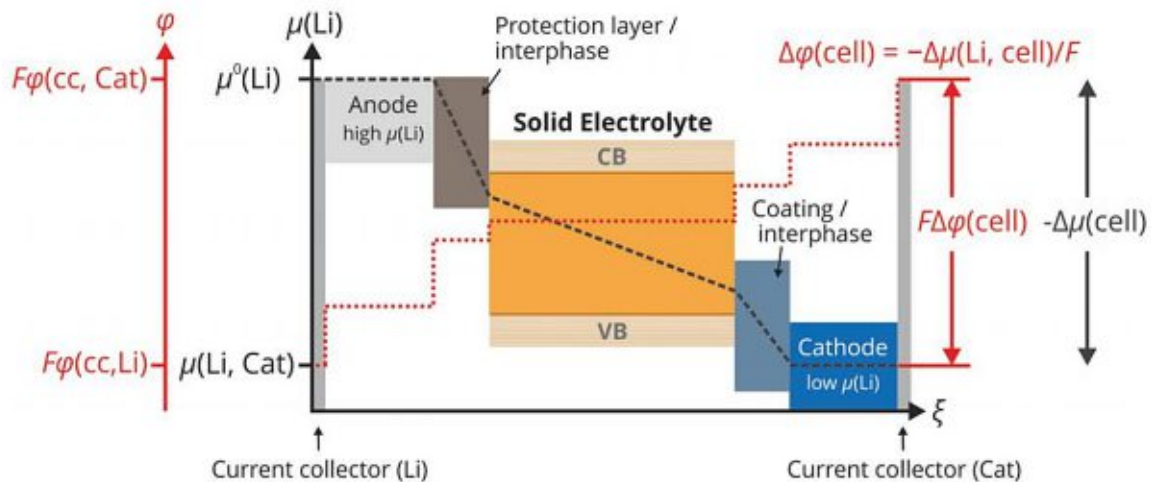


Figure 3: Schematic of the chemical potential of lithium in different components of a lithium ion battery [8].

Apart from the stability, the electrolyte must fulfil two requirements, it must be an excellent ionic conductor, and an electrical insulator. State-of-the-art batteries are using a mixture of organic solvents, e.g. EMC (ethyl-methyl-carbonate), DC (dimethyl-carbonate) or EC (ethylene-carbonate), and lithium salts such as  $\text{LiPF}_6$  (lithium hexafluoro-phosphate) or LiTFSI (lithium bis(trifluoromethanesulfonyl)imide) as electrolyte [2]. It has to be mentioned that nowadays there is a strong focus on solid state electrolytes for reducing safety issues related to the flammable solvents of liquid electrolytes. Another issue concerning liquid organic electrolytes is the already mentioned formation of an SEI (Solid electrolyte interface) layer, which consumes some of the electrolyte.

As cathode material several different lithium metal oxides are used. The first commercial LIB consisted of  $\text{LiCoO}_2$  as cathode material [5], which, however, is more and more substituted by other materials like LMO (lithium manganese oxide), LFP (lithium iron phosphate) or mixed oxides like NMC (nickel manganese cobalt oxide) [2].

In a charged battery the anode is fully lithiated but depending on the cathode material there is lithium remaining in the cathode side. Currently the most used anode material is graphite. Lithium intercalates in the graphene layers and causes only a small volume

expansion which is beneficial for the SEI layer. It grants that the SEI is not destroyed by mechanical stress as described afterwards. This system is well developed and optimised, it's stable over time and over thousands of cycles [9]. Lithium is stored in the graphite under forming  $\text{LiC}_6$ , which grants only a low specific capacity, calculated in the equation 1 below.

One of the currently investigated approaches for higher specific capacities is the usage of lithium metal as anode. One of the currently investigated approaches for higher specific capacities is the usage of lithium metal as anode. In this type of battery, no anode material is used (only current collector) and in the uncharged state, all the lithium is stored in the cathode side. If fully charged, lithium metal is directly plated onto the current collector rather than intercalated into another material as for conventional LIBs. This grants the highest possible specific capacity for an anode material.

Additionally, the lithium metal electrode will be required for next generation battery chemistries like the lithium sulphur (Li-S) battery and the lithium-air (Li-O<sub>2</sub>) batteries [10].

The theoretical specific capacity of different anode materials is calculated by the following equation 2, where  $v$  is the number of transferred electrons and  $MW$  the molecular weight.

$$Q_{el}^m = \frac{v * F}{MW} \quad (2) \quad [11]$$

With a Faraday constant of 96485.33 C/mol (F) the theoretical capacity ( $Q_{el}^m$ ) for a graphite anode is about 1338.8 C/g which equals around 372 mAh/g. The theoretical capacity of the lithium metal anode is about ten times higher with a calculated value of 3861 mAh/g. In addition, also lithium silicide can be used too with a theoretical specific capacity of 2011 mAh/g for  $\text{Li}_{4,4}\text{Si}$  if its fully discharged.

State-of-the-art batteries offer a specific energy of about 200 Wh/kg, which can be raised up to around 350 Wh/kg with the usage of lithium metal resulting in almost the doubling in the capacity. The following equation 3 shows the calculation of the capacity of a full cell.

$$Q_{full}^m = \frac{1}{\frac{1}{Q_{cathode}^m} + \frac{1}{Q_{anode}^m}} \quad (3) \quad [12]$$

As evident from equation 3, the specific capacity of a full cell is limited by the component with the lower value, either anode or cathode.

### 4.1.2 Lithium metal batteries and their drawbacks

At the beginning of the “batteries” era, zinc was used as anode material. Substitution of zinc by lithium was a promising step to increase the capacity of the batteries. The first lithium metal batteries were primary cells (only usable for one discharge cycle) with lithium as anode and iodine in a compound as cathode material. Up to 1970 all the lithium batteries were of primary cell type. Since the introduction of customer electronics scientists tried to produce a rechargeable lithium metal battery. A lot of problems, such as fire incidents led to the conclusion, that there were some problems with the usage of lithium metal. These problems are associated with the high reactivity of lithium metal, as well as the non-uniform deposition of lithium resulting in the formation of dendrites [13].

- SEI-formation

In the assembled cell lithium reacts spontaneously with the electrolyte forming the so-called solid electrolyte interphase (cf. Figure 3) often consisting of lithium oxide, lithium fluoride and lithium carbonate and other decomposition products of the electrolyte [14]. In this process the electrolyte is irreversibly consumed. AFM measurements showed, that this SEI-layer is highly inhomogeneous in terms of thickness and mechanical properties [15]. Since this layer is ionically conductive and electronically insulating it grows only until it reaches a certain thickness. Furthermore, the selection of the electrolyte influences the properties of the SEI-layer [16].

- Dendrites

The dendrite formation is a well-studied, but not fully understood process. There are several factors influencing the growth of dendrites. Among others the ion mobility and concentration within the electrolyte, applied current density, uniformity of the SEI layer and surface diffusion of lithium are important parameters in controlling the morphology of the electrodeposition [16].

Since the SEI-layer is inhomogeneous, it consists of thinner parts, where the resistance through this layer is less than on thicker parts. The variation in the composition also offers parts with lower and higher ionic conductivity, whereby beneath areas with the higher conductivity lithium deposition is more likely, resulting in mechanical stress which leads to cracks in the SEI. Afterwards the lithium gets plated on the pristine lithium resulting in dendrites.

- High reactivity with Oxygen, Nitrogen and Water

Since lithium is an alkali metal with an extremely high electro positivity it is very reactive with different kinds of substances. Under air exposure lithium firstly reacts fast under the formation of a black tarnish. Since a few reactions are happening simultaneously and sequentially the black substance forming on the surface it not quantified, whereby it is proved that one of the products is lithium nitride  $\text{Li}_3\text{N}$ . This reaction is followed by the formation of  $\text{LiOH}$  as reaction product of  $\text{Li}_3\text{N}$  with water. Finally the lithium hydroxide is absorbing  $\text{CO}_2$  from the environment under formation of lithium carbonate, which is a white solid [17].

- Formation of “Dead lithium”

Another disadvantage related with the formation of dendrites is the formation of “dead lithium”. In the discharging cycle, lithium is preferentially stripped from remaining dendritic structures of previous cycles, resulting in the formation of electrically isolated lumps on the surface. As pristine lithium reacts very fast with the electrolyte under SEI formation, the lumps are covered with an electrical insulation SEI layer at the whole surface which causes the electrical insulation from the rest of the anode as well as the current collector. Thus, some of the lithium is lost and does not participate anymore in the charging/discharging reactions. Additionally, while plating the lithium ions have to pass a layer of dead lithium, which becomes bigger and bigger after every cycle. A schematic of the formation of dead lithium is displayed in Figure 4.

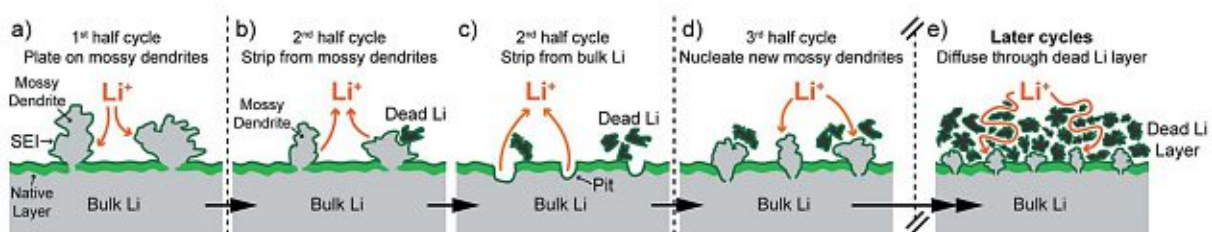


Figure 4: Formation of „dead lithium” in the first cycles [18].

- Volume change

One more drawback of using lithium metal as electrode is the volume change during cycling. Rough calculations assuming a dense deposition of lithium show that a loading of  $2 \text{ mAh/cm}^2$  result in a deposited thickness of around  $10 \mu\text{m}$  (starting with no lithium, i.e.,  $0 \mu\text{m}$ ). While the volume change of a graphite anode between the charged and discharged state is only  $6.5 \mu\text{m}$  when the same loading is regarded ( $2 \text{ mAh/cm}^2$ , starting with  $50 \mu\text{m}$ ). The relative volume changes thus amount to 13% for the graphite anode [19], whereas it is infinite for lithium metal anodes.

In Figure 5 the main problems with the usage of lithium metal are graphically displayed.

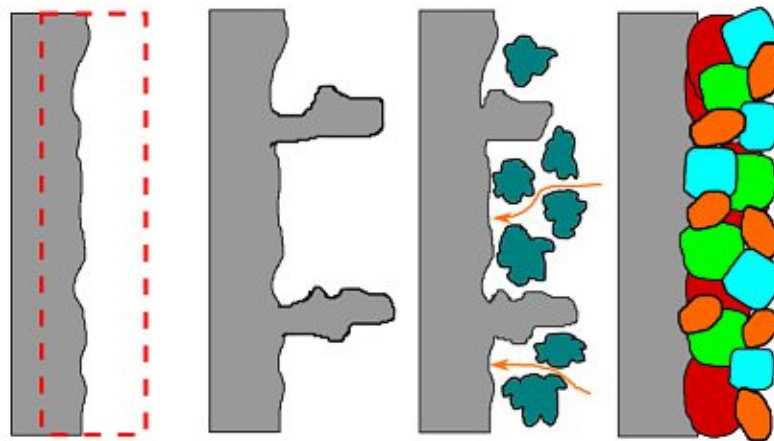


Figure 5: Problems occurring with the usage of lithium metal, f.l.t.r. volume change, dendrite formation, dead lithium formation, formation of a SEI layer.

### 4.1.3 Solutions for the drawbacks of lithium metal

Since the usage of lithium metal has high advantages, lots of effort is put in the research of techniques improving the chemical stability and cycling stability. Hence there are lots of approaches trying to get rid of the problems caused by the usage of lithium metal electrodes. Figure 5, which was adopted from Xiang et al. 2019, summarizes these techniques.

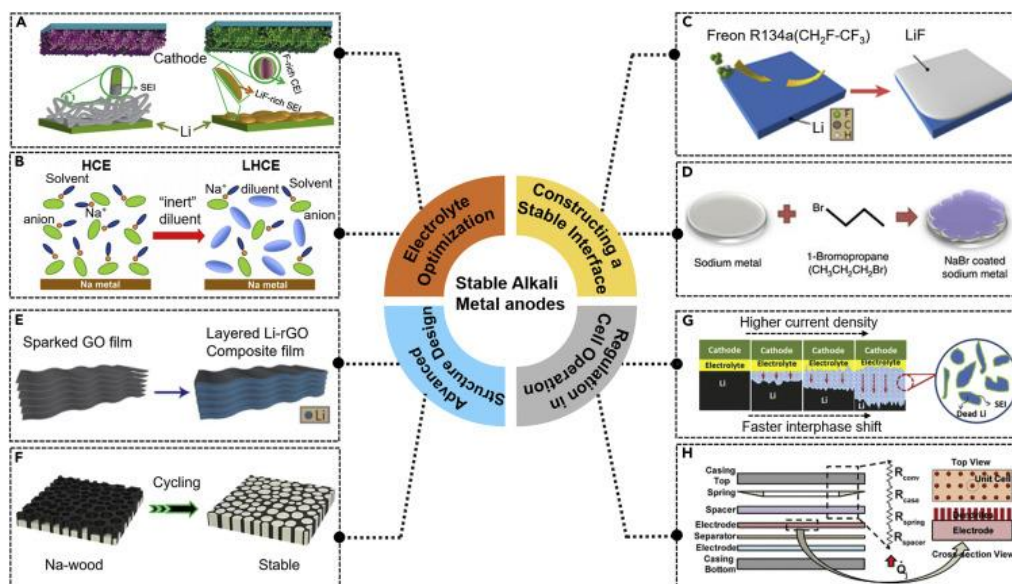


Figure 6: Pre-treatments of lithium electrodes for stabilization [20].

The different approaches to improve the stability of lithium metal can be classified into four groups as shown in Figure 6 above.

The first group mentioned is the optimisation of the electrolyte. As explained above, lithium reacts with the electrolyte under the formation of a SEI. Therefore, the selection

of the electrolyte has a huge influence on the composition as well as the morphology of the SEI-layer. Besides the standard components, the organic solvent and the lithium containing salts, additives are widely used to improve the stability of the lithium metal electrodes. VC (Vinylene carbonate) and FEC (Fluoroethylene carbonate) are adding a polymeric species to the SEI layer [21], whereas the exchange of the anion from the salt from  $\text{PF}_6^-$  to FSI offers a denser, LiF-rich SEI-layer resulting in a longer stability [22].

Another approach is advanced structural design. 3-D structures are used to compensate the volume change during cycling, preventing cracks and pulverization of the SEI as well as the anode itself. The operational procedure for this approach is highly complicated, often inhibiting application to larger scale [20].

The change of operating conditions could also give a beneficial effect, since a very low current density leads to a more uniform growth of lithium and prohibits dendrites from growing [20].

For industrial application of lithium anodes, the most appropriate approach should improve the stability in the cell during cycling, as well as the stability of lithium under ambient conditions for processing. One promising method in this regard is the formation of a protective coating, which is categorized as “constructing a stable interface” in Figure 6. The modification of the electrolyte would not give stability under ambient conditions, whereas the change of conditions such as lower cycling current is not feasible for many applications. The approach with 3-D structures is difficult to realize at large scale compared to surface coatings.

A protective coating for lithium metal electrodes must fulfil several requirements:

**High surface energy:** Since the growth of dendrites increases the surface area, a coating with a high surface energy should inhibit the dendrites from growing.

**Dense and pore free:** Furthermore, it is reported that only a dense layer could prevent the growth of dendrites, because already a few cracks could lead to inhomogeneous current distributions and concomitant dendrite growth in these areas [23]. On the other hand, a dense layer (unless high ionic conductivities are provided) offers the biggest resistance against electrochemical reactions compared to porous ones.

**Hydrophobic:** From the stability under ambient conditions point of view, a dense, hydrophobic layer would make the anode stable against air and humidity.

**Chemical and electrochemical stability:** Of course, an SEI-layer should be stable and not soluble in the electrolyte, while not reacting with oxygen, nitrogen, and water. The

chemical stability, given by the chemical potential of lithium in the SEI-film itself, should be in a proper range, to prevent the anode from reacting with the electrolyte as shown in Figure 3.

**Electronically insulating:** The artificial SEI-layer should be highly electronical insulating in order to prevent from further SEI growth on its surface. Electrons passing through this layer would lead to the plating of the lithium on this layer, which would make the initial layer useless [24].

**Mechanically stable:** The fact that the lithium metal is plated underneath the layer, indicates the appearance of mechanical stress. Therefore, excellent mechanical properties are important to avoid structural damage withing the layer during plating/stripping. In literature the Young's modulus is given as a value, quantifying the mechanical properties of an artificial SEI. Further investigations found that the mechanical properties of the layer are affected by more parameters e.g. ductility and toughness [24].

Due to their high surface energy in combination with the relatively low diffusion barrier at the surface the lithium halides are promising candidates for an artificial SEI-coating [23].

Since it is a part of the natural formed SEI, LiF was intensively investigated as artificial SEI material for protective coatings. It offers good mechanical strength [25], the highest Young's modulus among the natural occurring SEI components [24], low solubility in organic solvents [26] and relatively low solubility in water, which is needed to protect the lithium metal against ambient conditions. Furthermore, the low surface diffusion barrier is expected to prevent dendrite growth.

This artificial layer could be produced ex-situ before the cell assembling, or in-situ via additives in the electrolyte such as Fluoroethylene carbonate (FEC) which forces the formation of a LiF rich SEI [27]. But since the goal is to protect the lithium metal also under ambient conditions, only the ex-situ methods are regarded in this work. Furthermore, the additives forming a proper in-situ coating are consumed irreversibly by forming this SEI-layer which is a huge disadvantage in terms of long-term cycling.

### 4.2 Surface fluorination

The fluorination of the lithium metal could be done with very different methods, reported in literature. These approaches range from fluorination via different gases, to immersion in solution with different fluoride containing salts as well as unconventional techniques for instance the usage of ionic liquids. Furthermore, sputtering is a possible technique.



All these methods are reported to offer different benefits for the lithium metal battery, such as lower overpotential or longer, stable cyclability, while other studies show no positive influence of the LiF-layer to the lithium metal electrodes.

The outcomes of the different papers are quite contrary. Since these results were carried out using different setups (electrolytes, current densities, symmetric or full cells,...) it's difficult to compare the results directly.

In the column "Impact" of Table 1, the reported benefits of a LiF layer are displayed. The properties are shortened with the following shortcuts: CE – Coulombic efficiency, CL – Cycle life, OP - Overpotential, AS – Stability under ambient conditions analysed visual by taking photographs after different times, SC – obtainable specific capacity. The orientation of the arrow shows the influence of the layer reported in the different papers.

Table 1: Summary of surface fluorinations done in literature.

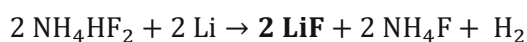
Author	Fluorination agent/ solvent	Reaction type	Reported thickness	Morphology	Impact
Yuan et al. [28], [29]	NH <sub>4</sub> HF <sub>2</sub> in DMSO	Immersion	~ 6.98 -77.4 μm [28] [29]	Multiple LiF cubes, porous	CE ↑, CL ↑ OP ↑, SC ↑ AS ↗ <sup>[29]</sup> , (vs Li-foil)
Lin et al. [30]	(R-134a) 1,1,1,2-Tetrafluoroethane	Gas-phase	~ 40 nm	Uniform, flat, smooth	CE ↑, CL ↑ OP ↓, DC ↑ AS ↑, (vs Li-rGO)
Lang et al. [31]	PVDF in DMF	Polymer-decomposition	~ 300 nm	Uniform, composite LiF/polymer	CE ↑, CL ↑ OP ↓, SC ↑ AS ↑, (vs Li-foil)
Fan et al. [32]	LiF Target	Sputter	~ 150nm	Uniform	CE ↗, CL ↑ OP ↗, SC ↑ AS /, (vs Li-foil)
Wang et al. [33]	Ionic liquid	Immersion	~ 115 nm	Uniform	CE →, CL ↑ OP ↓, SC ↑ AS /, (vs Li-foil)
He et al. [27]	NF <sub>3</sub>	Gas phase	~ 50 nm	-	CE /, CL / OP ↑, SC / AS ↑, (vs Li-foil)

For this thesis three of these reported methods were chosen and tested in a consistent manner using always the same electrochemical setup and materials (e.g. electrolytes).

a) Fluorination of the lithium metal in a  $\text{NH}_4\text{HF}_2/\text{DMSO}$  solution [28]

This fluorination method was reported by Yuan et al. in 2019. As a result, a crystalline and porous layer could be observed. The pores are coming from the formation of hydrogen during the reaction. It is reported that the growth of the lithium during plating starts at the surface of the lithium and fills the pores from the porous layer, combining the 3-D structuring approach with a stable artificial SEI. Furthermore, lithium dendrites were effectively inhibited from growing.

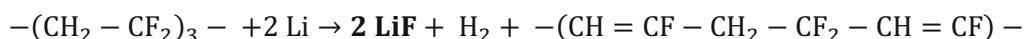
The formation of LiF happens via a reaction of  $\text{NH}_4\text{HF}_2$ , dissolved in DMSO, with lithium metal. The authors mentioned a reaction time of 24 h as the optimum for producing the coating in a feasible way.



b) Immersion in a PVDF/DMF solution [31]

This method was published by Lang et al. in 2018. It is proposed to be an efficient low-cost approach for the improvement of lithium metal electrodes. They describe the formation of a layer which consists of high amount of LiF but during XPS experiments they also show the formation of C-F bonds, standing for a fluoropolymer.

To obtain the described coating a Celgard three-layer polymer-separator (PE/PP/PE) is soaked with a PVDF in DMF solution and placed on the lithium for just 5 seconds. It is assumed that the reaction follows the following reaction equation:



The thermodynamics of this reaction was computationally calculated for different polymer chain-lengths, resulting in similar results, all indicating the feasibility of the reaction.

c) Reaction in the gas phase with 1,1,1,2-Tetrafluoroethane [30]

The gas phase fluorination of lithium metal was first mentioned by Lin et al. in 2017. Producing the LiF layer in a gas phase reaction grants a thin and conformal layer. Furthermore, the used agent R-134a offers no toxicity. XPS depth profile showed the existence of CF and  $\text{CF}_2$ -groups underneath the LiF layer.

For this method there is no clearly identified reaction equation. The fluorination happens over  $(\text{CH}_2\text{F}-\text{CF}_2)\text{Li}^+$  as intermediate followed by an  $\alpha$  or  $\beta$  elimination. This reaction takes place in a reactor with 0.5-1 atm R-134a gas at 150 °C.

In the following Figure 7 the received morphologies using different methods are displayed in SEM micrographs as well as in a schematic drawing.

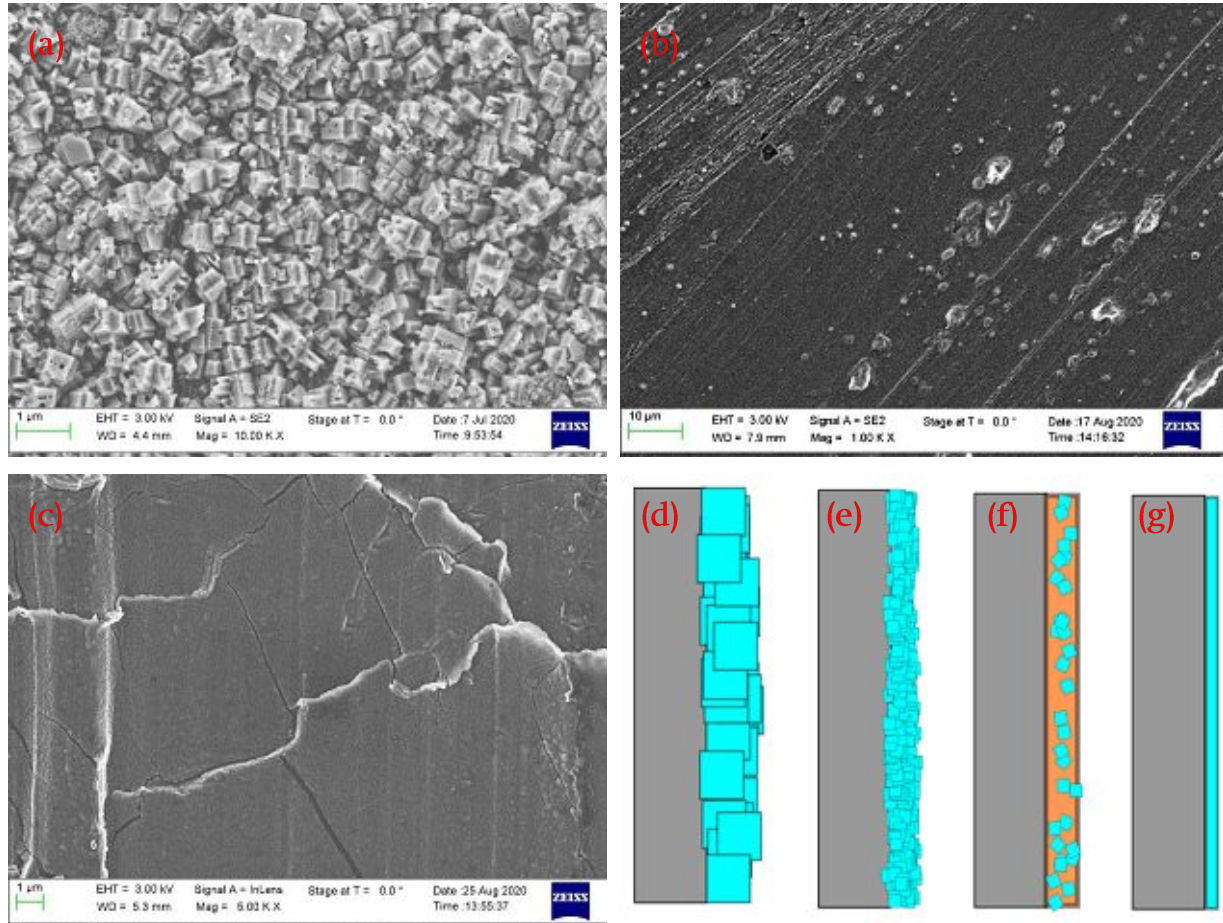


Figure 7: f.l.t.r. (a) cubic shaped layer from immersion coating, (b) compound coating from polymer (orange) and LiF crystals, (c) homogeneous, thin coating from the gas phase, (d-g) schematic pictures of the coatings (d) immersion coating for 120 h, (e) immersion coating for 24 h, (f) polymer-composite coating, (g) gas-phase coating.

## 5 Methodology

All the steps containing the handling of chemicals, cell parts and lithium metal were performed in a glovebox with <0.1 ppm of oxygen and <0.1 ppm of water under argon atmosphere.

### 5.1 Preparation of a LiF coating on lithium metal

Herein it is important to mention, that all the lithium metal electrodes used for measurements in cells or the coating process were scratched with a doctor blade before their usage. This step is necessary, because even though the lithium plates are stored in the glovebox, a thin oxide layer forms, visible through a dull, partially coloured surface.

#### 5.1.1 Polyvinylidene fluoride (PVDF) in dimethylformamide (DMF)

PVDF (Solvay, SOLEF® 5130) was dried for at least 2 hrs at 50 °C in a vacuum oven. After that, 50 mg were dissolved in 10 mL DMF (Sigma-Aldrich, anhydrous 99.8%) under stirring for 1 hour until it was fully dissolved. To apply the solution on a lithium foil, a Celgard separator (Celgard, three-layer PP/PE/PP, 25 µm thickness) was soaked with it, then put for 5 seconds on the Li foil. Next, the separator was removed carefully, trying to remove all the liquid. The so coated samples were dried in the glovebox for a minimum of one day to evaporate the rest of the solvent DMF. The formation of black coloured spots on the surface was observed rudimentarily on all the samples. It is referred to the breakdown of the PVDF-polymer under the formation of a LiF/polymer composite which contains double bonds causing that coloration [31], whereby a longer reaction time leads to a darker coloration. To minimize this, the separator was pulled off under the attention to remove all the liquid, preventing the carbon formation.

In a second approach, the whole lithium anodes were put in the solution for around 5 seconds and flushed with DMSO afterwards to get rid of the reactant solution.

To remove the remaining amount of the solvents DMF and DMSO, firstly the samples were dried under vacuum in the antechamber, but as shown later in the results, it led to the cracking of the surface layer. As a consequence, the samples were dried by storing them in the Glovebox for 24 h.

#### 5.1.2 Ammonium hydrogen difluoride (NH<sub>4</sub>HF<sub>2</sub>) in Dimethyl sulfoxide (DMSO)

Dimethyl sulfoxide (Sigma-Aldrich, >99.9%) was dried over a 3 Å molecular sieve. Prior, the molecular sieve received from Sigma-Aldrich was dried in a vacuum oven for at least 12 hrs at 250 °C. Then the sieve was directly transferred to the glovebox. About 80 g of DMSO

where dried with the molecular sieve. To receive a solution with 0.8 wt% of  $\text{NH}_4\text{HF}_2$  (Sigma-Aldrich, 99.999% trace metals basis) 0.64 g of it were dissolved in 80 g DMSO under vigorous stirring for 48 hrs.

Since some white precipitate remained in the solution, coatings with the filtered and unfiltered solutions were done. Furthermore, it is not mentioned in the paper how much  $\text{NH}_4\text{HF}_2$  is needed to coat a lithium anode of a certain size. To get reproducible results, each anode was immersed in its own glass vial, offering each anode the same amount of fluorination agent of around  $9,5 \text{ mg/cm}^2$ .

For the soaking of the lithium anode, 5 mL of this solution were poured into separate glass vials to ensure the equal amount of reactant for each sample and grant similar stirring conditions among the samples. Then the lithium metal chips were added, and the reaction was stirred very slowly. This reaction was performed over different times: 2 hrs., 24 hrs. and 5 days of immersion to receive different layers with different thicknesses and/or morphologies.

After this time, the anodes were washed in DMSO, in order to remove all the salt, the superfluous solvent was wiped off with a lint free towel and the anodes were stored in the glovebox for further drying. In the paper the liquid is only wiped off with a towel, the washing step was done, since after the wiping some of the white salt remained on the surface, which was removed after the washing step.

### 5.1.3 Gas-phase reaction with 1,1,1,2-Tetrafluoroethane (R-134a)

The reaction with R-134a, which is normally used as cooling agent in air conditioners, proceeded in a stainless-steel reactor.

The reaction was performed under a pressure of 1 atm R-134a gas (Suva R134a, Linde) and a temperature of approximately  $150 \text{ }^\circ\text{C}$ . In the literature the best results were achieved with a pressure of 0.5 atm R-134a. 1 atm pressure was used, since it's mentioned in the publication [30], that a higher pressure accelerates the reaction. It is reported in the publication that an optimised layer is received by a 20 h reaction time. Due to the limited timeframe of this work, a reaction time of 1h at  $150^\circ\text{C}$  using 1atm of the R-134a reactant was found to be also applicable to obtain a proper LiF-coating.

The required temperature of  $150 \text{ }^\circ\text{C}$  [30] could not be set very accurately because of the simple experimental setup used. A thorough measurement of the temperature at the bottom inside the reactor was not possible without severely reducing the tightness of the container. Nevertheless, a temperature calibration for the set temperature of the heating plate and the temperature within the reactor was conducted. The empty reactor was

equipped with two temperature sensors, one on the bottom of the reactor outside and one at the inner side. Then the temperature of the heating plate was varied until a constant temperature of 150°C could be maintained within the reactor. For the sample preparation, the same parameters were used. The reactor was filled with the anodes inside the glovebox, next it was evacuated and flushed three times with R-134a like seen in the next Figure 8.

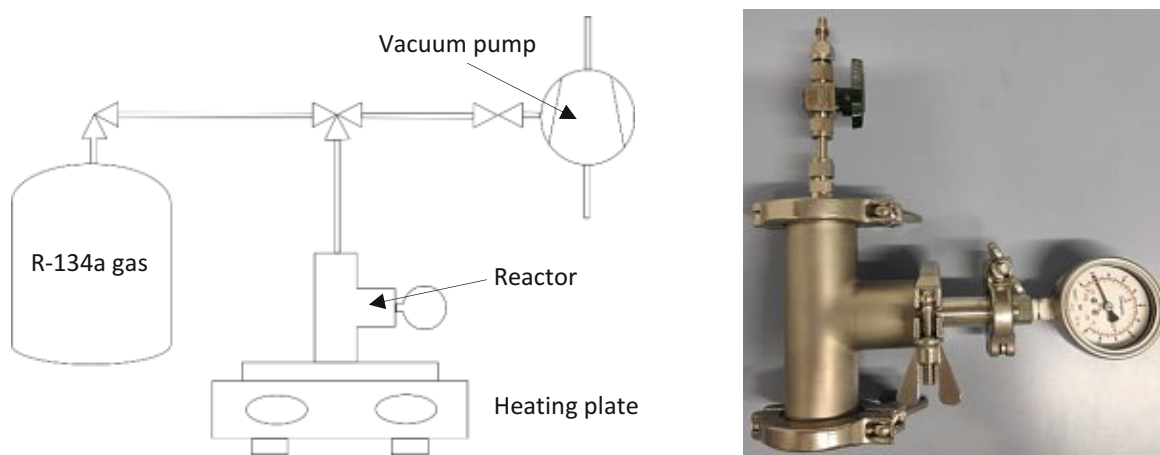


Figure 8: Reactor and experimental setup used for the gas phase fluorination.

The exclusion of air could be optically proofed by checking the reacted anodes in the glovebox for dark areas. Reactions with air or moisture would result in coloured, or in the worst case black areas of  $\text{LiOH}/\text{Li}_2\text{CO}_3$  or  $\text{Li}_3\text{N}$ . Three electrodes per batch were produced.

## 5.2 Electrochemical measurements

- Coin cells:

Due to their easy assembly coin cells are commonly used for testing new cathode- or anode materials as well as electrolytes. The following Figure 9 shows the schematic layout of a coin cell with the artificial LiF-layer on the lithium metal electrodes.

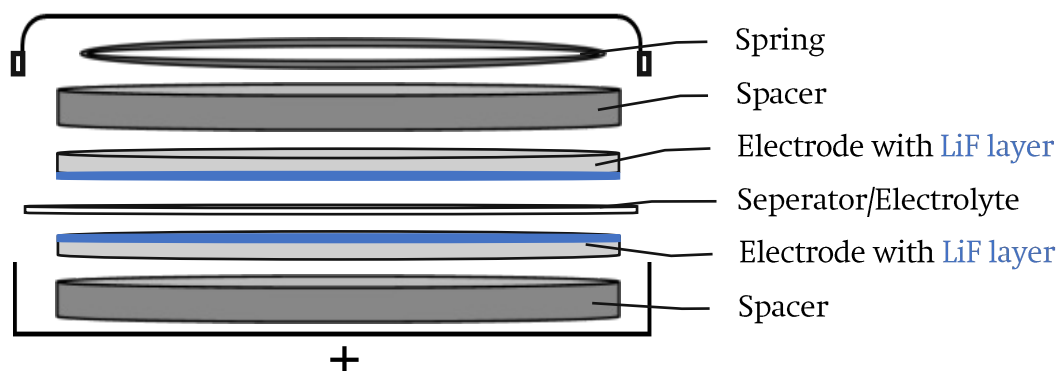


Figure 9: Schematic layout of a coin cell.

The following description is for the coin cell layout which was used during this thesis. All the measurements were done in symmetric cells, which means the anode and the cathode are made from the same material. The housing is made from stainless steel and has a diameter of 20 mm and a height of 32 mm. To separate cathode and anode the commercial separator “Celgard” (diameter 19 mm) which consist of three layers PP/PE/PP (PP Polypropylene, PE Polyethylene) was used. For applying adequate pressure in the cell, two spacers with a thickness of 0.5 mm and a spring with 1.1 mm height were used.

The assembling process starts with placing a spacer and one electrode in the middle of the bottom housing. Since symmetric cells were used exclusively in this thesis there is no defined anode and cathode. Next, 25  $\mu\text{L}$  of electrolyte were poured on the first electrode, then the separator was placed atop and another 25  $\mu\text{L}$  of electrolyte were applied. Finally, the spacer and the spring were put on the top electrode and finished with the top housing. In the last step a pressure of about 1000 psi ( $\sim 6.9$  MPa) was applied for 10 seconds to press and seal the cell. After the assembling the coin cell is tight and sealed.

The two used electrolytes were carbonate electrolyte: 1M  $\text{LiPF}_6$  (Lithium hexafluoro phosphate) in EC:EMC (Ethylene carbonate, Ethyl methyl carbonate) at the ratio of 3:7 with 2 wt.% VC (Vinylene carbonate), and ether electrolyte: 1M LiTFSI (Lithium bis(trifluoromethanesulfonyl)imide) in DOL:DME (Dioxolane, Dimethyl ethane) at a 1:1 ratio.

- 3-electrode test cell:

This cells from the company EL-CELL are totally different from coin cells. They consist of a massive housing and can be opened very fast allowing to modify the inner of the battery very easy e.g., it is possible to add more electrolyte between cycles. Another advantage is that the measurements can be carried out in a three-electrode setup allowing the precise measurement of the potential against a reference electrode. For all the 3-electrodes cell measurements done in this thesis, the carbonate electrolyte (200  $\mu\text{L}$ ) was used in combination with a 0.65 mm thick fibreglass separator (Whatman, Sigma-Aldrich). The following Figure 10 shows the setup of a such a cell.

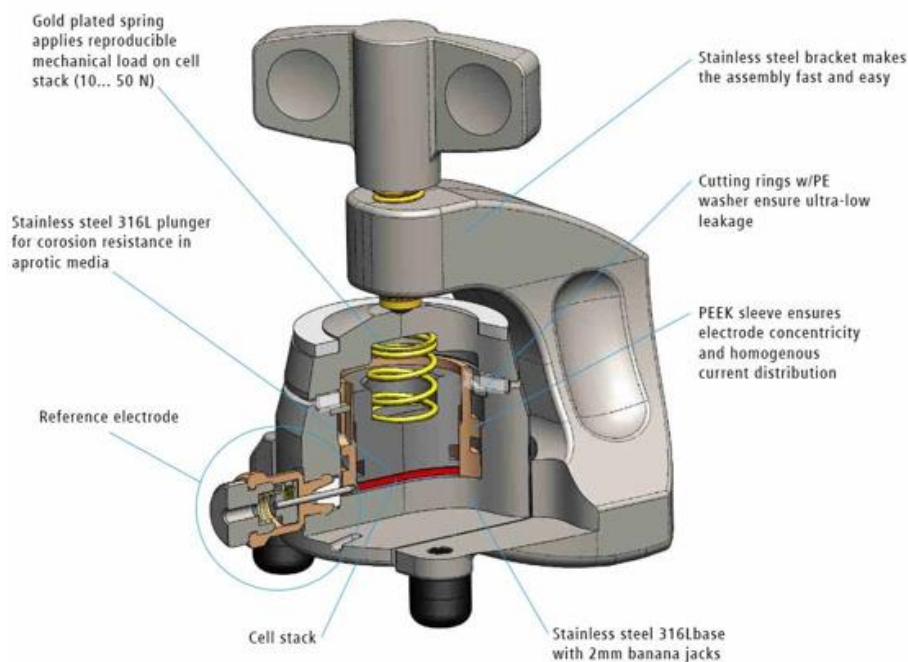


Figure 10: 3-electrode test cell layout “EL-CELL®”[34].

### 5.3 Analytical Methods

Each of the following electrochemical measuring methods was done on a BIOLOGIC-VSP or BIOLOGIC-MPG2 potentiostat, and the Software EC-Lab V11.33 from BIOLOGIC was used for the evaluation.

#### 5.3.1 Galvanostatic cycling/ cyclic chronopotentiometry

**Long-term cycling:** In this method, a constant current is applied to the specimen e.g. battery, for a certain time and the potential is recorded. Next the current is reversed and applied for the same time as before. This can be done for any number of cycles.

The kinetics of the lithium deposition can be determined by analysing the shape of the resulting potential curves [35]. Typically, current densities in a range of 1 to 5 mA/cm<sup>2</sup> are applied. In this work, current densities of 1mA/cm<sup>2</sup> and charge-discharge capacities of 1mAh/cm<sup>2</sup> were applied, as they were estimated to be close to practical applications. Nevertheless, at this current density the formation of dendrites generally happens as explained in chapter 4.1.2. Thus, it will be possible to evaluate the effectiveness of LiF coatings to inhibit dendrite formation using these values. In Figure 11 the applied current density versus time is displayed. After one charge-discharge cycle, a resting period of 10 min was used for the system to relax. Then an EIS measurement was performed, followed by the next cycle.



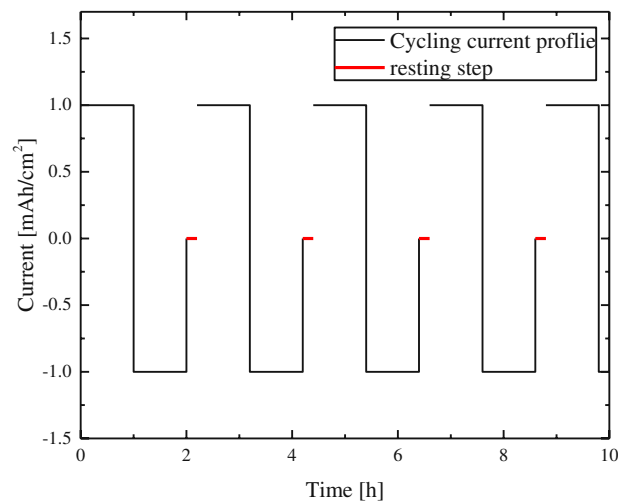


Figure 11: Current profile applied to the cells, with additional relaxing steps.

This applied current profile leads to an overpotential over time graph. In Figure 12(a), an overpotential graph without the formation dendrites is shown, as obtained by cycling lithium between an electrospun polymeric separator [35] whereas Figure 12 shows the peaking behaviour caused by the growth of dendrites using a commercial separator [35].

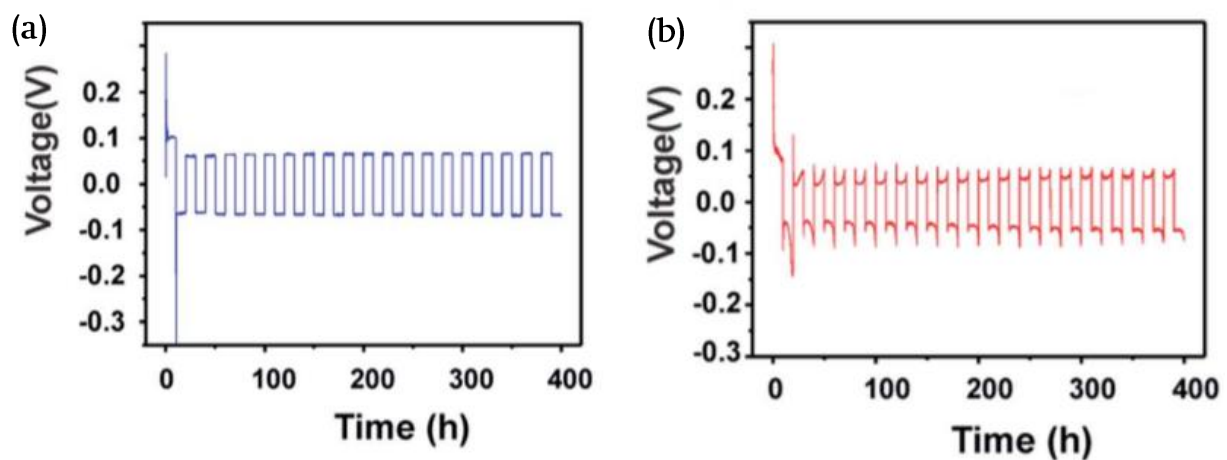


Figure 12: Galvanostatic cycling current profile. (a) cycling without dendrite formation, (b) GC-graph with dendrite formation [36]-modified.

In an electrochemical cell, the overpotential is the sum of the cathode- and anode overpotentials. The main reason for the shape of the recorded potential profiles are the different reaction pathways taken during the cycling of lithium metal [34].

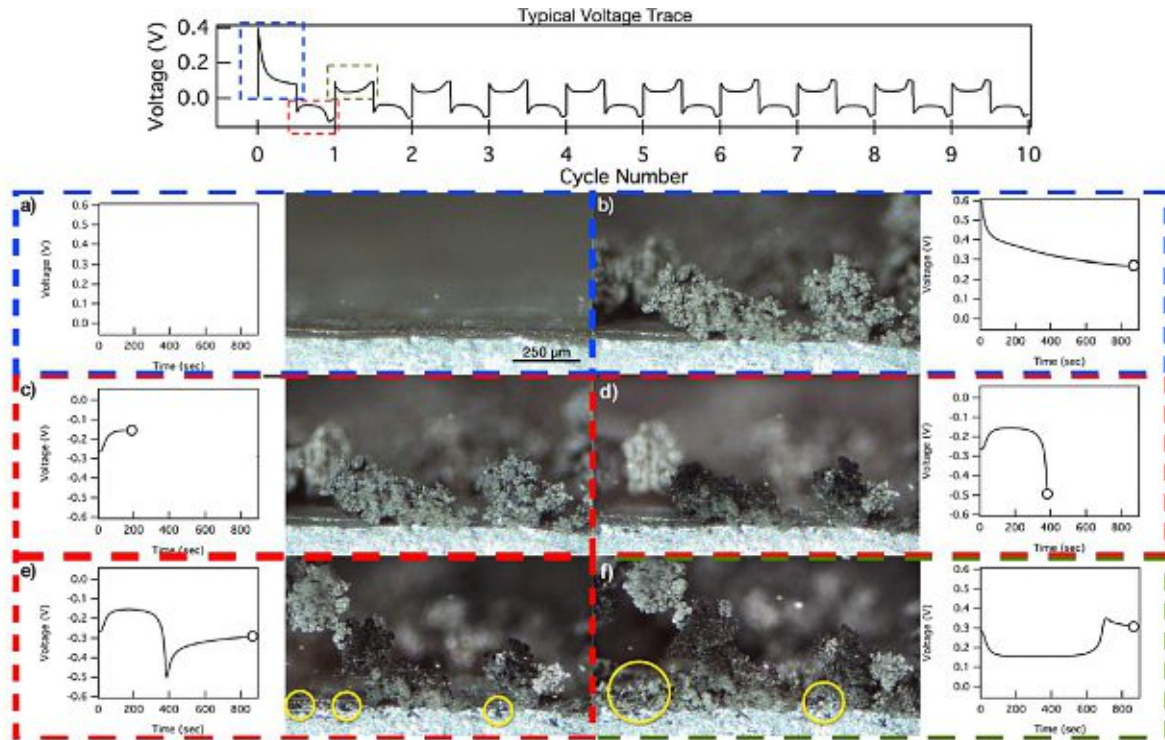


Figure 13: Overpotential over cycle numbers at symmetric pristine lithium cells with additional micrographs of the lithium-electrode surface [35].

During the first polarization, the working electrode undergoes a pitting process, whereas lithium gets plated on the counter electrode. Before the plating of lithium there needs to be some nucleation which happens on different kinds of layers as well as on lithium metal too. This nucleation process suffers from a high energy barrier. Therefore, at the first cycle the highest overpotential is reached. After the formation of nucleation sites for dendrites, the reaction path of lithium plating changes from lithium nucleation to dendrite growth, resulting in an decrease of the overpotential [35].

During the second half cycle, first the plated dendrites are stripped. When dendrites lose electrical contact during stripping, they become inactive (so-called “dead lithium”). Then the overpotential becomes higher again because of the pitting of the area around the dendrites, which is energetically less favourable.

**Cycling at low current densities:** stated in chapter 4.1.3 a lower current density prevents dendrites from growing. Therefore, the current density was shifted to lower values, increasing in certain steps. With this method the threshold potential, at which dendrites form could be detected. The cells were cycled at 1, 5, 10, 50 and 100  $\mu\text{A}/\text{cm}^2$  for one hour. Ten cycles for each current density were performed to check the stability at a certain current density over a few cycles and not just for one cycle.

The shape of this potential is related to the processes, including dendrite formation in the cells happening. If the potential occurs as stable, straight line we assume the cycling is reversible, meaning the anode is stable. In this case no dendrites are formed, and even no destruction of the layer happens.

**Relaxation potential during waiting periods:** The ten minutes resting step after each cycle during measurements of the potential was performed to establish equilibrium within the cell before the impedance measurement of the following cycle. This is needed since there is a concentration gradient forming in the electrolyte during polarization of the electrodes as well as the double layer at the interface between electrode-electrolyte gets charged during cycling [37].

Additional information is received from the potential-relaxation graph. This graph has a characteristic shape and approaches 0 V as shown in Figure 14.

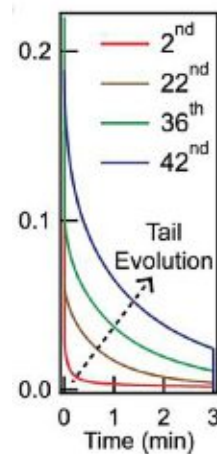


Figure 14: OCV relaxation of pristine lithium after certain cycle numbers [18].

It was reported by Chen in 2017 [18], that this tail is associated to the relaxation of the concentration profile within the cell. Accumulation of dead lithium on top of the electrodes leads to the evolution of a tortuous layer impeding the ion transport and thus increasing the time needed for the concentration profiles to get back to equilibrium.

This relaxation is done for the same length in time after each cycle. After a certain number of cycles, the zero voltage cannot be reached in this time, indicating the massive formation of dead lithium. To quantify this process, the last point (or for noisy signals, the average of the last ten points) of each potential profile during the resting step of the different samples was plotted.

### 5.3.2 Electrochemical impedance spectroscopy EIS

The EIS method is used to determine the complex impedance. An ideal electric resistance  $R$ , following Ohm's law, is a simplified concept. Thereby properties, such as the independence of the resistance from the frequency, or also the in-phase of current and voltage are assumed. In a real system, frequency dependent resistances like capacitors cause a much more complex behaviour. Therefore, the impedance is used to describe these systems.

Basically, an alternating voltage (PEIS) or current (GEIS) with a constant amplitude is applied on the sample while the complex impedance  $Z(f)$  is measured within a certain range of frequencies, detecting the phase shift of current and voltage. If there is only ohmic resistance the phase shift will be zero degrees. If there is just capacitance the phase shift is  $90^\circ$ . A combination (parallel or series) will result in a frequency dependent phase shift from  $0^\circ$  to  $90^\circ$  [38].

The data obtained from a conventional EIS measurement are often plotted in a Nyquist plot. Thereby the real part of the impedance ( $Z'$ ) is plotted on the X-axis and the imaginary part times -1 on the Y-axis ( $-Z''$ ) as shown in Figure 15. Each data point in the Nyquist plot represents the complex impedance at one certain frequency.

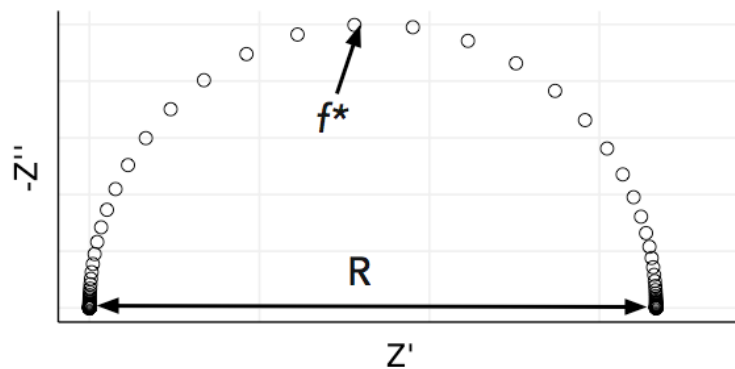


Figure 15: Schematic semi-circle in a Nyquist plot,  $f^*$  and  $R$  indicate the frequency of the datapoints and the ohmic resistance [39].

The shape of a Nyquist plot is characteristic for the underlying processes ongoing inside a cell and could be used to get real values for the resistance as well as the capacitance of certain elements by fitting the plot with a correct equivalent circuit. A semicircle obtained in a Nyquist plot could be modelled by the parallel connection of an Ohmic resistance ( $R$ ) and a capacitance ( $C$ ), which occurs at almost every electrochemical interface. On the one hand, a transfer of ions or electrons from/to the electrolyte to/from the electrode manifests itself as an Ohmic resistance  $R$ , on the other hand each double layer, built up at

the interface between electrode and electrolyte, gets charged if a potential is applied to the electrochemical cell, resulting in a capacitance  $C$ .

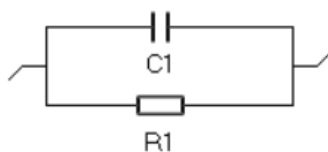


Figure 16: RC-element, representing a semi-circle in the Nyquist plot consisting of a resistance and a capacitor.

The measurement is done at different frequencies, allowing the quantification of different phenomena occurring in an electrochemical cell. A symmetric cell, as used in this Thesis, consist of different phenomena, explained below.

**Fitting Li-ion batteries:** In a battery, different phenomena and different interphases are occurring. Since the SEI layer is formed in a simultaneous reaction between lithium, salt, and electrolyte a multilayer structured layer is supposed to form. This SEI formation leads to the formation of new interphases SEI/electrolyte and lithium/SEI. The SEI itself is a complex structure often being described as a multi-layered interphase. Therefore, an electrochemical cell with pristine lithium as anode can be properly described only if e.g. five RC-elements and one ohmic resistance are fitted, which is reported by Aurbach et al. 1993 [40]. He assumes that the following equivalent circuit could be used to model a symmetric Li|Li cell in an carbonate based electrolyte [40].

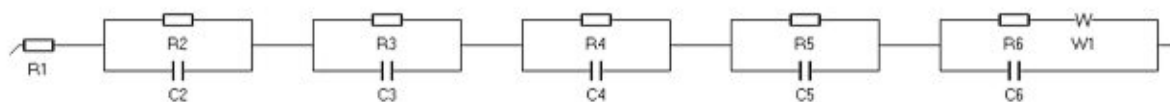


Figure 17: Proposed equivalent circuit for a symmetric Li|Li cell [40].

At very high frequencies ( $> 10^5$  Hz [41]) the capacitance offers almost no resistance, therefore the resistance at this high frequency belongs to the ohmic resistance of the system. This ohmic resistance belongs to the  $R_{el}$  (electrolyte resistance) as well as the resistance coming from the wiring in the device.

At medium frequencies ( $10^5$ - $10^2$  Hz [41]), the lithium electrode – electrolyte interphase is analysed. More precisely the layer formed on the lithium metal, which can be the natural formed SEI, as well as the artificial SEI consisting of LiF. The very low frequency part ( $< 10^2$  Hz [41]) of the impedance is related to the ionic diffusion. [42].

It is theoretically possible to calculate the different resistances which are occurring in an electrochemical cell from the measured complex impedance. In this thesis the impedance is described only qualitatively due to its complexity and the limited time available.

The following Table 2 shows the experimental parameters of the EIS measurement carried out for this thesis.

Table 2: Experimental parameters for the EIS measurements.

Method	Potentiostatic EIS (PEIS)
Frequency	20 kHz – 100 mHz
Amplitude	10 mV

### 5.3.3 Measurement of the exchange current $i_0$

In this method a potential sweep of 1 mV/min. from 30 mV to -30 mV is performed and the current is measured. The low potential ensures that no irreversible reactions occur. This method is normally used in the fields of corrosion and fuel cells. In our case the exchange current from the pristine/coated lithium to the electrolyte is determined. The exchange current ( $i_0$ ) is calculated with the Butler-Volmer (BV) equation.

$$i = i_0 * \left( \exp \left[ \frac{\alpha * z * F}{R * T} * \eta \right] - \exp \left[ \frac{-(1 - \alpha) * z * F}{R * T} * \eta \right] \right) \quad (4) \quad [43]$$

$i$ ...net current of the charge transfer reaction;  $\eta$ ...overpotential;  $\alpha$ ...charge transfer coefficient;  $R$ ...ideal gas constant;  $T$ ...temperature;  $z$ ...No. of transferred electrons;  $F$ ...Faraday constant

For large overpotentials, one of the exp-terms in the BV-equation becomes negligible. A straight line in the Tafel-plot as shown in Figure 18 can be assumed when the back reaction contributes less than 1 % of the current. Fast electrode kinetics lead to a mass-transfer-limited current, where no Tafel relationship could be seen, because this would require unlimited availability of reactants. If the electrode kinetics are slow, a high overpotential is required and a good Tafel-relation could be seen. Nevertheless this high overpotential leads to irreversible kinetics, which is not desired [44].

In a Tafel-plot  $\log(i)$  vs  $\eta$  is plotted. The linear parts of the anodic and cathodic branches can be used to determine the exchange current  $i_0$  which is shown in the Figure 18.

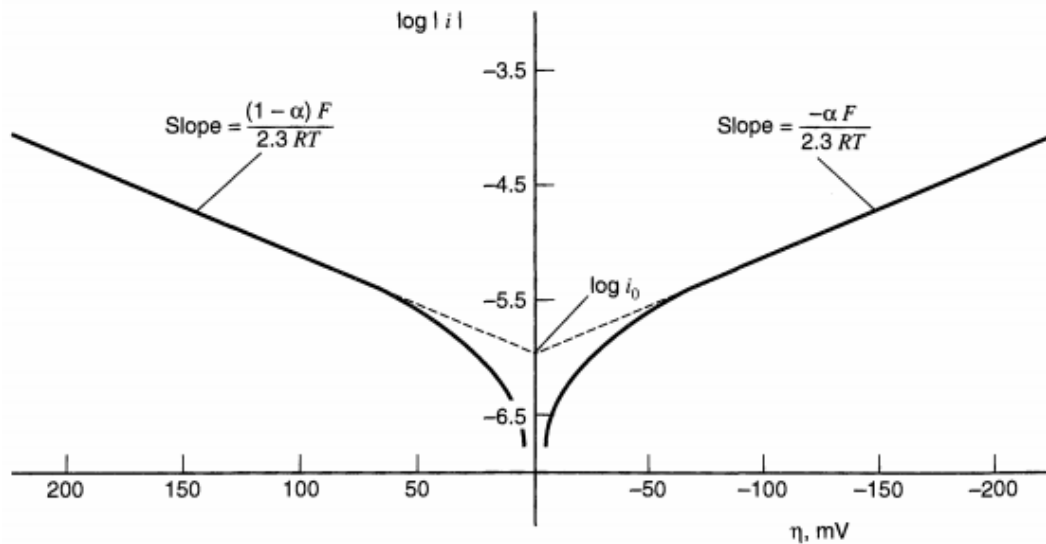


Figure 18: Schematic Tafel-plot with linear sections [44].

For small overpotentials, such as used to carry out the measurements in this thesis, the BV-equation could be approximated by using a Taylor series, which leads to the following formula:

$$i = i_0 \frac{F * \eta}{R * T} \quad (5) \quad [44]$$

This formula 5 shows that the current is linear proportional to the overpotential in a limited potential range near  $E_{eq}$  (potential at equilibrium), whereby the ratio of  $-\eta/I$  is called the charge-transfer resistance  $R_{ct}$ . Given this equation the exchange current can simply be calculated out of the current and the overpotential [44].

$$R_{ct} = -\frac{\eta}{i} = \frac{R * T}{F * i_0} \quad (6) \quad [44]$$

In case of a coating on the surface, this resistance depends on lots of different parameters. Out of this, we can get information about the combined overall properties of the coating. As seen in equation 6, a coating with a low charge transfer resistance should give the highest  $i_0$ , whereas a layer with a high  $R_{ct}$  should offer the lowest exchange current. The exchange current density  $i_0$  is received by dividing the exchange current by the surface-area.

The measurement of the exchange current, respectively the recording of the current while a potential sweep performed was done in a so called EL-Cell in a three-electrode-configuration with a pristine lithium as a reference electrode.

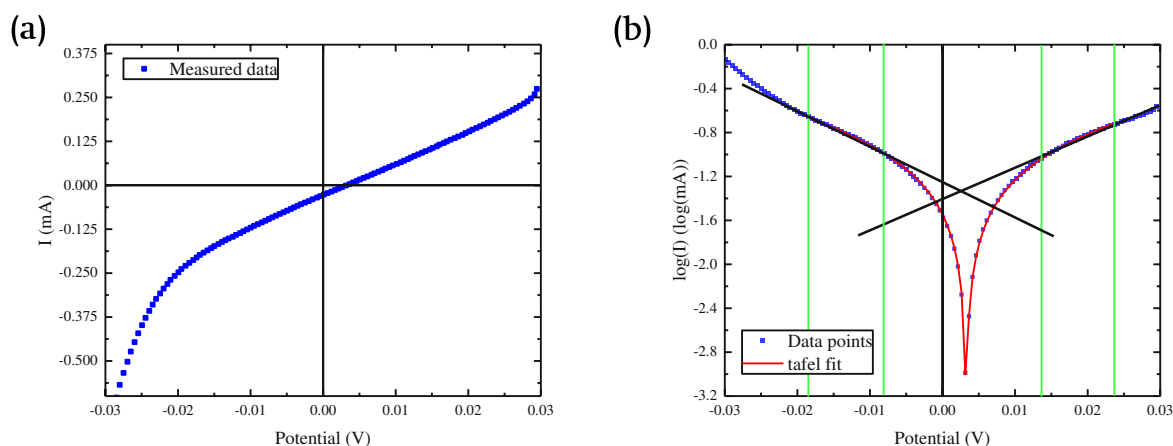


Figure 19: (a) Exchange current graph, (b) Tafel-plot, with fit for the linear Tafel regime at the anodic and cathodic branch for the determination of the  $i_0$  value.

For the fitting, the current-potential graph is plotted in a logarithmic scale, the Tafel-plot. Next the linear Tafel-regime was marked manually by the green lines Figure 19b whereby at lower potentials the back reactions are no more negligible and at higher potential irreversible reactions taking place, which are assumed to change the whole system. Therefore the “potential-windows” which can be used to obtain a Tafel-regime is hard to find. The slopes of both branches are calculated, at their intersection the exchange current could be received from the y-axis. The placement of the green lines is estimated so this measurement contains a huge error and cannot be used for the preservation of exact values.

### 5.3.4 Other measurements

The following measurements are not explained in detail, but the general instrumentation parameters are written down.

- XRD: For XRD measurement the device X'PERT (Powder) PRO was used within a  $2\theta$  angle of  $5-80^\circ$ . The specifications of the measurement: Radiation source: Copper target, step size:  $0.033^\circ$ , time per step: 200 s, beam mask: 10 mm and 45 kV/40 mA. To ensure the exclusion of air, a dome made from PMMA-polymer with a bottom of monocrystalline silicon was used.
- ATR FTIR: The device “Spectrum Two” from Perkin Elmer with a diamond crystal was used. The wavenumber was scanned from 400 up to  $4400\text{ cm}^{-1}$  within a scan rate of  $8\text{ cm}^{-1}$ .
- SEM: The SEM pictures were taken at the AIT. Therefore, the field emission SEM SUPRA 40 was used with a voltage of 3 kV.



- FIB SEM: The Focused Ion Beam SEM “FEI Quanta 200 3D DBFIB” was measured at the USTEM Center at the Vienna University of Technology.
- XPS: The XPS was proceeded at the Analytical Instrumentation Center at the Vienna University of Technology. A SPECS XPS-spectrometer equipped with a monochromatized Al-K $\alpha$  X-Ray source and a hemispherical WAL-150 analyser with an angle of 60° was used.

## 6 Results and discussion

### 6.1 Characterisation of the LiF coatings

#### 6.1.1 Polyvinylidene fluoride (PVDF) in dimethyl formamide (DMF)

The coating process in this method was difficult to perform reproducibly because the quality of the coating was directly connected with the operator's skills. If some of the PVDF/DMF solution remained after removal of the soaked separator, the formation of a black solid, assumingly consisting of a polymeric film incorporating C=C-groups, could be observed. To prevent the back side of the anode from being coated this approach was done on lint free paper towels. Optically a diffuse layer was visible at the surface.

Drying of the coated samples in vacuum, resulted in a cracked surface layer (ref. Figure 20). It is assumed that the rapid evaporation of the remaining solvent, which is assumed to be partly swelling the applied polymeric film, leads to mechanical stress and thus to crack formation. Therefore, the samples for cycling were used without drying in vacuum.

In order to achieve a higher reproducibility, a modified coating procedure was tested. The lithium samples were fully immersed into the PVDF-DMF solution. After removing the samples from the solution, the liquid remaining on the surface caused a very exothermic reaction. As a result, the formation of a lot of vapor was seen as well as a vigorous reaction on the surface, turning the whole surface of the sample brown/black. Furthermore, the solution left turned dark blue to black afterwards which is assumed to result from the formation of C=C double bonds. They are received as a result of the transformation of the PVDF polymer into polymer chains with more or less double bonds. Its reported in the literature that the longer the reaction takes place, the longer chains are formed. This agrees with our observations, at the beginning the solution was blue, turning darker until it was black after a few minutes. Since this reaction seems to be highly exothermic it is quite a challenge to get reproducible results.

It is not possible to perform the formation process with the application of a soaked separator in the same way for each sample, sometimes there is more liquid at the separator and sometimes less. It's also hard to guarantee the exact reaction time of 5 seconds. To sum up, difficulties in the preparation of the samples are expected to impact the reliability of the data obtained from subsequent measurements. A higher standard deviation for the electrochemical performance indicators is expected for samples obtained by reaction with PVDF.

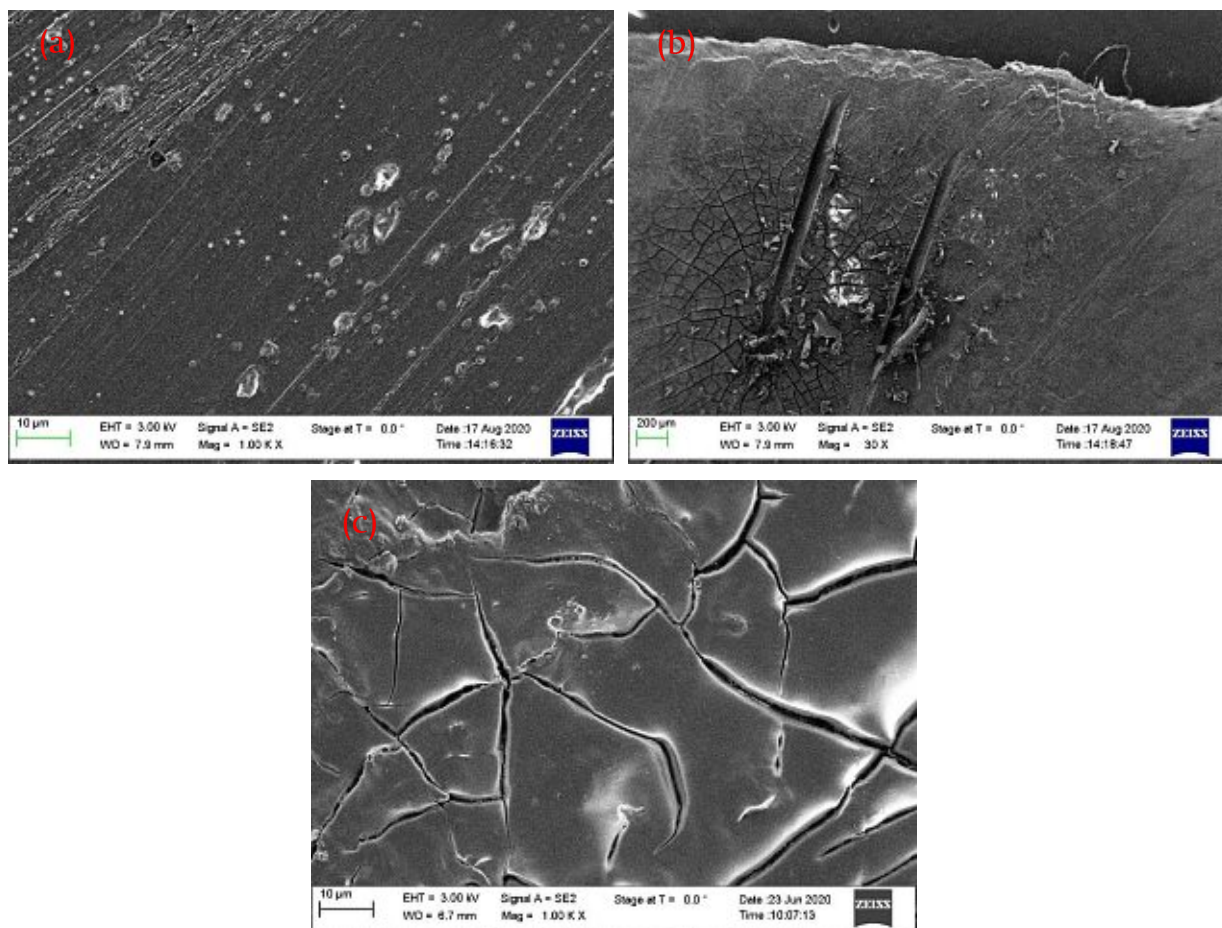


Figure 20: (a) Intact LiF/PVDF layer, (b) damaged layer via scratching the surface, (c) PVDF layer after drying the coated sample in vacuum.

Figure 20(a) shows a coated Li metal foil after reaction with PVDF. The obtained coating is flat and rather smooth, while Figure 20(c) shows a pattern of a cracked surface obtained after drying under vacuum. In Figure 20(b) the coated anode was scratched in order to stress the surface mechanically which leads to enormous crack formation.

The XPS analysis showed a composition of around 19 at.% F and 38 at.% Li. Furthermore around 20 at.% O and 10 at.% C were found. After long time of sputtering (1800 s) there are still some significant amounts of C left. The ratio Li:F is reduced to 6:1 after 300 s, which shows that the content of F is reduced within the sample. The calculated sputtering time of a 200 nm thick layer of pure LiF is about ten times higher (>10000s) than the effectively used time, assuming the thickness of the layer as either significantly thinner than 200 nm or more easily removed by sputtering. In the XPS spectra itself, the occurrence of LiF and C-F bonds can be observed.

It could be said that the layer is a composite of LiF and a fluoride-containing polymer, which is also reported in the literature.

Table 3: XPS quantification of the PVDF decomposition coated LiF layer.

Ar-sputtering time	Element / at.%						
	C	F	Li	N	Ni	O	Si
Pristine	15.1	18.6	37.9	3.4	0.5	23.0	1.5
300 s	15.3	8.5	44.8	4.1	0.2	27.1	
600 s	14.9	7.3	42.5	6.6	0.2	28.5	
900 s	11.2	5.2	52.5	6.3		24.8	
1200 s	11.3	4.8	52.2	5.9		25.8	
1500 s	8.6	4.3	52.3	7.5		27.3	
1800 s	8.8	3.9	55.2	6.6		25.6	

### 6.1.2 Ammonium hydrogen difluoride

The solution of  $\text{NH}_4\text{HF}_2$  in DMSO can be produced and applied easily to the Li metal. A few varieties were tested, like different concentrations, immersion times and filtered/unfiltered solutions.

As mentioned in the theoretical part, solutions of  $\text{NH}_4\text{HF}_2$  in DMSO were filtered to remove remaining precipitate. Both, filtered and unfiltered solutions have been tested. The comparison of the filtered and unfiltered solution showed no optical difference in the layer. Therefore all the anodes measured were processed by the unfiltered solution with the same concentration as mentioned in the paper [28].

In Figure 21, the trend of the LiF layer produced by the  $\text{NH}_4\text{HF}_2$  immersion method is displayed. The variation of the soaking time showed a huge difference in the morphology and crystallite size of the layer as it is revealed in Figure 21.

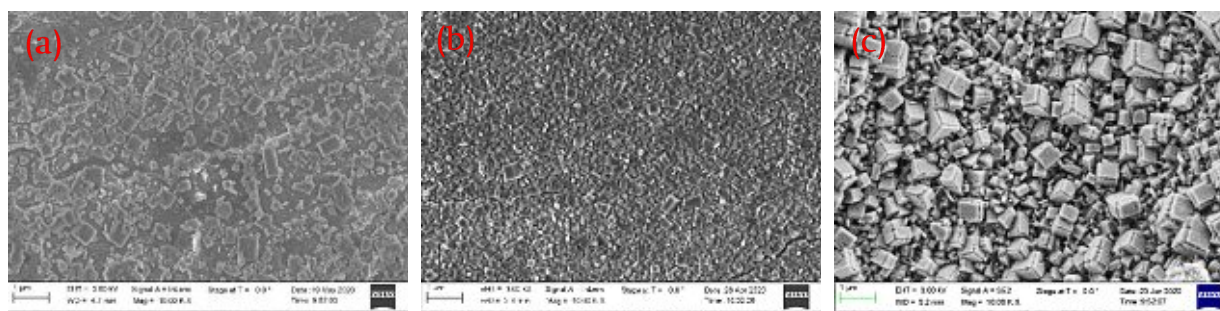


Figure 21: Coating after different immersion times: (a) 2 hrs., (b) 24 hrs. and (c) 5 days.

Coating for 2 hrs. only leads to a partial coating of the surface, whereas the 24 hrs. and 5 days immersion results in coverage of the whole surface.

In the course of the thesis, the received crystallite morphologies received by the immersion coating changed over time. The first batches performed showed a uniform distribution of LiF cubes with similar sizes of around 1  $\mu\text{m}$ . Whereas the last batches

which were done about 8 month later, using the same chemicals as before, showed deteriorated big cubes with lots of small cubes in between as displayed in the following Figure 22.

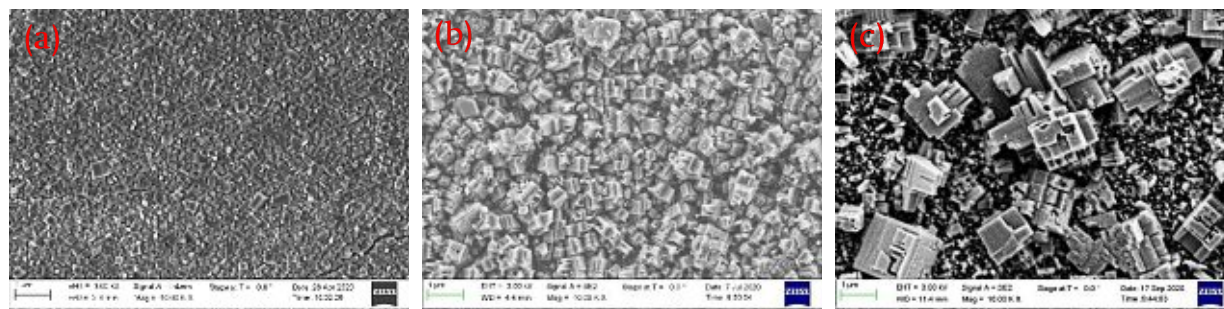


Figure 22: LiF-layer produced by immersion reaction, (a) at the beginning of the thesis, (b) around 4 months later, (c) around 8 months later. Whereby a new immersion solution was produced about every two weeks.

Figure 22(a) and (b) shows a uniform distribution of the LiF cubes which could be received on a few samples. The coating produced after 8 months shows a different morphology, whereby a few big LiF crystals are visible with lots of small crystallites in between.

One possibility to describe this difference is the condition of the chemical ammonium hydrogen difluoride, precisely the water content, since this substance is hygroscopic and does react with water [45]. Therefore, the  $\text{NH}_4\text{HF}_2$  and the solvent DMSO were dried, the DMSO over a 3 Å molecular sieve and the fluoride salt at 80 °C under vacuum. Even with the dried substances the obtained LiF-layer did not look different.

In order to estimate the thickness of the applied LiF-layer, FIB-SEM measurements were performed (Figure 23).

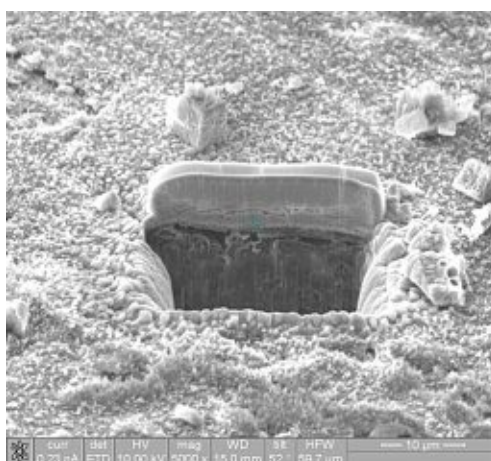


Figure 23: FIB-SEM picture of the coated lithium anode (the grey bar is platinum).

However, it is reported the lithium metal suffers from morphological damage, resulting in a clogged looking shape after the ion cutting process [46]. It was not possible to get the exact thickness of the layer in terms of nanometers. Nevertheless, we were able to roughly

estimate the layer-thickness to be around 1  $\mu\text{m}$ , the same as the size of the single LiF cubes. Compared to the literature where thicknesses of around 7-77  $\mu\text{m}$  [28][29] are reached, thinner layers were obtained.

In order to obtain the same thickness as reported, a few variations of the coating procedure were done. To remove all the salt after the immersion, the coated anodes were washed with DMSO afterwards, which is not done in the original publication. However, for coatings received from samples not cleaned after immersion the SEM micrographs did not show major difference in terms of the morphology. The only difference observed was the deposition of undefined solid deposits between the crystals as shown in Figure 24 by red circles.

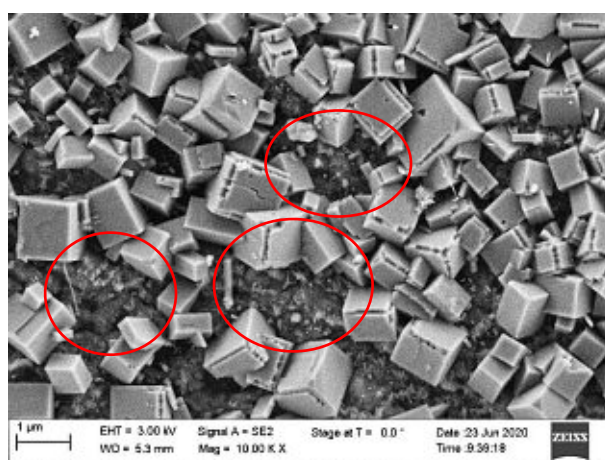


Figure 24:  $\text{NH}_4\text{HF}_2$  immersion sample without the DMSO washing step, the unidentified solid is marked with red circles.

XPS measurements showed equal amounts of Li and F in at.% for the coated Li foils. This confirms the existence of LiF. During the sputtering process, the amount of carbon, which comes from the few seconds of air exposure during transfer of the samples into the measuring device, is decreasing during Ar-sputtering. Even after a long time of sputtering the relative composition of the analysed material is 1:1 Li:F, verifying a thickness in the  $\mu\text{m}$ -range rather than nm-range.

Table 4: XPS quantification of the  $\text{NH}_4\text{HF}_2$ -immersion coated LiF layer.

Sample state	Element / at.%								
	Al	C	F	Li	N	Na	Ni	O	Si
Pristine	1.4	5.3	42.7	43.8	2.3	0.4	1.2	2.2	0.8
45s sputtering	0.8	1.6	44.2	49.2	0.7	0.4	1.2	1.2	0.7
300s sputtering	0.3	0.6	45.6	49.9		0.1	1.1	1.9	0.5

## 6.1.3 Gas-phase reaction with R-134a

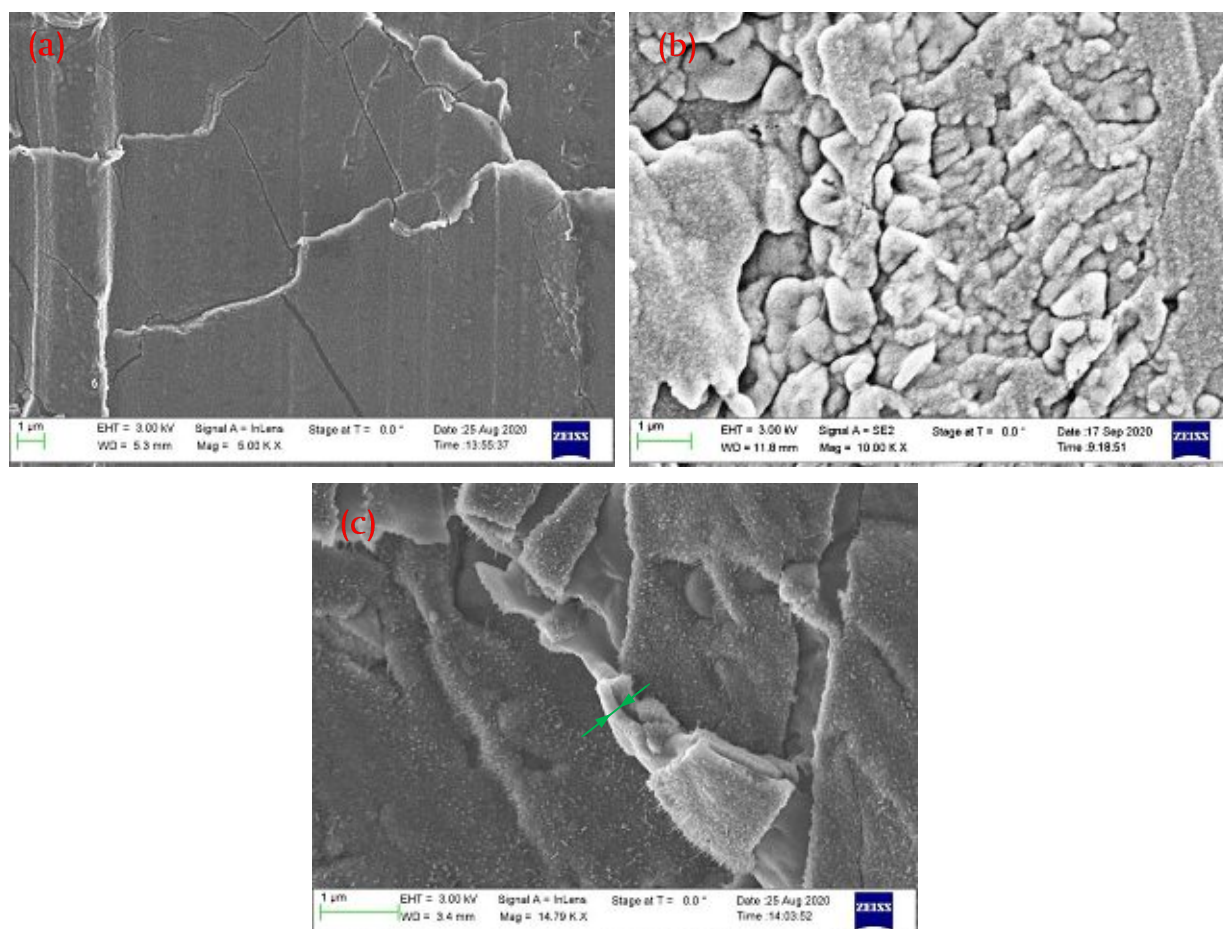


Figure 25: (a) LiF layer with cracks, (b) spherical areas at the surface, (c) layer fragments of the coating, whereby the thickness of the layer could be estimated visually between the green arrows.

The overview of the gas-phase coated sample (Figure 25(a)) shows a uniform coating, with a few cracks. Since the scratched lithium metal anodes were placed on metal spacers and the lithium is very sticky it comes to deformation when the anode is removed from the separator for doing further analysis. This may result in the formation of cracks within the coated surface, as seen in Figure 25(a).

Since the layer (“spiky tiles”) could be visually separated from the flat lithium metal substrate it is possible to estimate the thickness of these coatings. As shown in Figure 25(c) the thickness of the layer is roughly 200 nm. In Figure 25(b) it is displayed that there are some areas on the surface which are showing a spherical morphology, but they are still coated with the LiF layer. These areas are most likely coming from a partial melting of the lithium [29] since its melting point is about 180.5 °C [47]. Nevertheless, almost every measurement which were done have shown that the samples coated by reaction with R-134a are highly reproducible which means the coating process offers high reproducibility.

## 6.1.4 XRD characterisation of the layers

The following graphs show a detailed diffraction pattern of the sample treated with  $\text{NH}_4\text{HF}_2$ .

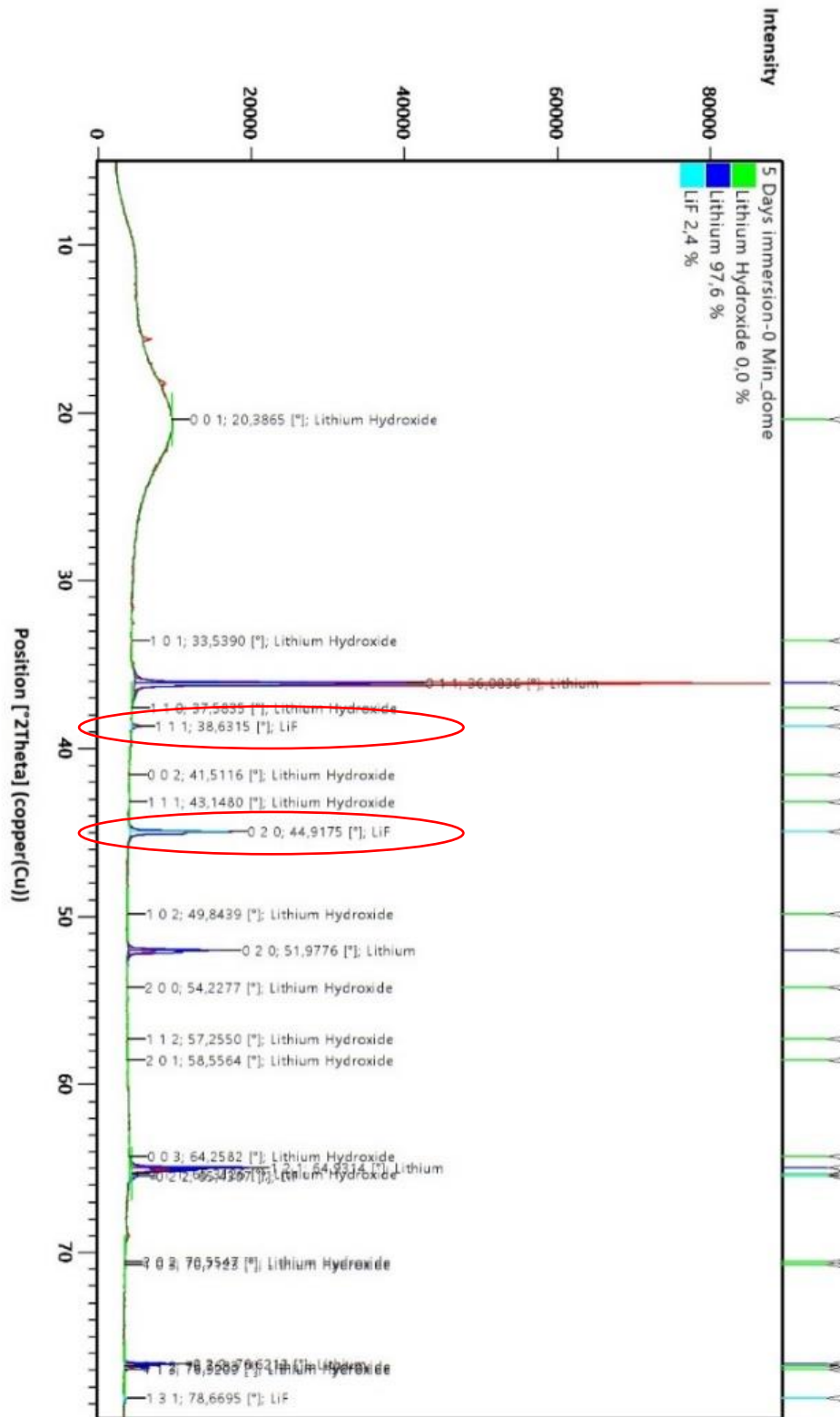


Figure 26: XRD pattern of the  $\text{NH}_4\text{HF}_2$  immersion coated sample. The LiF peaks are marked with red circles.



The broad peak in the pattern at around  $20^\circ$  2-Theta stems from the polymer cap of the “XRD-dome” which consists of PMMA (Poly(methyl methacrylate)) [48].

The sample treated with  $\text{NH}_4\text{HF}_2$ , whose layer consisted of the LiF cubes was the only one where LiF could be found and quantified by XRD. The other coated samples, plotted below, are showing no LiF peaks. On the one hand it could be that the layers are consisting of an amorphous layer, on the other hand the detection limit for XRD is around 1 wt.% [49]. It may be that the PVDF and gas-phase coated layers, which are way thinner than the LiF cubes from the immersion method are below this detection limit.

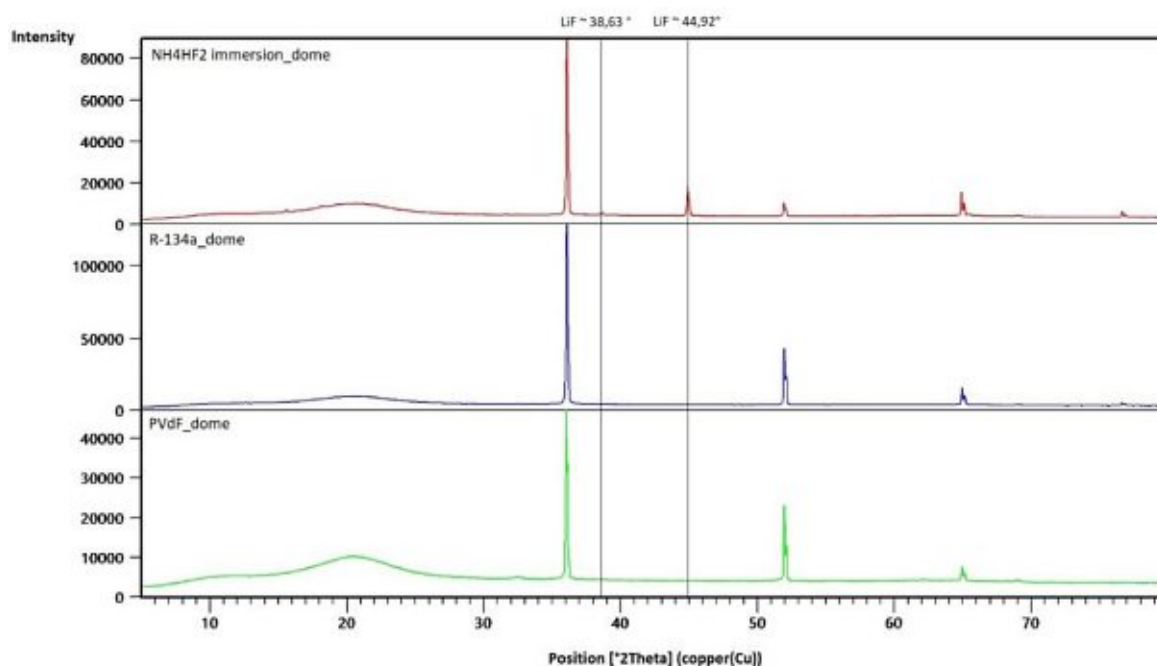


Figure 27: XRD- pattern of the different coated samples, red:  $\text{NH}_4\text{HF}_2$ -immersion, blue: R134a gas-phase, green: PVDF. The LiF peaks are marked with black lines.

The direct comparison of the XRD-patterns from the differently treated samples points out, that only the immersion method yields samples with representative LiF peaks.

## 6.2 Electrochemical investigations

The electrochemical investigations are divided into two main parts, the analysis of uncoated Li and exact description as the reference system with a symmetric cell, and the comparison with LiF-coated samples in order to investigate the influence of this artificial protection layer qualitatively and quantitatively.

### 6.2.1 Pristine lithium reference system

For the reference system pristine lithium electrodes were used in symmetric cells. It's important to analyse the behaviour as well as the reproducibility in terms of cycling performance, to get valid information about the influence of the LiF layer on top of these electrodes.

#### 6.2.1.1 Galvanostatic cycling

The cycling was carried out using the measurement program explained in detail in chapter 5.3.1 in detail. The cycling experiments were carried out with the carbonate and the ether electrolyte.

The next graph (Figure 28) shows a cycling profile of pristine lithium cells in carbonate-based electrolyte and ether-based electrolyte. Each cell was cycled for at least 150 h, which equals 75 cycles with a current density of 1 mA/cm<sup>2</sup>. To get the cycle number out of the following CP-graphs the time must be divided by the factor two.

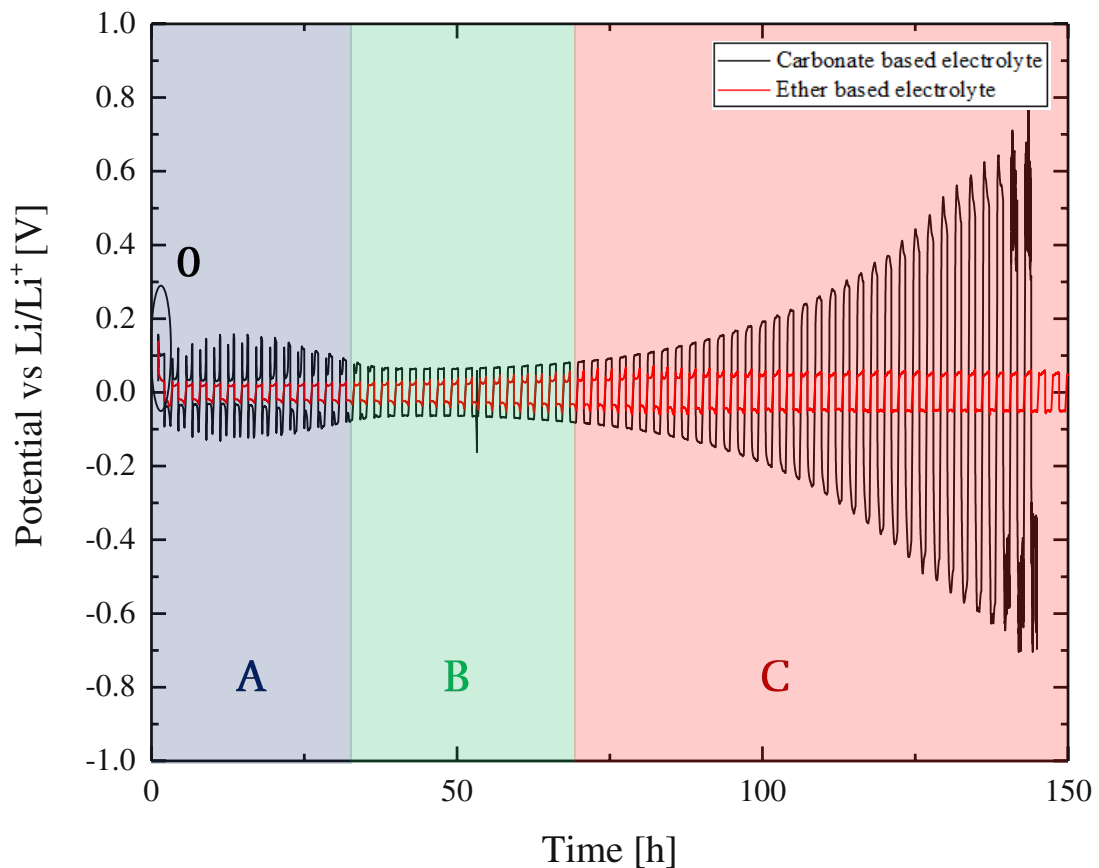


Figure 28: Galvanostatic cycling of pristine lithium cells in carbonate- and ether-based electrolyte.

The cycling profile could be roughly divided into four parts, concerning the progress of the potential. The first part “0” is the high overpotential at the first cycle, which is not considered here but analysed in chapter 6.2.3 since it is not really connected to the long-term behaviour. In the second part A, a heavy peaking behaviour can be observed. In sector B the total potential increases almost constantly but very slow. In the fourth section C, the overpotential increases dramatically, resulting finally in the shortcut of some of the cells. Three representative cycles of each section are plotted in Figure 29.

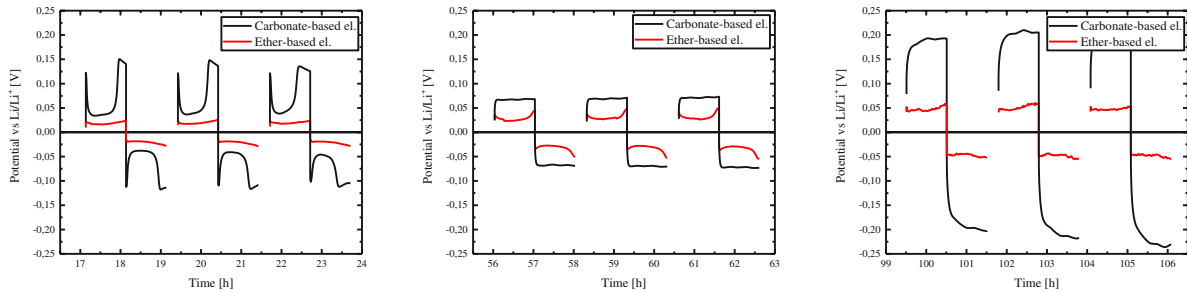


Figure 29: Three cycles of the different sections in the galvanostatic cycling profile of pristine lithium.

Generally, the carbonate-based electrolyte shows a huge variation in the shape and values of the overpotential, which is reported by Wood\_2016 [35] in detail. Whereas the ether-based electrolyte shows an almost continuous shape of the profile over 150 cycles, with only a slight increase in the potential, almost one order of magnitude lower than the carbonate one.

At the earlier cycles, the carbonate graph shows a “peaking” behaviour. The peaks come from the formation of dendrites and pitting processes, as well as the formation of dead lithium, due to the local deposition and stripping processes [cf. chapter 5.3.1]. The later cycles show a steady increase in potential over time, ending in a plateau. This can be referred to the limited diffusion of Li-ions through a thick layer of dead lithium [18]. It takes time for the lithium to establish the concentration gradient throughout the electrolyte during polarization impeded by this layer. Once a quasi-stable gradient is reached, the potential shows a plateau from the diffusion limitation of lithium ions [18].

The four parts in the graph are described in more detail.

**Part 0:** This part is defined as the first cycle and is discussed later in chapter 6.2.3

**Part A:** On the pristine Li surfaces, heavy “peaking” is observed and lithium dendrite formation and growth as well as the evolution of dead lithium are dominating this part of the measurement.

**Part B:** Due to the continuous accumulation of dead lithium on the surface of the electrodes, diffusion is becoming more and more the limiting factor for lithium deposition/stripping. Thus, lithium dendrite formation only seems to be reduced. However, it was reported that the “peaking” behaviour, as observed in part A, is only concealed by the sluggish kinetics and can be again observed using e.g. GITT.

**Part C:** Dead lithium continues to form and constantly consumes electrolyte, due to the formation of SEIs. Eventually the cell dries out and the cell impedance increases steadily as not enough electrolyte remains to properly contact both electrodes.

To confirm this hypothesis a 3-electrode cell (EL-CELL) with the quadruple amount of electrolyte (200  $\mu\text{L}$ ) compared to the standard coin cell (50  $\mu\text{L}$ ) was built and cycled with the standard procedure at a current density of 1  $\text{mA}/\text{cm}^2$ .

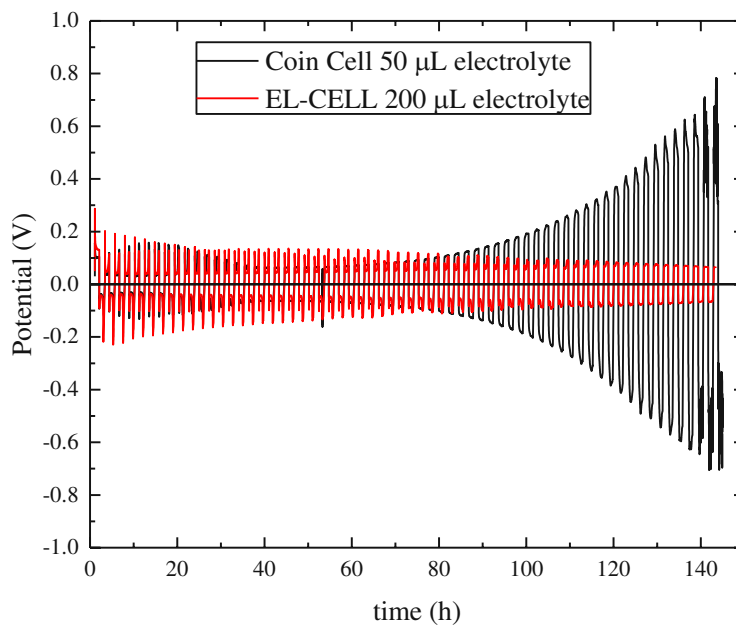


Figure 30: Comparison of the influence in the cycling profile of different electrolyte amounts

Figure 30 shows that, for the carbonate-based electrolyte, the amount of electrolyte is one of the limiting components of an electrochemical cell’s cycling life, especially in coin cells regarding the limited available space inside the casings. Due to the formation and destruction of the SEI at each cycle lots of electrolyte and/or the electrolyte salt is used irreversibly.

Generally, it could be stated, that the selection of the electrolyte has a massive influence in the cycling stability of lithium metal batteries. The two electrolytes used in this thesis differ from the other by two parameters. On the one hand, the organic solvents used are

carbonate-based and ether-based, which makes a huge difference, because of the different reactivity with the lithium metal. The usage of ethers like DOL/DME as electrolyte mitigates the dendrite growth due to its low viscosity and low reduction potential. However the ether electrolytes suffer from a low boiling point and low flash point which makes them less safe [50]. A much heavier drawback is the low oxidation stability of common ethers up to a maximum of around 4.0 V vs Li/Li<sup>+</sup> [51]. Whereas the LiTFSI salt grants a higher density of the plated lithium [52]. It's proven that LiTFSI offers higher capacities and a more reversible redox reaction than LiPF<sub>6</sub>, proven by cyclic voltammetry in cells consisting of a lithium metal anode and a LiFePO<sub>4</sub> cathode [53]. Since in this thesis the used setup consists of symmetric cells with lithium as cathode and anode, it can be assumed that the LiTFSI will positively influence the cycling behaviour. However LiTFSI also leads to the corrosion of the aluminium current collector on the cathode side [54].

### 6.2.1.2 Open-circuit-voltage relaxation

After each cycle at the galvanostatic cycling a resting step of ten minutes was performed and the voltage recorded. This “tail” shows the relaxation of the potential after polarization of the electrodes during galvanostatic cycling.

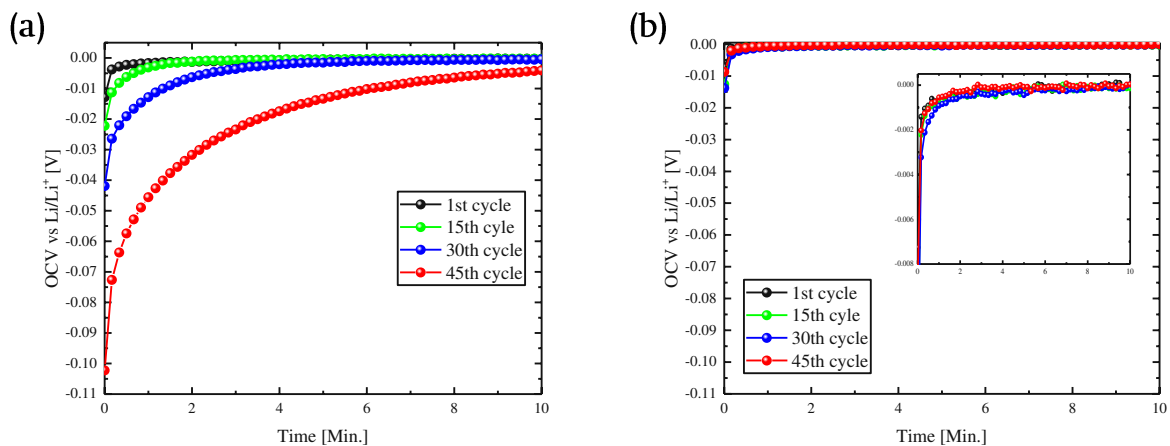


Figure 31: Potential „tails“ during resting steps between cycling, (a) carbonate- (b) ether-based electrolyte.

For the carbonate-based electrolyte, the tails of the relaxation potential are becoming bigger after each cycle. This is referred to the diffusion of lithium ions in the electrolyte, which becomes slower by the formation of more and more dead lithium at each cycle. Thus, the concentration gradient of ions, which is built up during galvanostatic charging/discharging takes a continuously longer time to dissipate.

In the ether electrolyte no such trend could be observed. The relaxation of the tail is constant over 60 cycles. The carbonate-based electrolyte shows at around 25 cycles, that the ten minutes resting step is not enough anymore to reach the equilibrium of the cell,

meaning a potential of 0V vs. the counter electrode. This behaviour could be a prove that the ether-based electrolyte forms less or almost no amounts of dead lithium, compared to the carbonate one.

To quantify the relaxation “tails”, the potential at the end of the relaxation step was recorded and plotted vs. the cycle number. For data with a high level of noise, the average of the last five values was used. The onset of these curves was determined by visual inspection of the graphs. This allows us to compare the different coated samples, including the deviation between equal samples.

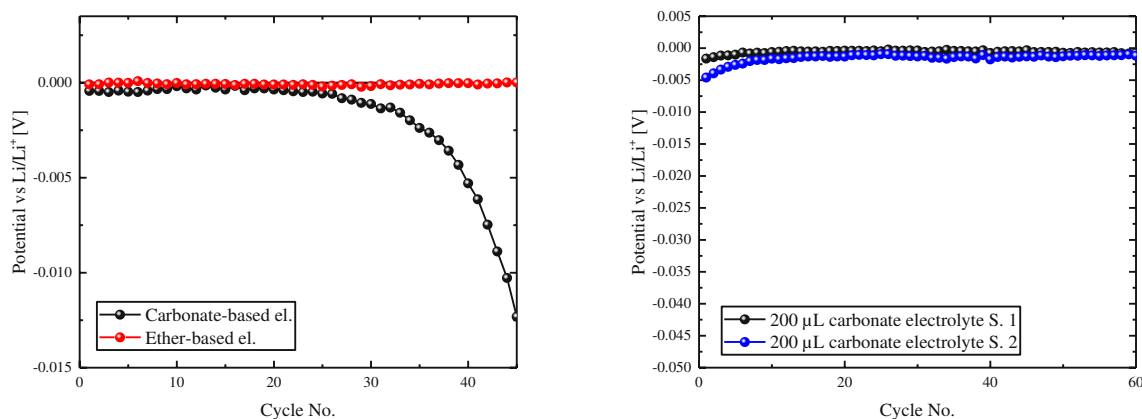


Figure 32: (a) OCV over cycle number. Added lines are guides for the eyes. (b) Potential over cycle number for pristine lithium EL-Cells with 200  $\mu\text{L}$  electrolyte.

Generally, the carbonate-based pristine lithium sample shows an increase in the OCV after around 20-25 cycles, which probably stems from the drying of the cell. The comparison between the cycling of pristine lithium in carbonate-based electrolyte in the coin cell (50  $\mu\text{L}$ ) and the EL-Cell (200  $\mu\text{L}$ ) shows the absence of the increase in potential in the EL-Cell with more electrolyte.

In the ether-based electrolyte an almost constant OCV at the end of the relaxation cycle could be recorded.

### 6.2.1.3 Electrochemical impedance spectroscopy

Before the beginning of galvanostatic cycling and furthermore after every GC-cycle an EIS measurement was performed to measure the change in the resistance of the cell, as well as detecting some change in the structure of the cell, especially the SEI layer.

It must be stated, that referring to the Ohm's law, the potential and the resistance of a system are directly connected via the current. Since in our measurements the current was

held constant, the initial resistance of the cell could be calculated from the obtained overpotential.

**Carbonate-based electrolyte:** In Figure 33 the EIS spectra of the Li/Li cells at different cycle numbers are displayed.

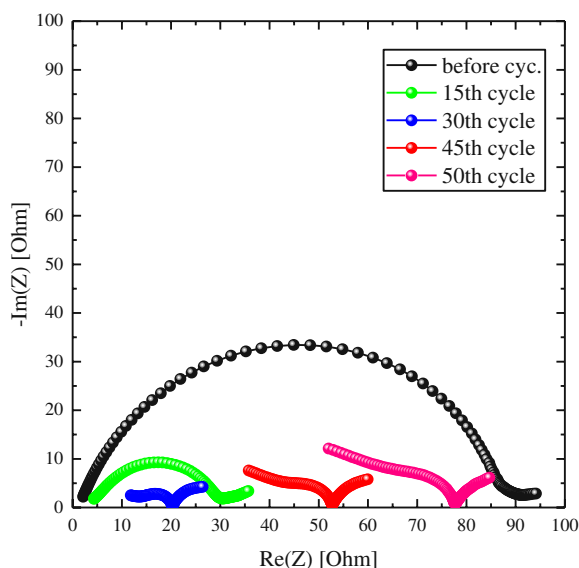


Figure 33: EIS spectra for pristine lithium cells in carbonate-based electrolyte at different cycle numbers.

Among all samples, the first impedance measured, which is done before the start of the cycling shows the highest resistance. Since the shape of the EIS-spectra, which is explained in detail in the theoretical introduction (cf. chapter 5.3.2), offers information about the (electro-)chemical phenomena happening inside the cell, a few characteristic features after a certain number of cycles are listed below:

- Before cycling: Visually there is only one semi-circle noticeable, but as discussed in the theoretical introduction Aurbach et al. showed that this structure can be fitted with five R-C elements. Thereby two of them stem from the interphases lithium/SEI and SEI/electrolyte and the rest from the inner part of the SEI layer [40].
- After 15 cycles: After 15 cycles the impedance graph is like that one before cycling but shifted to lower values. The surface area becomes higher due to the formation of dendrites, which also lowers the resistance [55].
- After 30 cycles: At a cycle number of around 30, the resistance reaches a minimum. The shape of the impedance response changes, giving rise to three distinct depressed semi-circles. Due to instrumental limitations, the EIS measurement was done at a frequency from 20 kHz-100 mHz. For a more detailed analysis of the high-

frequency range, another measurement was carried out at a different device starting from 1 MHz as shown in Figure 34(b).

The fitting of this Nyquist plot with the equivalent circuit of Aurbach shown in Figure 17 displays, that the second visible semicircle ( $\sim 3 \cdot 10^3 - 10^2$  Hz) offers far the highest capacitance, almost three sizes of magnitude higher than the other semicircles. So, this part could be referred to the formation of dendrites, generating a higher surface resulting in a higher capacitance.

- From 30 to 50 cycles the impedance is increasing strongly, while each semi-circle is shifted to higher values. To check if this increase stems from the formation of dead lithium, or the drying of the cell (due to excessive electrolyte decomposition), the impedance data of the EL-CELL where the amount of electrolyte is four times higher than the coin cell are plotted at different cycles in Figure 33(a).

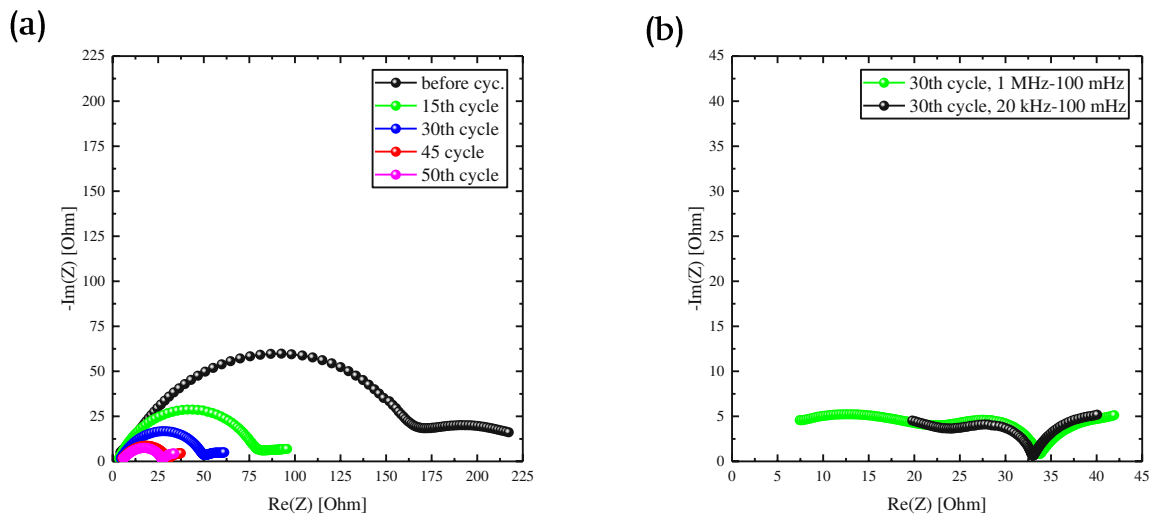


Figure 34: (a) EIS spectra for pristine lithium EL-CELL (200  $\mu$ L electrolyte) in carbonate-based electrolyte at different cycle numbers, (b) EIS spectra for pristine lithium cells within different frequency ranges measured in a coin cell setup.

Figure 34 allows us to assume, that the increase in impedance or resistance after the 30<sup>th</sup> cycle is referred to the drying of the cell.

**Ether-based electrolyte:** The ether-based electrolyte shows a different behaviour to the carbonate one, as observed also during galvanostatic cycling. The impedance over time is displayed in Figure 35.



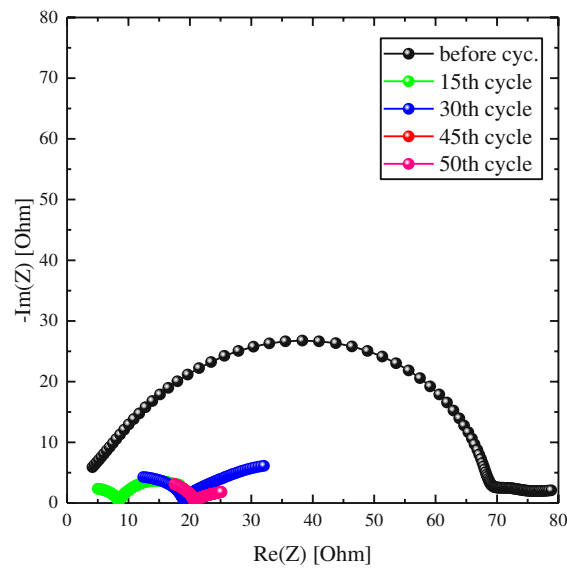


Figure 35: EIS spectra for pristine lithium cells in ether-based electrolyte at different cycle numbers. The graphs for the 45<sup>th</sup> and the 50<sup>th</sup> cycle are almost equal.

Same as seen in the carbonate electrolyte, before cycling the highest resistance is observed. Followed by a decrease of the resistance until around 20 cycles. Afterwards the resistance becomes a bit higher, getting almost stable from cycle 30 on until the end of our measurement which was at around 100 cycles. The absolute value is somehow alternating in a constant area, which could happen by irregular destruction of the SEI and formation of dead lithium.

The shape of the impedance graphs from 30 cycles on and more stays almost constant.

## 6.2.2 Comparison of pristine lithium and LiF-coated lithium

In this chapter, the differences between the differently coated samples are compared among themselves, as well as with the pristine lithium which is analysed properly in chapter 6.2.1.

### 6.2.2.1 Galvanostatic cycling

**Carbonate-based electrolyte:** The cycling was done for pristine and differently coated lithium metal electrodes. In the following graphs, there are at least two measurements of the different coatings shown with pristine lithium as a reference.

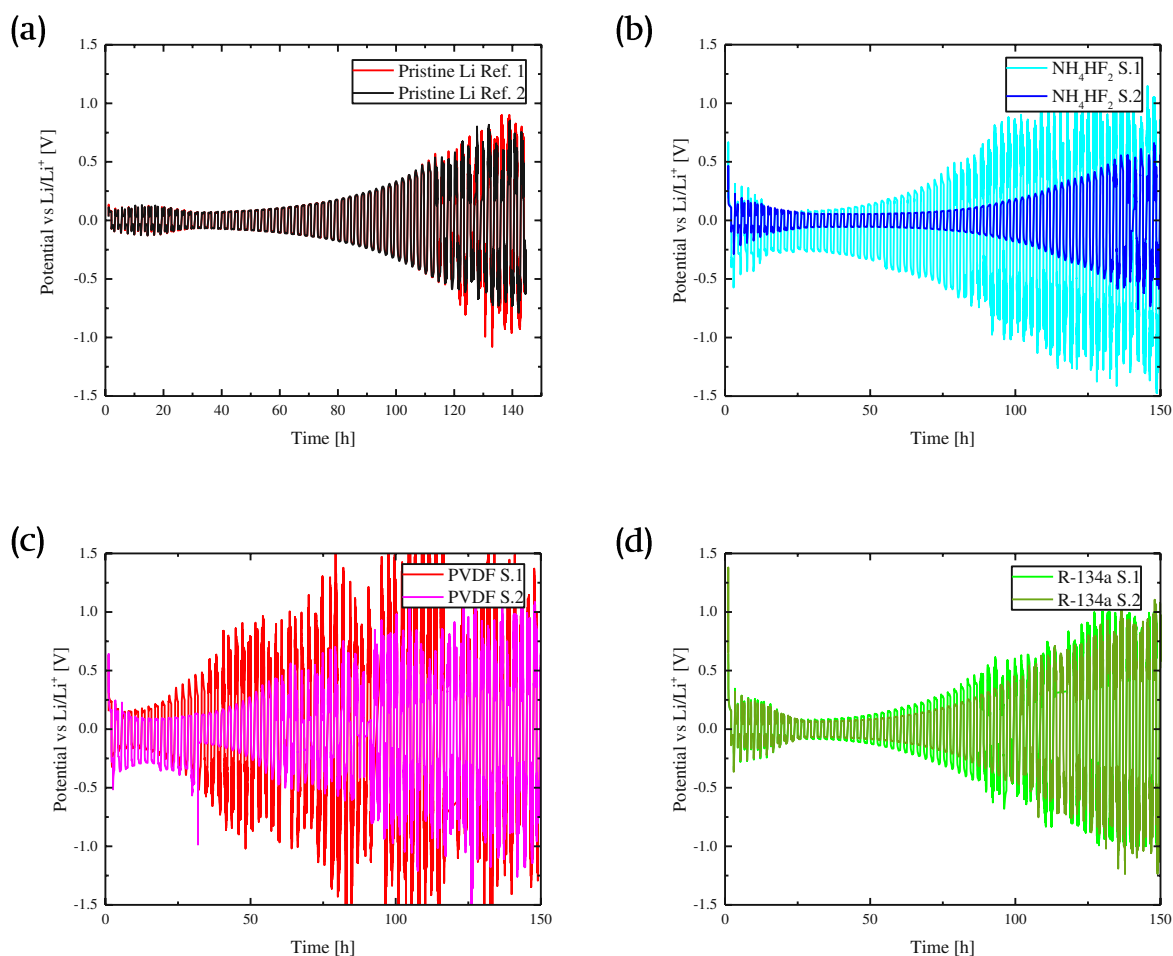


Figure 36: Cycling behaviour of pristine lithium and different coated electrodes in the carbonate-based electrolyte, (a) pristine, (b)  $\text{NH}_4\text{HF}_2$ , 5 days immersion (c) PVDF, (d) R-134a.

Each of the coated electrodes shows similar or poorer performance during cycling compared to the pristine lithium cells as displayed in Figure 36. It is also visible that the results from different samples obtained by reaction with  $\text{NH}_4\text{HF}_2$  and PVDF are very different. This implies that the methods of applying the LiF-layer are offering a poor reproducibility. Especially the  $\text{NH}_4\text{HF}_2$  immersion-coated samples overpotential is different by almost the factor three. For the PVDF coated sample the two cells vary at a factor of around two. This deviation is important to evaluate if changes are significant or not.

It must be mentioned, that for this Thesis the three coating methods were directly adopted from literature and only minor efforts to optimize the processes were conducted.

Its published by Wood, 2016 [35] that in the first cycle, pitting happens on the stripped site, while nucleation is the only process happening at the plating site. In combination with the research done by He, 2019 [27], it is revealed that the initially high overpotential and the subsequent decrease is related to the breakdown of the artificial SEI. The high

overpotential is referred to the transport of the Li-ions through the LiF layer. Thus, inhomogeneities in the layer promote the formation of defect-hotspots since the nucleation is preferred in areas with a low ionic resistance. [27]

These first cycles and their shape are discussed in the chapter 6.2.3.1 “Stability threshold of the layer” in detail.

As done for the description of the pristine lithium reference cell, potential-time curves of three cycles of each section A (the early cycles e.g. 1-10), B (middle cycles e.g. 10-25) and C (very late cycles e.g. 25 +) was plotted for the different coatings.

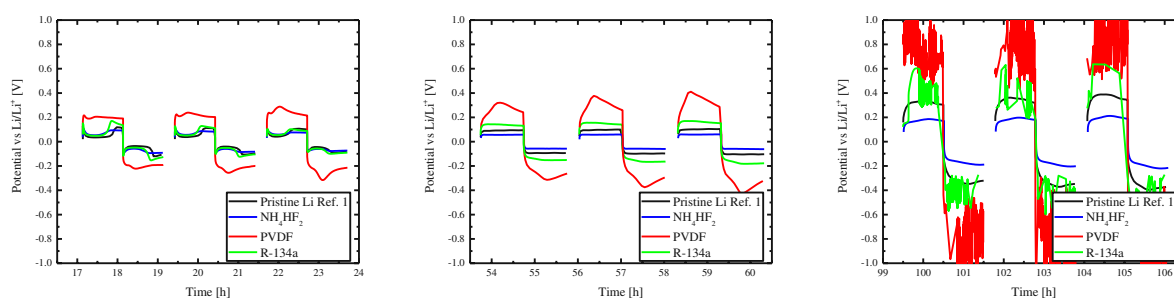


Figure 37: Overpotentials at different time ranges for differently coated electrodes in carbonate electrolyte.

In the early cycles, here cycle 8-10, peaking behaviour is observed as described in chapter 4.1.2. whereby each sample except the PVDF treated ones show similar values (Figure 37). Additionally, the shape of the potential, which stands for the formation of dendrites in the earlier and the formation pitting of the surface in the late cycles is comparable.

This behaviour continues in the subsequent cycles up to 30 cycles. In the late cycles, the PVDF and  $\text{NH}_4\text{HF}_2$  samples are showing a high noise. It was not clarified in this Thesis where this noise comes from, but the drying of the cell might be one possible solution.

The PVDF-treated samples show a strong difference in the potential profiles compared to the other samples. The overpotential is almost twice as high as for the other cells, and the shape of the peaks is quite different. When the carbonate-based electrolyte was added during assembling the cell, its colour turned from colourless to yellow/brown. So, it may be that a reaction between this electrolyte and the LiF/polymer coating happened, resulting in a quite different behaviour of these cells than the others. But it is not confirmed that this coloration influences the behaviour of the battery. Nevertheless, it is reported that the interaction between polymer coatings with the electrolyte might have a significant influence on the performance [56]. However, the change in the colour is supposed to stand for a reaction happening, which was not quantified due to the limited time.

**Ether-based electrolyte:** The cycling process was done for at least two specimen for each coating also in the ether electrolyte, displayed in Figure 38.

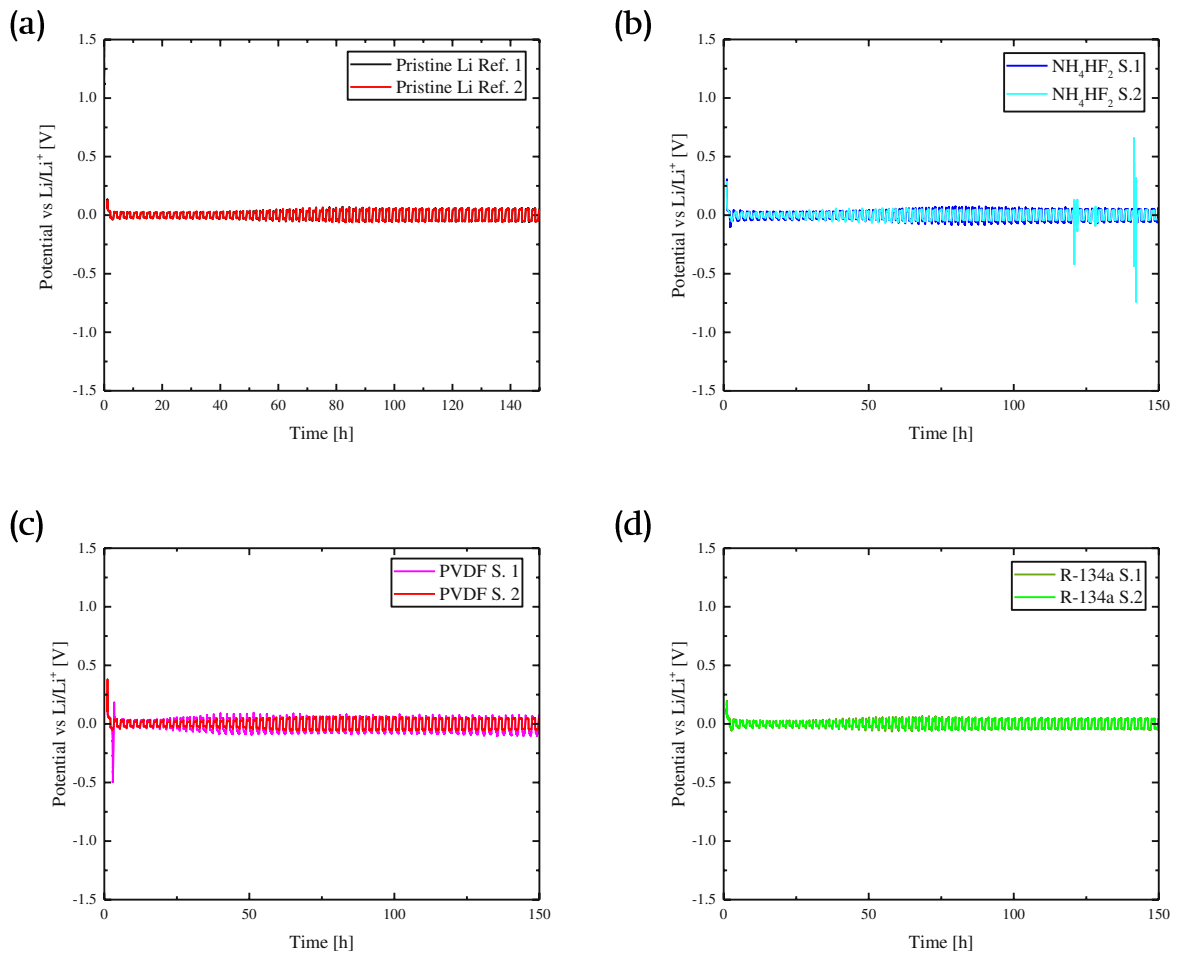


Figure 38: Cycling behaviour of pristine lithium and different coated electrodes in the ether-based electrolyte, (a) pristine, (b)  $\text{NH}_4\text{HF}_2$ , (c) PVDF, (d) R-134a.

Generally, as shown in chapter 6.2.1.1, the overpotential occurring in the ether electrolyte is lower than in the carbonate-based as seen at the comparison of Figure 36 and Figure 38. Furthermore, the differences between the coated and uncoated samples are insignificant, only samples obtained by reaction with PVDF show a higher overpotential, as well as a higher deviation among samples treated with the same coating procedure.

A detailed look at the shape of the overpotential at three different regions of the cycling, early (cycle 1-10), middle (c. 10-25) and late cycles (c. 25+) is shown below.

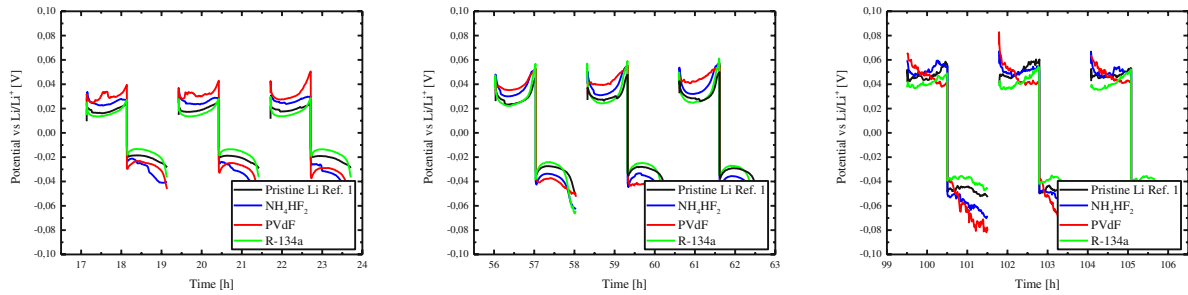


Figure 39: Overpotentials at the three different sections A, B and C in the cycling from different coated electrodes in ether electrolyte.

Figure 39 shows, that the behaviour among all samples is quite similar at the different time ranges depicted.

Even the PVDF treated samples show almost the same shape of the potential profile as the other ones. This observation further affirms the finding, that the coatings on the samples treated with PVDF might react, or at least physically interact with the carbonate-based electrolyte, whereas no reaction is observed with the ether electrolyte.

**Estimation of the reproducibility:** In the following graph, one representative measurement of each cell is displayed. The values and an estimated error for the first four cycles are shown in the Table 6.

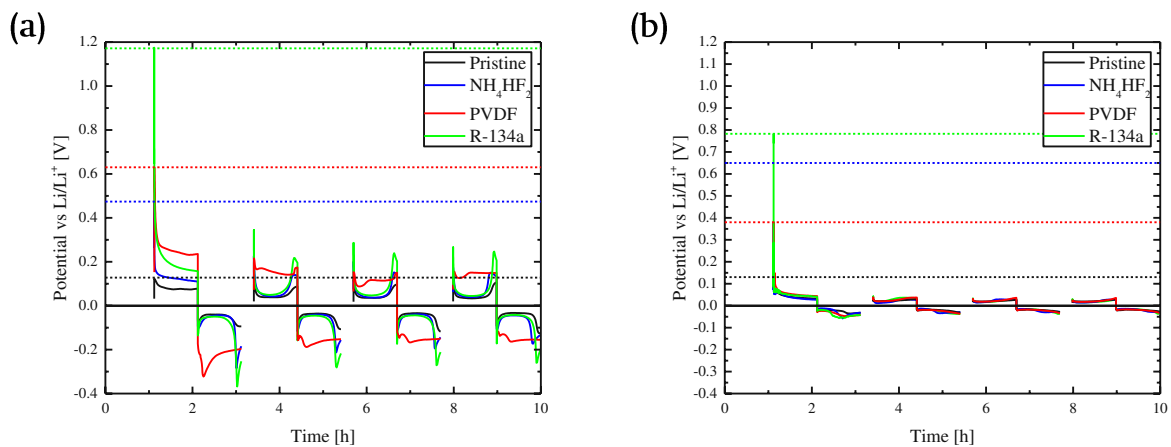


Figure 40: Cycling profile of (a) coated lithium cells in carbonate electrolyte, (b) different coated cells in ether electrolyte.

In Figure 40 the highest overpotential at the first cycle is marked with a dashed line. Since the current is constant for every cycle, this overpotential is proportional to the resistance. All the coated samples are showing a higher overpotential than the uncoated one. The gas phase coating, which is very dense and uniform, gives the highest overpotential in both electrolytes, while the uncoated one gives far the lowest resistance. These values are verified by the EIS-data in the following chapter.

To receive statistically valid data, the first three cycles of each coating in each electrolyte are plotted with their highest overpotential. In Figure 41 (see Table 6 appendix) the statistics of the different coated samples in the carbonate electrolyte are displayed. Figure 42 (see Table 7 appendix) shows the maximum overpotential values for the samples within the ether-based electrolyte.

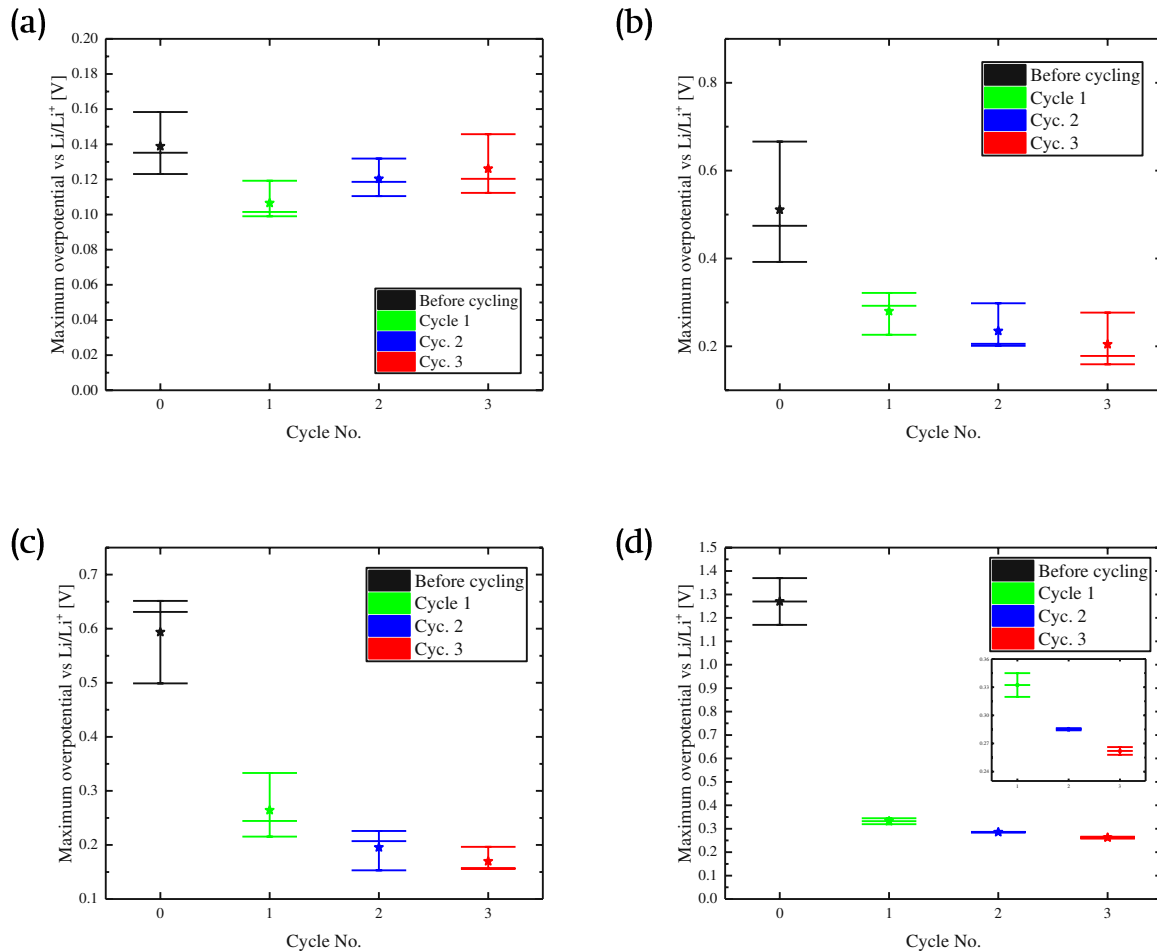


Figure 41: Maximum value of the overpotential before cycling and the first three cycles of different coated samples in the carbonate -based electrolyte. The star in each measurement series represents the average value. (a) pristine lithium, (b)  $\text{NH}_4\text{HF}_2$  immersion coated lithium, (c) PVDF polymer-coated lithium, (d) gas-phase coated lithium.

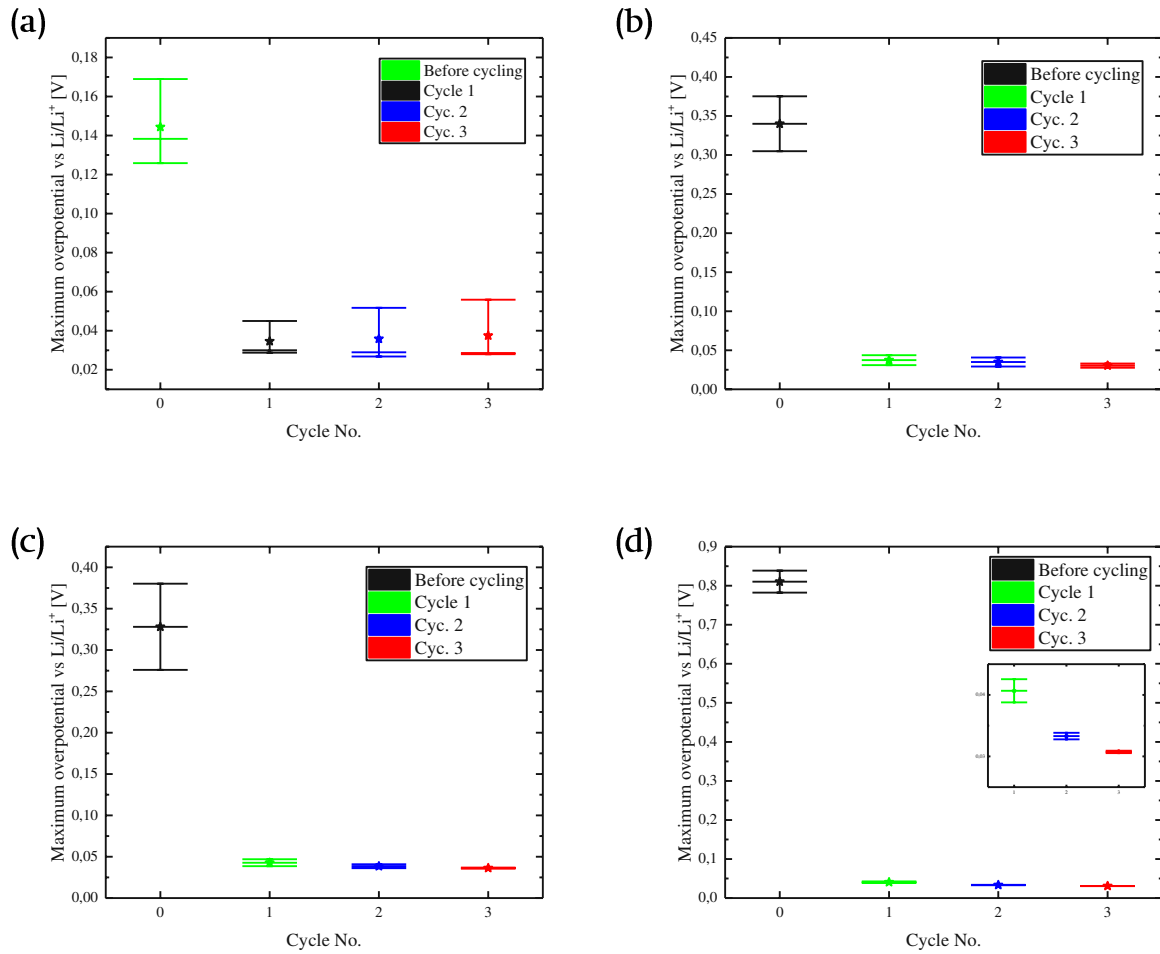


Figure 42: Maximum value of the overpotential before cycling and the first three cycles of different coated samples in the ether-based electrolyte. The star in each measurement series represents the average value. (a) pristine lithium, (b)  $\text{NH}_4\text{HF}_2$  immersion coated lithium, (c) PVDF polymer coated lithium, (d) gas-phase coated lithium.

## 6.2.2.2 OCV – relaxation

As done on pristine lithium, after each cycle at the galvanostatic cycling a resting step of ten minutes was performed too, while recording the voltage. The last OCV value, at high variations the average of the last ten values, was plotted over cycle number, Figure 43.

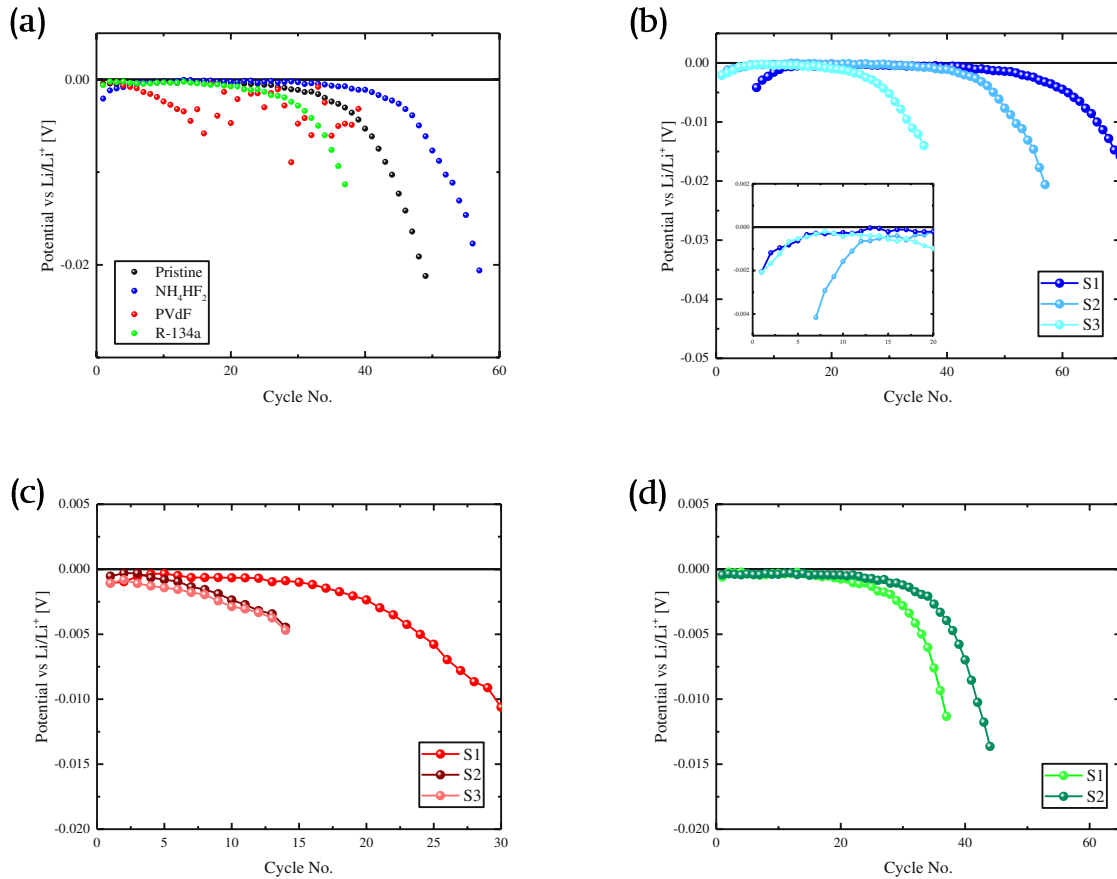


Figure 43: Potential after ten minutes resting in carbonate-based electrolyte, (a) one sample for each coating (b) three samples of the NH<sub>4</sub>HF<sub>2</sub> coated anodes, (c) three samples of the PVdF decomposition-coated samples, (d) two samples of the gas-phase coated samples.

Generally, each sample measured in coin cells, shows an increase in the OCV after the 10 min relaxation period after an increase in the cycle number. Compared to the 3-electrode cell measurement see Figure 32(b) with a four times higher amount of electrolyte, where no increase happens, it could be stated, that this increase in the overpotential after the relaxation period stems from the drying of the cells, and not from the growth of dead lithium, which could inhibit the lithium-ions from diffusing to the lithium metal.

The anode coated with the immersion method in NH<sub>4</sub>HF<sub>2</sub> shows a little decrease in the OCV after the first five cycles. Since this layer is supposed to be porous, it may be that the lithium ions are hindered from diffusion by these pores. After 5-7 cycles the OCV reaches the zero value, which may be referred to the destruction of the layer and the formation of major dendrites as discussed at the overpotential.



The PVDF treated sample shows an increase in the potential at the end of the relaxation period from the beginning on. This behaviour may result from the different composition of the layer. It is possible that the faster drying of the cell, compared to the other coated samples comes from the swelling of the polymer, which consumes some of the electrolyte. Nevertheless, it's not really possible to quantify this phenomenon since the composition of the layer is not known.

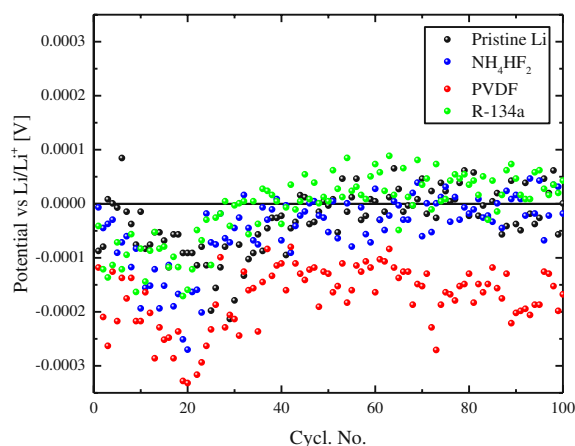


Figure 44: Average OCV after the resting step in ether-based electrolyte.

As seen in Figure 44, the ether-based electrolyte, the OCV values are at very low values of around  $-0.3$  mV. Nevertheless, a minimal trend could be observed. At the first 20-30 cycles the OCV value is increasing very little and decreasing afterwards this “peak”. Since this trend appears on the coated lithium as well as on the pristine lithium metal electrodes, it could not be linked with the artificial LiF-layer on the surface.

### 6.2.2.3 Electrochemical impedance spectroscopy

Aurbach 1993 [40] showed, that the impedance spectra which is received by the measurement with pristine lithium electrodes needs five R-C semi-circles to fit them. Due to the complicated relationship between the impedance behaviour and the structural features and electrochemical processes, it was not possible within the framework of this thesis to quantify the impedance of the coated electrodes in detail. The coating would add at least three more interfaces: coating/lithium, coating/” natural SEI”, coating/electrolyte which makes it very hard to fit and quantify.

**Carbonate-based electrolyte:** As on pristine lithium, EIS analysis was done after each cycle of the GC. In the following Figure 45 the results of the impedance analysis of the first cycles are displayed for the pristine and the different coated electrodes.

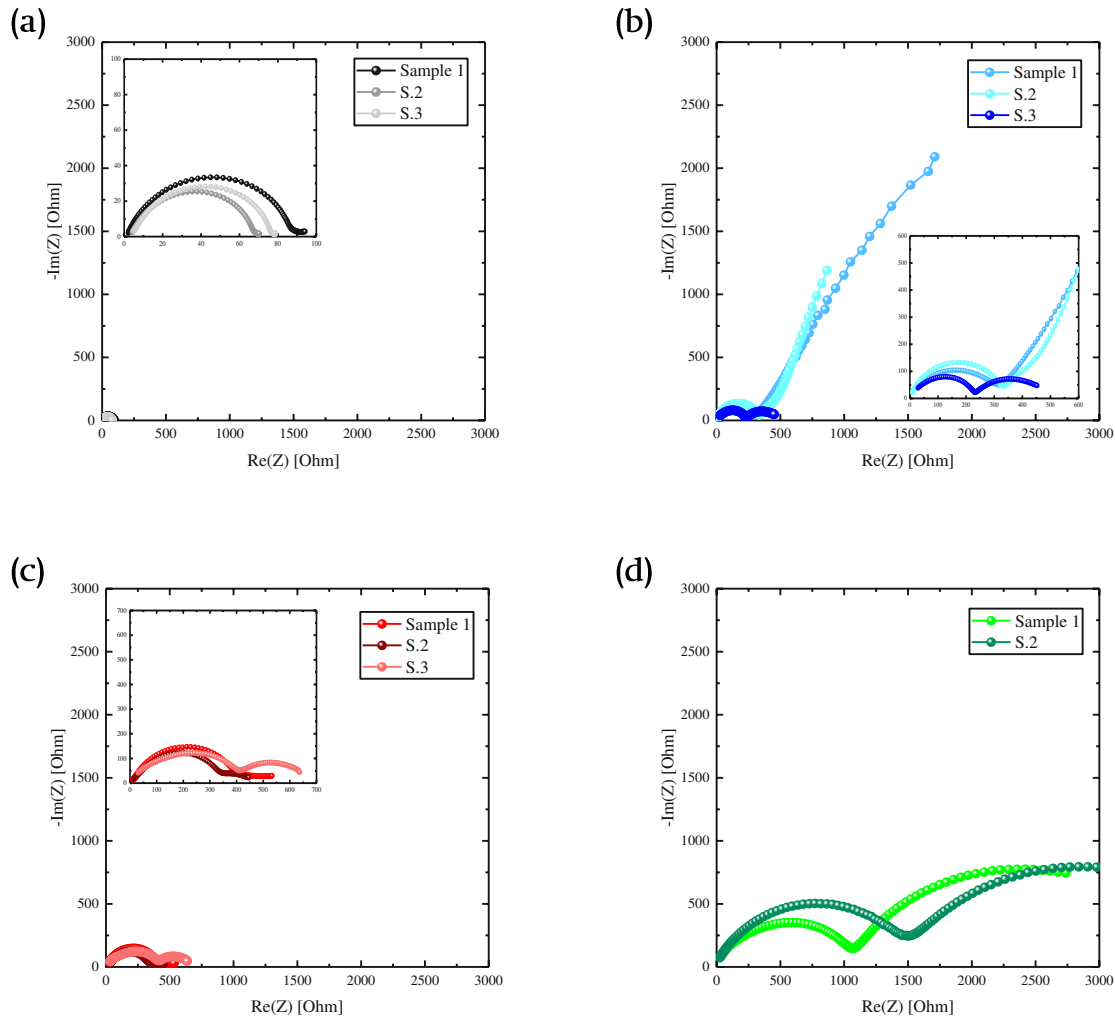


Figure 45: EIS spectra before cycling in carbonate electrolyte, (a) pristine lithium, (b)  $\text{NH}_4\text{HF}_2$  immersion-coated, (c) PVDF decomposition-coated, (d) R-134a gas-phase coated lithium.

The pristine, uncoated lithium shows far the lowest resistance before cycling, as there is no layer on it. An error of around 25% could be estimated from the impedance spectra of pristine lithium. However, the different coated samples are showing errors of 50% up to a completely different spectra. Possible reasons for this observation could be different layer thicknesses and homogeneities for different samples used in different cells as well as differences in the coating of the two electrodes used within one cell.

The porous layer produced by the immersion coating in a  $\text{NH}_4\text{HF}_2$  solution shows a huge difference among the different samples. Not only the values of the resistance differ, but the shape is also different. Ender, 2017 [57] published, while measuring cells in the three-electrodes configuration with a lithium reference electrode, that the geometry of the cells influences the shape of the Nyquist-plot considerably. Therefore, symmetric cells with different sized anodes were analysed, resulting in the splitting of one semi-circle into two while one of the anodes is bigger than the other [57]. Since it is discussed that the  $\text{NH}_4\text{HF}_2$ -

immersion method is poorly reproducible among different approaches, these different shapes in Figure 48(b) could result from asymmetric cells.

The  $\text{NH}_4\text{HF}_2$  treated sample with the lowest resistance among the coated samples, ranges in the area of the resistances of the PVDF treated samples.

The dense and uniform coated lithium obtained by reaction with R134a, shows the highest resistance before cycling, at relative similar values.

All of the coated samples are showing the same shape of the EIS-graph, consisting of one very small ohmic resistance at the highest frequency, followed by two semicircles, which are more or less visible. Since there is such a high resistance observed at the coated samples compared to the uncoated one, it indicates that the lithium ions are migrating through this LiF-layer [27].

For a direct comparison of the samples with the lowest impedance for each coating, graphs of the impedance before cycling, after the first cycle and after the 8<sup>th</sup> cycle are plotted in Figure 46.

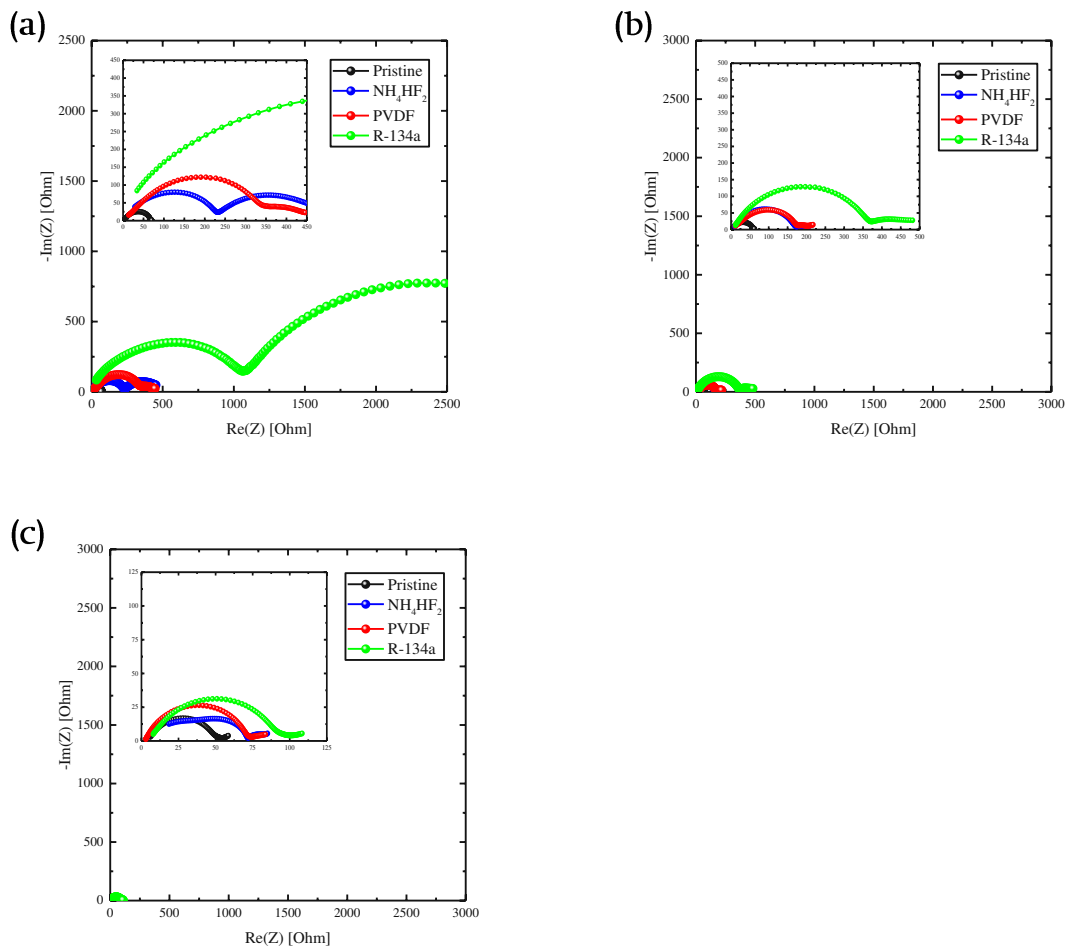


Figure 46: EIS spectra of different coated samples in the carbonate electrolyte. (a) before cycling and (b) after the first cycle, (c) after the 8<sup>th</sup> cycle.

The comparison of the resistances before cycling and after the 8<sup>th</sup> cycle displays the convergence of the resistances after a few cycles. This equal resistance means, that there is no more layer adding extra resistance to the pristine lithium. Since the coated samples are showing a second semi-circle before cycling, while pristine lithium does not it can be argued that this second semicircle is referred to the artificial LiF layer. However, the composition and the morphologies meaning the structure of the layer, being flat or including cracks has a huge influence on the EIS response. Even though after eight cycles there is no more second semi-circle observable, which again would stand for the absence of an artificial layer.

In the carbonate-based electrolyte the shape of the EIS spectra after the few cycles shows a similar shape of the semicircle, which makes the Nyquist-plot look like at pristine lithium. As a consequence, we can assume that the layer has been destroyed in the first few cycles.

**Ether-based electrolyte:** The comparison of the impedance spectra carried out in the ether electrolyte shows almost the same behaviour as in the carbonate electrolyte, but at lower values of the impedance.

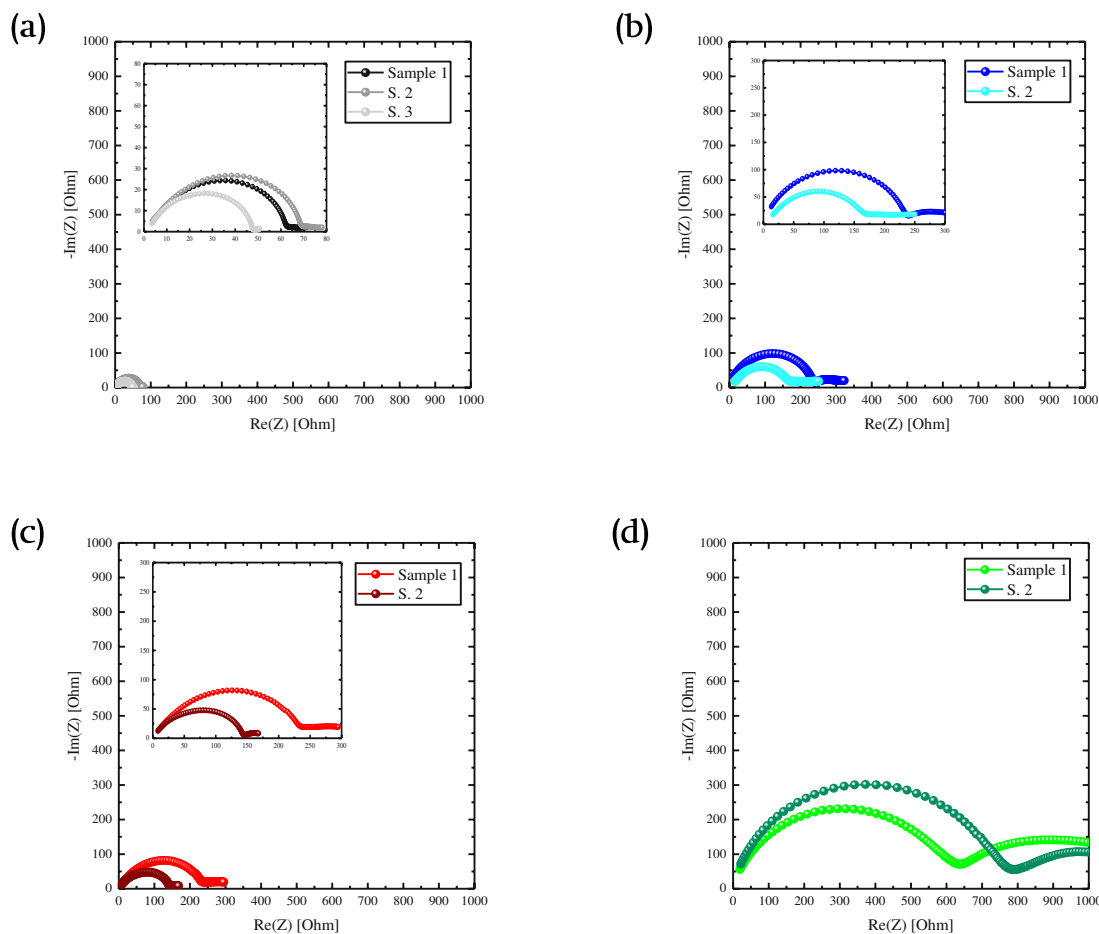


Figure 47: EIS spectra before cycling in ether electrolyte, (a) pristine lithium, (b) NH<sub>4</sub>HF<sub>2</sub> immersion-coated, (c) PVDF decomposition-coated, (d) R-134a gas-phase coated lithium.

The estimated error of the pristine lithium cells is around 30% which is similar to around 25% received in the carbonate-based electrolyte. However, the coated samples are showing much higher errors up to more than 50%. Again, the uncoated sample with the “natural” SEI shows the lowest impedance.

Figure 48 shows the Nyquist-plot of the samples offering the lowest impedance for each different coated sample, before cycling and after the 2<sup>nd</sup> and the 8<sup>th</sup> cycle.

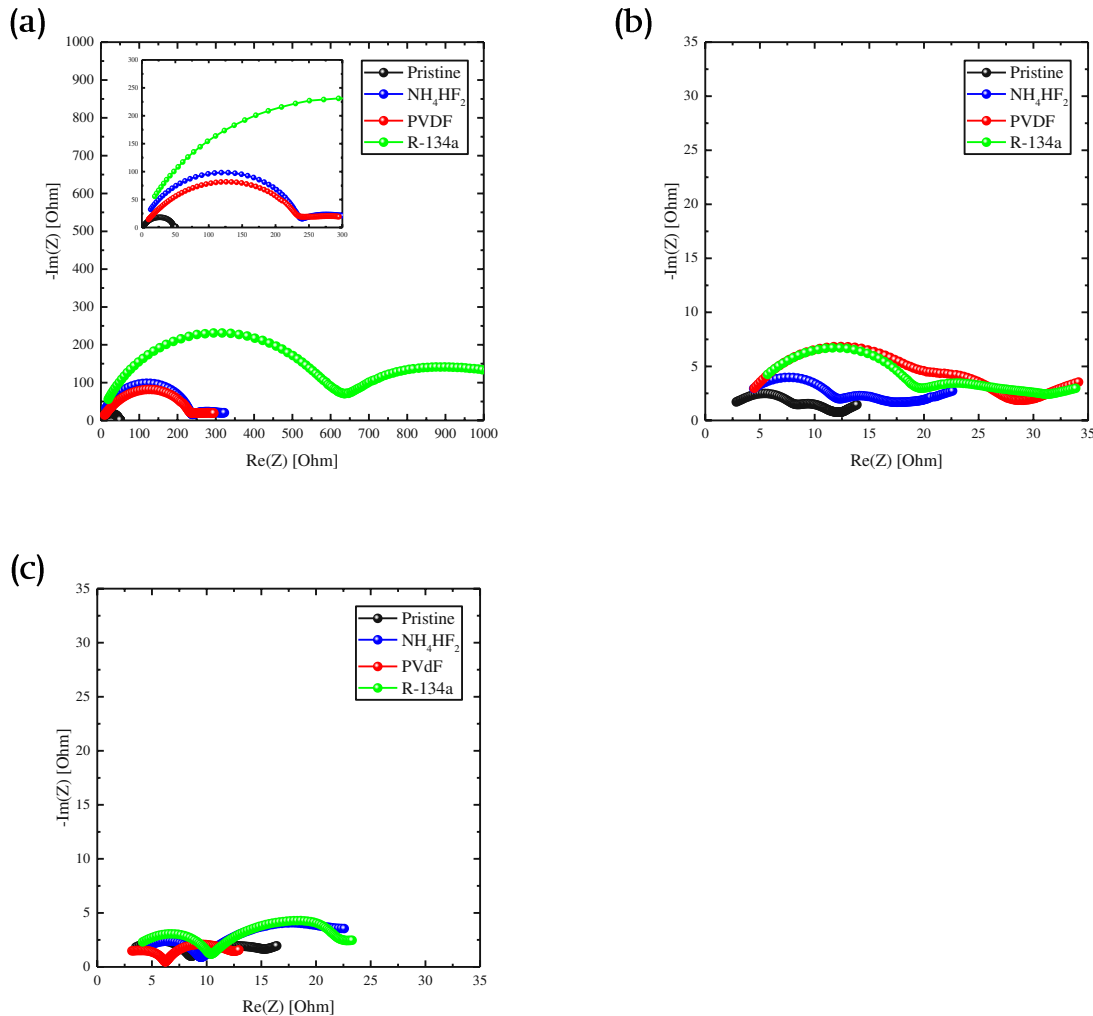


Figure 48: EIS spectra of different coated samples in the ether electrolyte. (a) before cycling and (b) after the first cycle, (c) after the 8<sup>th</sup> cycle.

The values of the impedance for the different samples after one cycle ranges almost in the same area, same as in carbonate-based electrolyte, whereas after eight cycles the impedance is more or less at the same values.

Compared with the carbonated electrolyte the resistances of the tested cells in the ether electrolyte are around 5 times lower for the pristine lithium and up to ten times lower for the coated samples. Furthermore, the shape of the spectra, which stands for the (electro-) chemical processes ongoing in the cell is quite different.

## 6.2.2.4 Capacity measurements in full cells

To verify the results from the symmetric cells closer to real applications, two full cells of each coating were built with NMC622 as cathode material and the standard carbonate electrolyte.

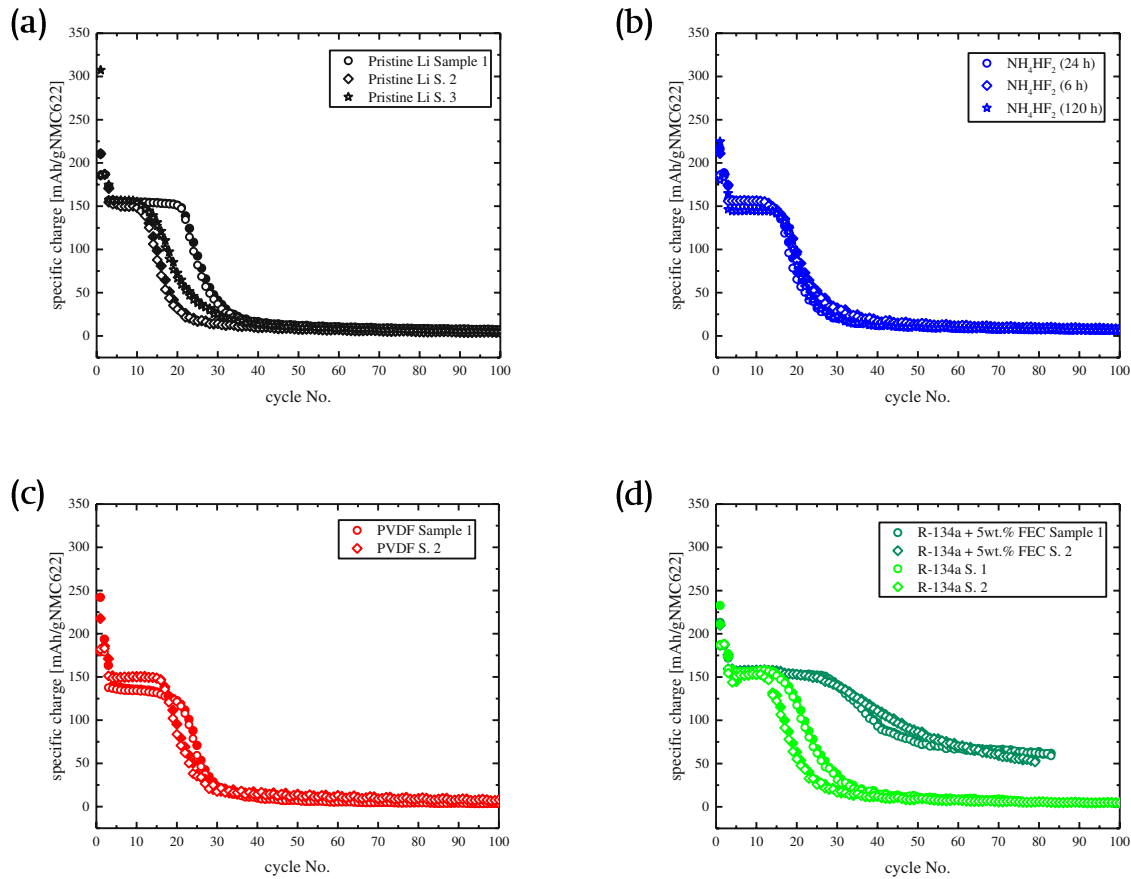


Figure 49: specific charge of full cells against NMC622, (a) pristine lithium, (b)  $\text{NH}_4\text{HF}_2$  immersion coated, (c) PVDF decomposition coated, (d) gas-phase coated lithium electrodes.

No difference in the specific charge over 100 cycles could be observed in the full cells. To avoid a malfunction of the measurement itself or the setup, two cells with R134a treated lithium were filled with electrolyte containing 5 wt.% FEC as additive. FEC as additive improves the cycle lifetime of lithium electrodes by the quick formation of a thin SEI layer, resulting in a better protection of the lithium metal, compared to electrolytes without FEC. Unfortunately the FEC is consumed during this process [27]. However, within the number of cycles investigated, the full cell with additional FEC (dark green) showed a much better performance than the cells with the standard carbonate electrolyte (light green). This shows that a simple LiF-coating does not improve the electrochemical performance in full cells, whereas using FEC as additive to the electrolyte does.

### 6.2.2.5 Conclusion

To sum up, the reference system with symmetric pristine lithium cells was characterised carefully, showing an experimental estimated error of around 25-30% for the overpotential and the resistance as they are connected by the Ohm's law. Therefore, the influence of a protective layer, has to be quite significant to observe it within the used measurements. Furthermore, the deviation between equal samples is very high, or even they show a different behaviour in the Nyquist-plot.

The measurements of the overpotential and the impedance spectroscopy as well as the potential-relaxation agree well. Whereby the PVDF treated samples show a quite different behaviour, which may be referred to the different coating type compared to the other samples.

Even though none of the coatings offered a better performance than the uncoated, pristine lithium in symmetric cells, the change of the electrolyte has a huge influence on the overpotential and the cycling behaviour. Also, the full cell measurement showed no beneficial behaviour of a LiF coating, whereby the addition of 5 wt.% FEC to the electrolyte improves the performance significantly.

### 6.2.3 Validation of the destruction of the layer

After the cycling measurements in symmetric and full cells, it becomes clear that the layer has no positive influence on the long-term cycling stability. So, it is important to analyse what happens to the layer at the first cycles. For that reason, the cycling was done at lower current densities to get the threshold current density at which the layer gets destroyed. In addition, SEM pictures of the plated structures were taken after a specific amount of charge has been applied. In addition, the first cycles from the galvanostatic cycling are analysed properly.

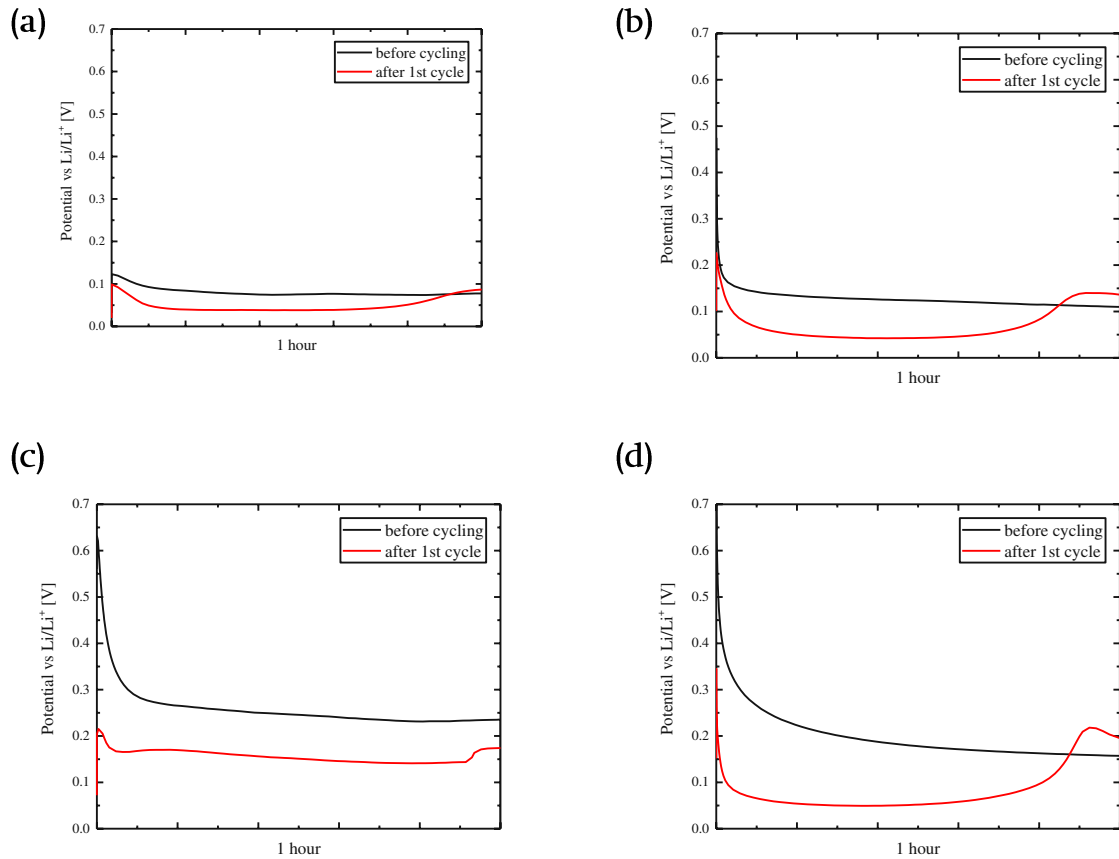


Figure 50: Overpotential measurements before and after the first cycle, (a) pristine lithium, (b)  $\text{NH}_4\text{HF}_2$ , (c) PVDF, (d) R-134a.

According to the publication from He 2019 [27], the first half cycle of the coated samples shows a higher overpotential due to the additional layer, where Li-ions are migrating through. The potential after one full cycle shows the estimated peaking behaviour as reported by Wood 2016 [35] and described in the theoretical introduction in detail (cf. chapter 4.1.2). It looks like the lowest potential valley is almost at the same overpotential for all the coated samples except the PVDF treated one.

At the beginning of the second cycle the lithium is stripped from the dendrites first. After all the dendrites are stripped, the new pits on the surface are created, whereas the artificial SEI layer, offers a higher resistance. Of course, a dense layer offers higher resistance against pitting compared to a porous layer. In the porous layer the pitting (dissolution of the lithium) could start inside pores, where the ionic conductivity is lower than at the rest of the surface, equal to the formation of dendrites as explained in chapter 4.1.2. a perfect flat layer offers no such exposed areas.

Furthermore the pitting generates a larger surface, whereby the surface energy must be overcome in this process [58]. A comparison of the surface energy from pure LiF with that one of the compounds found a native SEI ( $\text{LiOH}$ ,  $\text{Li}_2\text{CO}_3$ ) shows that LiF offers far the



highest surface energy [23]. This could also explain the higher potential which is needed to pit the LiF coated samples.

The PVDF treated sample offers a higher overpotential over all the cycles. This is expected to come from the different type of the layer, a LiF/polymer composite. Although, since the polymer is not characterised, it may offer a much lower ionic conductivity than the pure LiF, which would also result in a higher overpotential.

### 6.2.3.1 Stability threshold of the layer

It is shown by Wood 2016 [35], that the peaking behaviour of the overpotential is referred to the growth of dendrites. It is also mentioned by Xiang et. al [20] that a cycling at low current densities prevents the lithium metal from dendrite growth. Therefore, the uncoated and different coated cells were cycled at very low current densities, to find the threshold current from which the dendrite formation starts.

Besides the low cycling current, the exchange current of the different samples was measured in a potential window between -30 mV to 30 mV vs. Li/Li<sup>+</sup> at a rate of 1 mV/minute. For the exchange current the linear  $\eta/I$  and the logarithmic Tafel-plot is displayed in Figure 51.

To get the current density (assuming a flat surface), the current  $I$  must be divided by the area of the anodes which is 1.91 cm<sup>2</sup>.

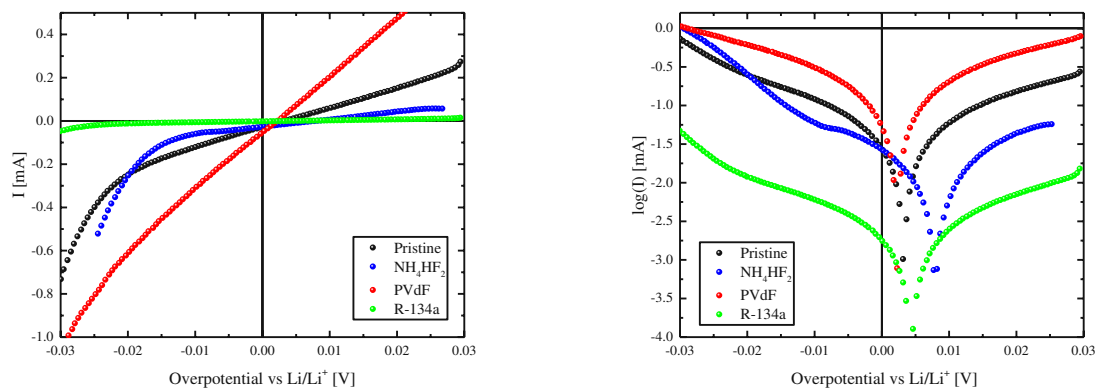


Figure 51: Potential sweep measurements of the different coated samples. (a) Potential/current-graph, (b) Tafel-plot.

In a steady, reversible system, the Tafel-plot shows a certain potential range where the graph is almost linear. As discussed in chapter 5.3.3, at very low potentials the back reaction is no more negligible and at higher overpotentials the reaction may be limited by the mass-transfer. In between an almost linear part in the Tafel-plot was used to fit the exchange current, whereby the following result were obtained.

## 6 Results and discussion

Table 5: Apparent exchange current density (assuming a flat surface) of the different coated samples in carbonate-based electrolyte

Coating method	Fitted value for the $i_{ex}$ per $cm^2$
None	60,7 $\mu A/cm^2$
$NH_4HF_2$	12,0 $\mu A/cm^2$
PVDF	169,6 $\mu A/cm^2$
R-134a	5,0 $\mu A/cm^2$

As displayed in the theoretical part, this exchange current depends on the charge-transfer resistance. Therefore, the sample with the highest exchange current (PVDF) should offer the highest stability against the dendrite formation, because the high exchange current, standing for a low charge-transfer resistance is assumed to lower the hot-spot behaviour resulting in a more homogeneous plating. Whereas the gas-phase coated sample with the lowest exchange current, shows the breaking of the layer at very low current density, which seems to promote the dendrite growth trough hotspot formation.

Furthermore, the potential/current graphs are compared with the cycling at increasing current density graphs.

In the Tafel-plot, each sample shows an increase in the slope at around 20 mV, which is assumed standing for the lowering of the  $R_{ct}$  and/or the increase of the surface i.e. the growth of dendrites. This happens at a certain current, which is very different among the different coated samples. A comparison of the current value where this increase starts, with the behaviour of the overpotential whilst cycling with different current densities could offer information about the stability threshold of the layer, more precise the limit in potential and current for a reversible cycling.

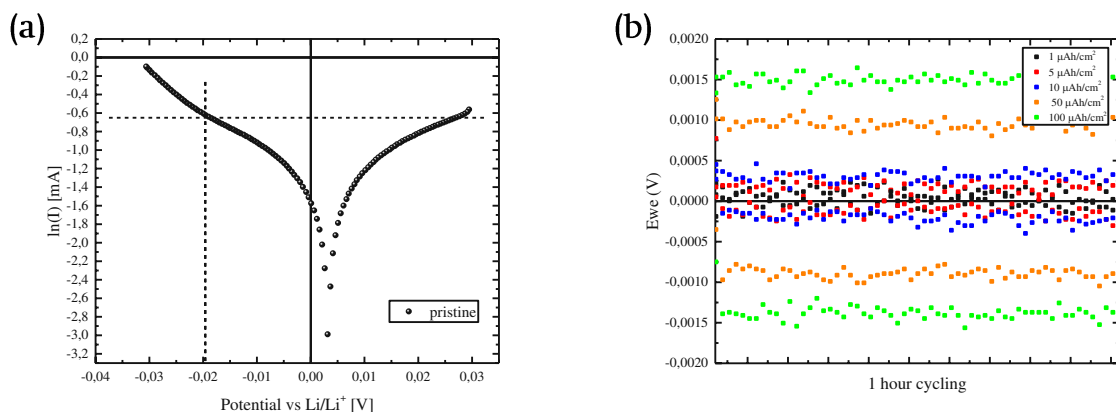


Figure 52: Pristine lithium cells, (a) tafel-plot, (b) linear U/I-plot, (c) overpotential at different current densities.

The increasing current density shows a linear behaviour for the pristine lithium cells up to  $100 \mu\text{Ah}/\text{cm}^2$ . According to the publication of Wood et al. 2016 [35], we can state that due to the flat shape of the potential over time during each half cycle, the pristine lithium does not show a major dendrite formation up to this current density for the used setup within the carbonate electrolyte. Similar measurements are done by He et al. 2019 [27], whereby they used chronoamperometry to determine the stability, the current was measured while applying a constant potential. They showed that pristine lithium shows a stable cycling behaviour up to 50 mV or around  $50 \mu\text{A}/\text{cm}^2$ . Nevertheless, their  $\text{NF}_3$  treated lithium anode with a dense LiF layer on it, showed a 10 times lower current at a certain voltage compared to pristine lithium, verifying that the layer adds a high resistance to the cell. At around  $2 \mu\text{A}/\text{cm}^2$  or a voltage of 20 mV they showed the beginning of the breakdown of the layer [27].

The following Figure 53 shows the overpotential at different current densities of the three different coated samples.

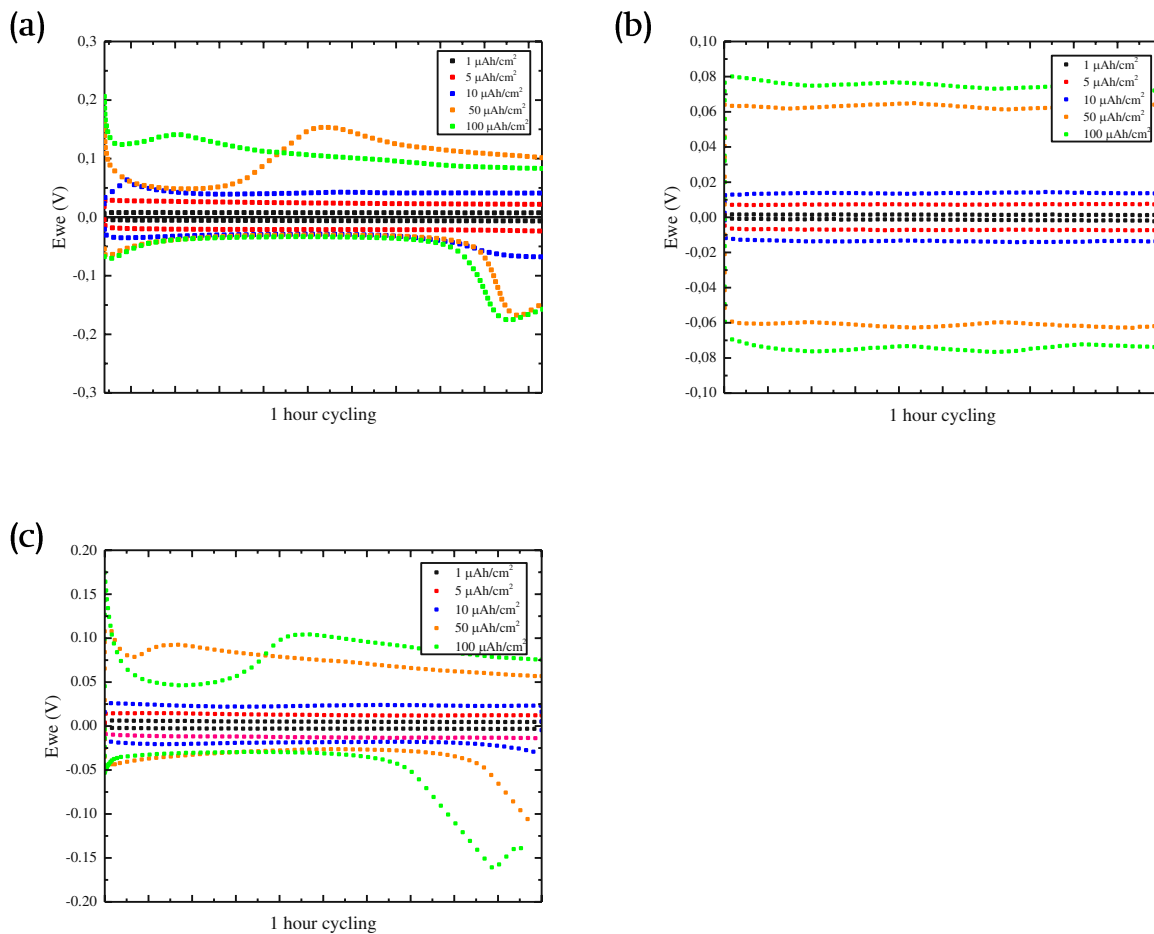


Figure 53: Overpotential at different current densities. (a) 5 d  $\text{NH}_4\text{HF}_2$  immersion-coated, (b) PVDF composition-coated, (c) R-134a gas-phase-coated.

For the PVDF coated samples, which show a quite different behaviour in the long-term cycling too, the “stability-area” received from the Tafel-plot Figure 51(b) reaches up to around 600  $\mu\text{A}$ , meaning around 310  $\mu\text{A}/\text{cm}^2$ . As seen at pristine lithium, the comparison with the increasing current (Figure 53(b)) shows, that PVDF is stable for up to at least 100  $\mu\text{Ah}/\text{cm}^2$  as this is the highest value at which the measurement was performed.

The comparison of the fitted exchange current density of the pristine lithium ( $\sim 60 \mu\text{A}/\text{cm}^2$ ) and the PVDF coated lithium ( $\sim 169 \mu\text{A}/\text{cm}^2$ ) displays that the PVDF coated one offers a three times higher exchange current density. Similar results were received for others artificial SEI-coatings for instance a mixed layer of  $\text{Li}_2\text{O}$ ,  $\text{LiF}$  and  $\text{Li}_3\text{N}$  done by Yao et al. 2019 [59].

The gas-phase coated sample shows the begin of the increase in exchange current at 20 mV at around 10  $\mu\text{A}$  or 5.3  $\mu\text{A}/\text{cm}^2$ . Which means the growth of dendrites begins at a very low current. The increasing current experiment again confirms these obtained results. Even at a current density of 10  $\mu\text{Ah}/\text{cm}^2$  a slight peaking behaviour is observable. Analysing the  $\text{NH}_4\text{HF}_2$ -coated sample offers relatively similar values as the gas-phase coated one, showing the slight beginning of dendrite formation almost around 10  $\mu\text{Ah}/\text{cm}^2$ .

However, these experiments must be carried out by using the ether-based electrolyte too. It can't be excluded that the different behaviour of the PVDF coated sample stems from a chemical or physical reaction of the coating with the carbonate electrolyte.

### 6.2.3.2 Plating/stripping morphologies

To get information of the morphologies of the plated or stripped lithium a current of 1  $\text{mA}/\text{cm}^2$  was applied on symmetric cells for 30 minutes, which equals the half of a cycle done at the long-term cycling. This was done to see the plating morphology of the lithium, without a thick layer of dead lithium. The cells were disassembled and washed with DME to get rid of the salt dissolved in the electrolyte.

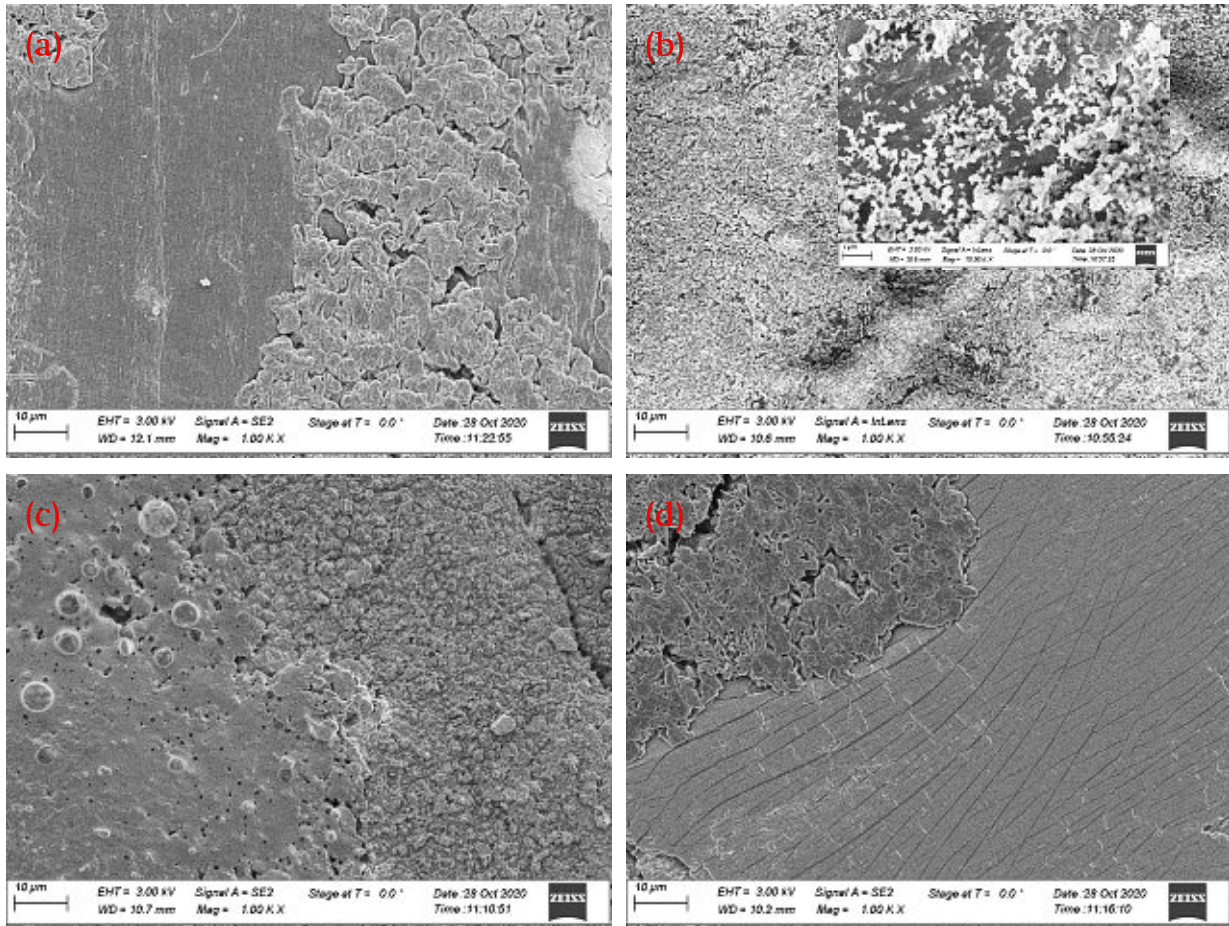


Figure 54: Different lithium plating morphologies after  $\frac{1}{2}$  cycle, (a) pristine lithium, (b) PVDF compound coated sample, the inlayer has a 10 times higher zoom, (c)  $\text{NH}_4\text{HF}_2$  immersion coated sample (120 h), (d) gas phase coated sample.

Each sample shows the plating happening on certain spots and not uniformly over the whole surface, which would be the best mechanism theoretically. On the one hand this could be referred to the uneven plating which stems from the inhomogeneous layers, on the other hand the amount of plated lithium may be too less to cover the whole surface.

The plating structure of the pristine lithium (a) is bulky with spherical shape, as estimated from literature reports [60].

The PVDF composite coated sample (b) shows the plating of lithium in tiny balls with diameters of around 100 nm. The plated lithium seems to be more evenly distributed, than on each other coating. Lopez et. al [56] received a similar plating morphology plating on PVDF-coated copper. They reported that the thickness of the polymer coating influences the average size of the deposited lithium spheres.

The  $\text{NH}_4\text{HF}_2$  coated lithium (c), which is supposed to be porous, and far the thickest coating shows an almost uniform plating of the lithium on top of the LiF layer. This structure agrees with the published literature [29], where it is mentioned that the lithium starts growing inside the pores, resulting in a flat waver like shape on top of the surface.

The R-134a gas phase coated anode shows the same plating behaviour as the pristine lithium. The cracks at the unplated area are supposed to be induced from the removal of the coated electrode from the spacer (used as specimen holder) used during the reaction with the reactant. Due to the brittleness of the layer, it gets cracked very easily by the deformation of the anodes.

Nevertheless, the lithium is plated above rather than beneath the different coatings. As explained in the theoretical chapter, this plated lithium reacts with the electrolyte under the formation of new SEI, which finally results in the growth of dendrites during plating/stripping.

### 6.3 Stability under ambient conditions (Photographs, XRD, FT-IR)

Several methods were used to determine the stability under ambient conditions. The average condition while performing these tests were a relative humidity of around 65% and a temperature of 22 °C.

Photos of the anodes were taken after varying lengths of time under air exposure. This method is quite inaccurate but can offer a simple qualitative estimation if there is any protective effect or not.

To quantify the amount of reaction products which are formed during the air exposure, XRD and FTIR measurements were carried out. Both methods allow in general to determine the amount of the two main reaction products  $\text{Li}_2\text{CO}_3$  and  $\text{LiOH}$ .

#### 6.3.1 Photographs

The coated and uncoated samples were placed on a Teflon plate in the laboratory. The temperature was 23 °C and the relative humidity was around 65 %. The camera was placed 20 cm above the samples and then pictures were made in defined timesteps.

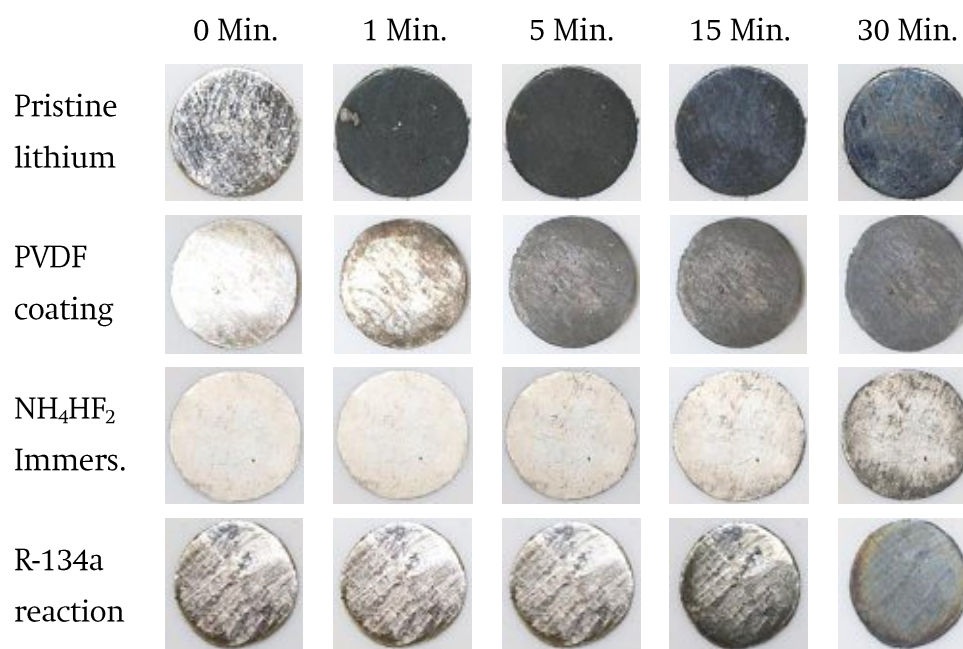


Figure 55: Photographs of different coated lithium samples after different times of air exposure.

According to the reactions mentioned in chapter 4.1 the samples are turning black at the beginning. On pristine lithium this reaction happens within a few seconds of air exposure. Afterwards the uncoated lithium shows the formation of white LiOH respectively Li<sub>2</sub>CO<sub>3</sub>.

These photos point out, that none of the coatings protects the lithium, not even for 30 minutes. The formation of black coloured solid consisting of e.g. Li<sub>3</sub>N is observed at each sample after 5 minutes. The difference between those coated anodes could be explained by the different layer thicknesses and morphologies. The NH<sub>4</sub>HF<sub>2</sub> coated sample with the thickest layer shows the best protection. However, it could be that the layer is just covering the reaction products. To quantify the amounts of reactions products which are formed under reaction with air, analytical methods like XRD and FTIR were done.

### 6.3.2 X-Ray diffraction

The samples were measured with X-Ray diffraction after different times of air exposure. To prohibit a further reaction during the measurement, that sample were put in an argon filled XRD-Dome made from polymer (PMMA). For the quantification of the protectiveness the amount of LiOH was calculated from the spectra and plotted over time. It must be mentioned that the lithium hydroxide was the only reaction product which showed detectable peaks in the spectrum.

In the following Figure 56, the amount of LiOH over time for the different coated lithium metal electrodes is plotted.

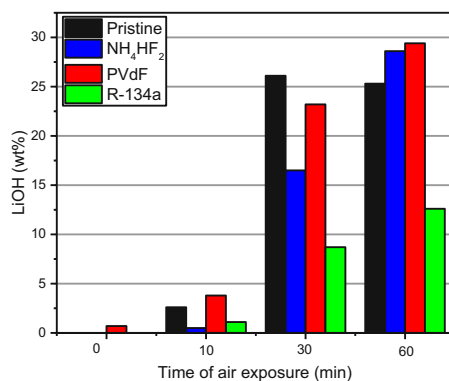


Figure 56: Amount of LiOH over time after a certain time of air exposure for pristine lithium and different LiF coatings.

The Figure 56 shows the same trend in each sample, after a longer time of air exposure there is a higher amount of LiOH formed. Only the uncoated, pristine lithium sample shows no increase of LiOH between 30 and 60 Minutes which could be explained by the last reaction happening at lithium metal in air, the formation of  $\text{Li}_2\text{CO}_3$ . The uncoated sample should offer the fastest reaction, so the formation of LiOH happens ways faster and afterwards the reaction to  $\text{Li}_2\text{CO}_3$  is beginning earlier. Nevertheless, the error of these measurements is quite high, coming from the deformation of the lithium anodes under air exposure, resulting in a “wavy” surface.

The comparison of the three coated electrodes is showing some minor differences, the gas phase coated one gives the best protection as estimated because of the tightness of the layer, but generally none of the coatings protects the lithium for more than 10 minutes, only the reaction rate of lithium and air components seems to be lowered a bit.

In general, the XRD-Data validation in this case is quite hard because the lithium “plates” are underlying a huge deformation process while reaction with air. The edges of the anodes are getting curled up and the whole surface becomes wavy. Another drawback of the XRD measurement of these kind of samples, is that all of the measured elements are very light, so they have a small scattering factor. This leads to a minor radiation yield which makes the quantification harder compared to heavy elements [61].

### 6.3.3 FTIR-Spectroscopy

The samples were taken out of the glovebox and measured at the ATR FTIR instrument. The peaks of two different reaction products LiOH (respectively  $\text{LiOH}\cdot\text{H}_2\text{O}$ ) and  $\text{Li}_2\text{CO}_3$  are marked with black lines and used for analysis. The lithium hydroxide shows a sharp peak at  $3672\text{ cm}^{-1}$ , and  $\text{LiOH}\cdot\text{H}_2\text{O}$  at  $\sim 3570\text{ cm}^{-1}$ . The main peak of  $\text{Li}_2\text{CO}_3$  is between  $1475\text{ cm}^{-1}$  and  $1429\text{ cm}^{-1}$  and another peak at  $870\text{ cm}^{-1}$  [62].



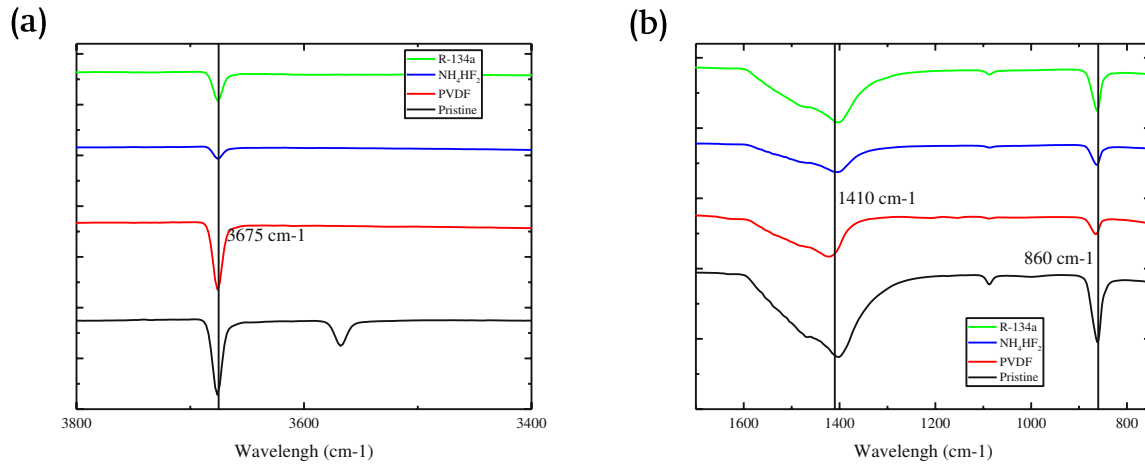


Figure 57: FTIR spectra of different coated anodes after 10 minutes air exposure.

After 10 minutes of air exposure, the FTIR measurements (Figure 57) show the same peaks at each sample, coated and uncoated. The pristine lithium and the 5 day immersion-coated lithium are showing an additional peak at a wavelength of  $\sim 3570$   $\text{cm}^{-1}$  which is the  $\text{LiOH}\cdot\text{H}_2\text{O}$ , however this has no influence on the general conclusion. A quantification of the amount of the reaction products  $\text{LiOH}$  and  $\text{Li}_2\text{CO}_3$  is not possible since the measurement setup needs to be calibrated with defined amounts of  $\text{Li}_2\text{CO}_3$  for instance.

The confirmation of the polymer/LiF compound coating was also done with FTIR for samples measured immediately after they were taken out from the glovebox. The PVDF treated samples showed a pronounced peak at  $1625$   $\text{cm}^{-1}$  (cf. Figure 58) which is characteristic for the C=C bond with a wavenumber of around  $1678$   $\text{cm}^{-1}$ - $1600$   $\text{cm}^{-1}$  depending on the chemical environment [63]. This peak was only visible at the PVDF treated sample.

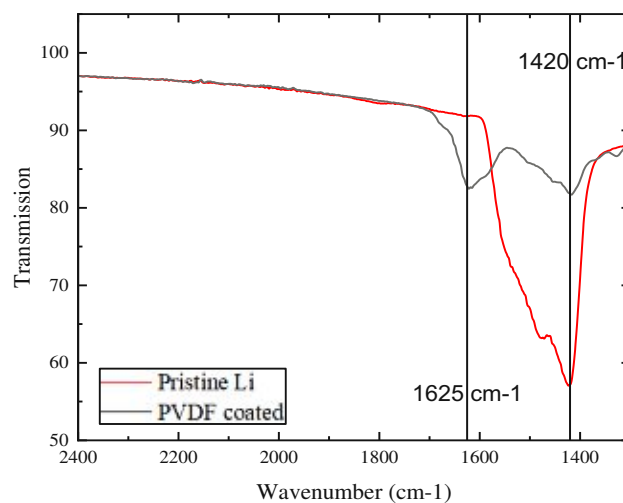


Figure 58: FTIR spectra of pristine lithium and LiF/PVDF composite-coated lithium.

### 7 Conclusion

All the measurements were done with pristine lithium first, to characterise the system, and receiving a reference for the coated lithium samples. Already the pristine lithium shows a high deviation e.g. for the overpotential the deviation is about 30%. The lithium metal anodes were scratched manually before assembling them in a cell or even coating them. Despite they were stored in the glovebox, a slightly matt layer was present on all the lithium metal chips. Since the scratching was done manually it results in different scratched chips, whereby some of them were scratched perfectly, others may have received a higher surface area due to cracks formed through the scratching and so on, which results in a bad reproducibility.

It must be mentioned that in none of the reported approaches, where coatings on lithium metal were applied and compared with pristine lithium, statistical evaluations were done, each paper offers only one sample for each measurement e.g. EIS or CP.

To sum up the results from the coated electrodes, none of the coatings offers a better cycling stability than the pristine lithium in both electrolytes which is completely contrary to the publications e.g. Yuan et al. [64] and Lin et al. [30]. Each of those shows the long-term cycling graph whereby the coated lithium shows a much lower overpotential over the whole timeline, whereas our experiments showed the opposite.

At the beginning of the cycling the existence of a LiF-layer is detectable by a high overpotential in the cycling-profile and a high resistance in the impedance spectroscopy. After around ten cycles in the carbonate, and 1 cycle in the ether electrolyte, the overpotential as well as the shape of the impedance response are quite similar between the coated and uncoated electrodes, what shows the absence of the layer in the later cycles. Highly contrary results are obtained by Wang et al. [33] and Yuan et al. [64], as they are showing EIS-spectra where the “LiF-rich” SEI offers a lower resistance than the uncoated one at 1-10 cycles.

The biggest problem for comparing obtained results from different publications is the high variation in almost each parameter e.g. the selection of the electrolyte system, the cell construction or the cycling rates. Therefore, there can't be any direct comparison among the different coatings. Furthermore, the different compositions of the electrolytes and different salts, makes it hard to determine whether the protecting effect comes from the LiF-layer itself, or from the “self-healing” properties of the salts for instance. Even though it's possible that only a special combination of a certain solvent and salt leads to protective properties for lithium metal electrodes. According to He et al. [27] much more

fundamental studies on the protective role of LiF, especially regarding its intrinsic properties is needed.

Among the coated samples in this thesis, the gas phase reaction obviously delivers the most reproducible and densest layer. The PVDF decomposition reaction itself is very difficult to control, which makes the formation of reproducible results hard. Also, the  $\text{NH}_4\text{HF}_2$ -immersion coated anodes deliver a bad reproducibility which may be related to the long reaction time under stirring, whereby no statistical evaluation was done in the papers at mentioned before.

The composition of the layer was determined by XPS-measurement, whereas no value for the thickness was obtained before reference scans at pristine LiF would have to be done. The best method to obtain exact thicknesses of the LiF-layers would be Cryo FIB-SEM [46]. However, especially for the  $\text{NH}_4\text{HF}_2$  the proposed thicknesses of  $\sim 7\text{-}77\ \mu\text{m}$  [28][29] could not be received. We suppose that once a LiF layer is formed, it prevents the lithium from further reacting with the agent.

The PVDF decomposition-coated sample plays a special role, during cycling with the carbonate-based electrolyte. In the publication it is reported, that the PVDF/LiF coating prevents the lithium metal against reaction with carbonate electrolytes [31]. Contradicting results were observed, during the assembling of the coin cells, the electrolyte turned brown/yellow when in contact with the carbonate electrolyte. The cycling profile showed a much higher overpotential at the PVDF-coated sample. A quite different behaviour of the PVDF sample is also confirmed by OCV-relaxation, whereby the PVDF sample shows a lower relaxation on the beginning than the others. Nevertheless, cycling of the cells at very low current densities, showed the stability area of the coating, whereas the PVDF composite coated shows far the best behaviour among the different coatings. These results are verified by the measurement of the exchange current. One explanation could be that the composite coating which contains LiF and polymer could offer a higher ionic conductivity.

The gas-phase coating led to the highest resistance of the layer before cycling, which may come from the high density and uniformity of the layer.

Coin cells and 3-electrode cells were built and cycled with the developed combined measurement successfully. Since the overpotential and the resistance are connected, the galvanostatic cycling and the electrochemical impedance showed consistent results. The artificial coating adds a huge resistance to the cell, before cycling and during the first cycles. After a few cycles there is no higher resistance observable, which indicates the absence of a layer. We assume that the destruction of the layer happens equal to the

destruction of the “natural” SEI during cycling, whereby the nucleation of the lithium leads to crack formation in the coating. In the first few cycles the artificial SEI or LiF-layer underlies this process which goes hand in hand with the formation of dendrites which are getting covered by a “natural” SEI afterwards, making the artificial SEI from the beginning irrelevant.

Between the two different electrolytes, the carbonate based with  $\text{LiPF}_6$  and the ether-based with LiTFSI as salt, a huge difference is visible as shown many publications [50], [54], [65]. The overpotential of the ether electrolyte is at least half as high as in the carbonate one. The tests in full cells showed that a change in the electrolyte parameters, for example the addition of FEC, changes properties such as the capacity. Hereby it is proven that the system is working, and changes in this system influences the performance significantly.

None of the stability measurements of the coated lithium under air exposure showed a protective effect of the layer. The optical method, done by He et al. [27] and Yuan et al. [29] showed no reaction product up to 40 min at Yuan and 6 h at He. We state that this optical method is not really feasible for proving the stability, because the layer on the lithium metal can simply cover the reaction products making it impossible to observe them visually. Therefore, stability measurements were carried out with XRD, to quantify the amount of the reaction products. These measurements under air exposure showed a poor protection of lithium by the layer. The densest, gas-phase-layer showed a slower formation of LiOH at the surface of lithium by the factor two. But in terms of industrial application 10% instead of 25% after 30 minutes exposure still shows the ongoing of a fast reaction. The black colouration which is formed immediately after the air exposure is not qualified or quantified at all.

The dissemination of this thesis was done via online poster session at the Young Chemist Summit 2020 (online). The poster is attached in the appendix.

## 8 Literature

- [1] J. Liu *et al.*, “Pathways for practical high-energy long-cycling lithium metal batteries,” *Nat. Energy*, vol. 4, no. 3, pp. 180–186, Mar. 2019, doi: 10.1038/s41560-019-0338-x.
- [2] G. Zubi, R. Dufo-López, M. Carvalho, and G. Pasaoglu, “The lithium-ion battery: State of the art and future perspectives,” *Renew. Sustain. Energy Rev.*, vol. 89, pp. 292–308, Jun. 2018, doi: 10.1016/j.rser.2018.03.002.
- [3] A. J. Bard, R. Parsons, J. Jordan, and I. U. of P. and A. Chemistry., *Standard potentials in aqueous solution*. New York: M. Dekker, 1985.
- [4] Dylan Trotsek, “Lithium ion batteries,” *Journal of Chemical Information and Modeling*, 2017. [Online]. Available: <https://www.ucl.ac.uk/institute-for-materials-discovery/research/clean-energy/lithium-ion-batteries>. [Accessed: 05-Nov-2020].
- [5] J. B. Goodenough and K.-S. Park, “The Li-Ion Rechargeable Battery: A Perspective,” *J. Am. Chem. Soc.*, vol. 135, no. 4, pp. 1167–1176, Jan. 2013, doi: 10.1021/ja3091438.
- [6] A. Ramasubramanian, V. Yurkiv, T. Foroozan, M. Ragone, R. Shahbazian-Yassar, and F. Mashayek, “Lithium Diffusion Mechanism through Solid-Electrolyte Interphase in Rechargeable Lithium Batteries,” *J. Phys. Chem. C*, vol. 123, no. 16, pp. 10237–10245, Apr. 2019, doi: 10.1021/acs.jpcc.9b00436.
- [7] D. Aurbach, “A short review of failure mechanisms of lithium metal and lithiated graphite anodes in liquid electrolyte solutions,” *Solid State Ionics*, vol. 148, no. 3–4, pp. 405–416, Jun. 2002, doi: 10.1016/S0167-2738(02)00080-2.
- [8] S. P. Culver, R. Koerver, W. G. Zeier, and J. Janek, “On the Functionality of Coatings for Cathode Active Materials in Thiophosphate-Based All-Solid-State Batteries,” *Adv. Energy Mater.*, vol. 9, no. 24, p. 1900626, Jun. 2019, doi: 10.1002/aenm.201900626.
- [9] J. Asenbauer, T. Eisenmann, M. Kuenzel, A. Kazzazi, Z. Chen, and D. Bresser, “The success story of graphite as a lithium-ion anode material – fundamentals, remaining challenges, and recent developments including silicon (oxide) composites,” *Sustain. Energy Fuels*, vol. 4, no. 11, pp. 5387–5416, 2020, doi: 10.1039/D0SE00175A.
- [10] T. Kim, W. Song, D.-Y. Son, L. K. Ono, and Y. Qi, “Lithium-ion batteries: outlook on present, future, and hybridized technologies,” *J. Mater. Chem. A*, vol. 7, no. 7, pp. 2942–2964, 2019, doi: 10.1039/C8TA10513H.
- [11] P. Tan, Z. Wei, W. Shyy, and T. S. Zhao, “Prediction of the theoretical capacity of non-aqueous lithium-air batteries,” *Appl. Energy*, vol. 109, pp. 275–282, Sep. 2013, doi: 10.1016/j.apenergy.2013.04.031.
- [12] C. H. Hamann, A. Hamnett, and W. Vielstich, *Electrochemistry*, Second, Co. WILEY-VCH Verlag GmbH & Co. KGaA, 2007.
- [13] B. Scrosati, “History of lithium batteries,” *J. Solid State Electrochem.*, vol. 15, no. 7–8, pp. 1623–1630, Jul. 2011, doi: 10.1007/s10008-011-1386-8.
- [14] A. Wang, S. Kadam, H. Li, S. Shi, and Y. Qi, “Review on modeling of the anode solid electrolyte interphase (SEI) for lithium-ion batteries,” *npj Comput. Mater.*, vol. 4, no. 1, p. 15, 2018, doi: 10.1038/s41524-018-0064-0.
- [15] J. Zhang *et al.*, “Direct Observation of Inhomogeneous Solid Electrolyte Interphase on MnO Anode with Atomic Force Microscopy and Spectroscopy,” *Nano Lett.*, vol. 12, no. 4, pp. 2153–2157, Apr. 2012, doi: 10.1021/nl300570d.
- [16] J. Steiger, “Mechanisms of Dendrite Growth in Lithium Metal Batteries,” Karlsruhe Institut für Technologie, 2015.
- [17] M. M. Markowitz and D. A. Boryta, “Lithium Metal-Gas Reactions.,” *J. Chem. Eng. Data*, vol. 7, no. 4, pp. 586–591, Oct. 1962, doi: 10.1021/je60015a047.

- [18] K. H. Chen *et al.*, “Dead lithium: Mass transport effects on voltage, capacity, and failure of lithium metal anodes,” *J. Mater. Chem. A*, vol. 5, no. 23, pp. 11671–11681, 2017, doi: 10.1039/c7ta00371d.
- [19] S. Schweidler, L. de Biasi, A. Schiele, P. Hartmann, T. Brezesinski, and J. Janek, “Volume Changes of Graphite Anodes Revisited: A Combined Operando X-ray Diffraction and In Situ Pressure Analysis Study,” *J. Phys. Chem. C*, vol. 122, no. 16, pp. 8829–8835, Apr. 2018, doi: 10.1021/acs.jpcc.8b01873.
- [20] J. Xiang *et al.*, “Alkali-Metal Anodes: From Lab to Market,” *Joule*, vol. 3, no. 10, pp. 2334–2363, Oct. 2019, doi: 10.1016/j.joule.2019.07.027.
- [21] A. M. Haregewoin, A. S. Wotango, and B.-J. Hwang, “Electrolyte additives for lithium ion battery electrodes: progress and perspectives,” *Energy Environ. Sci.*, vol. 9, no. 6, pp. 1955–1988, 2016, doi: 10.1039/C6EE00123H.
- [22] Gaojing Yang, Yejing Li, Shuai Liu, Simeng Zhang, Zhaoxiang Wang, and Liquan Chen, “LiFSI to improve lithium deposition in carbonate electrolyte,” *Energy Storage Mater.*, vol. 23, pp. 350–357, 2019, doi: 10.1016/j.ensm.2019.04.041.
- [23] Y. Ozhabes, D. Gunceler, and T. A. Arias, “Stability and surface diffusion at lithium-electrolyte interphases with connections to dendrite suppression,” Apr. 2015.
- [24] P. Zhai, L. Liu, X. Gu, T. Wang, and Y. Gong, “Interface Engineering for Lithium Metal Anodes in Liquid Electrolyte,” *Adv. Energy Mater.*, vol. 10, no. 34, p. 2001257, Sep. 2020, doi: 10.1002/aenm.202001257.
- [25] H. Shin, J. Park, S. Han, A. M. Sastry, and W. Lu, “Component-/structure-dependent elasticity of solid electrolyte interphase layer in Li-ion batteries: Experimental and computational studies,” *J. Power Sources*, vol. 277, pp. 169–179, Mar. 2015, doi: 10.1016/j.jpowsour.2014.11.120.
- [26] K. Tasaki and S. J. Harris, “Computational Study on the Solubility of Lithium Salts Formed on Lithium Ion Battery Negative Electrode in Organic Solvents,” *J. Phys. Chem. C*, vol. 114, no. 17, pp. 8076–8083, May 2010, doi: 10.1021/jp100013h.
- [27] M. He, R. Guo, G. M. Hobold, H. Gao, and B. M. Gallant, “The intrinsic behavior of lithium fluoride in solid electrolyte interphases on lithium,” *Proc. Natl. Acad. Sci.*, vol. 117, no. 1, pp. 73–79, Jan. 2020, doi: 10.1073/pnas.1911017116.
- [28] Yanxia Yuan, Feng Wu, Guanghai Chen, Ying Bai, and Chuan Wu, “Porous LiF layer fabricated by a facile chemical method toward dendrite-free lithium metal anode,” *J. Energy Chem.*, vol. 37, pp. 197–203, 2019, doi: 10.1016/j.jechem.2019.03.014.
- [29] Yanxia Yuana *et al.*, “Regulating Li deposition by constructing LiF-rich host for dendrite-free lithium metal anode,” *Energy Storage Mater.*, vol. 16, pp. 411–418, 2019, doi: 10.1016/j.ensm.2018.06.022.
- [30] D. Lin *et al.*, “Conformal Lithium Fluoride Protection Layer on Three-Dimensional Lithium by Nonhazardous Gaseous Reagent Freon,” *Nano Lett.*, vol. 17, no. 6, pp. 3731–3737, Jun. 2017, doi: 10.1021/acs.nanolett.7b01020.
- [31] Jialiang Langa *et al.*, “One-pot solution coating of high quality LiF layer to stabilize Li metal anode,” *Energy Storage Mater.*, vol. 16, pp. 85–90, 2019, doi: 10.1016/j.ensm.2018.04.024.
- [32] L. Fan, H. L. Zhuang, L. Gao, Y. Lu, and L. A. Archer, “Regulating Li deposition at artificial solid electrolyte interphases,” *J. Mater. Chem. A*, vol. 5, no. 7, pp. 3483–3492, 2017, doi: 10.1039/C6TA10204B.
- [33] G. Wang *et al.*, “A Scalable Approach for Dendrite-Free Alkali Metal Anodes via Room-Temperature Facile Surface Fluorination,” *ACS Appl. Mater. Interfaces*, vol. 11, no. 5, pp. 4962–4968, Feb. 2019, doi: 10.1021/acsami.8b18101.
- [34] E.-C. (R), “No Title.” [Online]. Available: <https://el-cell.com/products/test-cells/standard-test-cells/ecc-combi/>. [Accessed: 27-Sep-2020].

- [35] K. N. Wood *et al.*, “Dendrites and Pits: Untangling the Complex Behavior of Lithium Metal Anodes through Operando Video Microscopy,” *ACS Cent. Sci.*, vol. 2, no. 11, pp. 790–801, Nov. 2016, doi: 10.1021/acscentsci.6b00260.
- [36] Y. He *et al.*, “Effectively suppressing lithium dendrite growth via an es-LiSPCE single-ion conducting nano fiber membrane,” *J. Mater. Chem. A*, vol. 8, no. 5, pp. 2518–2528, 2020, doi: 10.1039/C9TA12783F.
- [37] C. Uhlmann, J. Illig, M. Ender, R. Schuster, and E. Ivers-Tiffée, “In situ detection of lithium metal plating on graphite in experimental cells,” *J. Power Sources*, vol. 279, pp. 428–438, Apr. 2015, doi: 10.1016/j.jpowsour.2015.01.046.
- [38] G. Instruments, “Basics of Electrochemical Impedance Spectroscopy.” [Online]. Available: <https://www.gamry.com/application-notes/EIS/basics-of-electrochemical-impedance-spectroscopy/>. [Accessed: 28-Nov-2020].
- [39] Matt Lacey, “Simple circuits with resistors and capacitors.” [Online]. Available: <http://lacey.se/science/eis/simple-circuits/>. [Accessed: 29-Nov-2020].
- [40] D. Aurbach and A. Zaban, “Impedance spectroscopy of lithium electrodes,” *J. Electroanal. Chem.*, vol. 348, no. 1–2, pp. 155–179, Apr. 1993, doi: 10.1016/0022-0728(93)80129-6.
- [41] R. Bouchet, S. Lascaud, and M. Rosso, “An EIS Study of the Anode Li/PEO-LiTFSI of a Li Polymer Battery,” *J. Electrochem. Soc.*, vol. 150, no. 10, p. A1385, 2003, doi: 10.1149/1.1609997.
- [42] Joanna Conder, Claire Villevieille, Sigita Trabesinger, Petr Novák, Lorenz Gubler, and Renaud Bouchet, “Electrochemical impedance spectroscopy of a Li-S battery: Part 1. Influence of the electrode and electrolyte compositions on the impedance of symmetric cells,” *Electrochim. Acta*, vol. 244, pp. 61–68, 2017, doi: 10.1016/j.electacta.2017.05.041.
- [43] M. Ecker, T. K. D. Tran, P. Dechent, S. Käbitz, A. Warnecke, and D. U. Sauer, “Parameterization of a Physico-Chemical Model of a Lithium-Ion Battery,” *J. Electrochem. Soc.*, vol. 162, no. 9, pp. A1836–A1848, Jun. 2015, doi: 10.1149/2.0551509jes.
- [44] A. J. Bard and L. R. Faulkner, *Electrochemical Methods: Fundamentals and Applications*, 2nd ed. Wiley, 2001.
- [45] “SDS Ammonium Bifluoride,” 2016. [Online]. Available: <https://eki-chem.com/docs/SDS/1490-011516.pdf>. [Accessed: 09-Dec-2020].
- [46] J. Z. Lee *et al.*, “Cryogenic Focused Ion Beam Characterization of Lithium Metal Anodes,” *ACS Energy Lett.*, vol. 4, no. 2, pp. 489–493, Feb. 2019, doi: 10.1021/acsenerylett.8b02381.
- [47] Pubchem, “LITHIUM, ELEMENTAL,” *Hazardous Substances Data Bank (HSDB)*. [Online]. Available: <https://pubchem.ncbi.nlm.nih.gov/source/hsdb/647>. [Accessed: 25-Nov-2020].
- [48] C. Y. Abasi, D. Wankasi, and E. D. Dikio, “Adsorption Study of Lead(II) Ions on Poly(methyl methacrylate) Waste Material,” *Asian J. Chem.*, vol. 30, no. 4, pp. 859–867, 2018, doi: 10.14233/ajchem.2018.21112.
- [49] M. Secchi *et al.*, “Mineralogical investigations using XRD, XRF, and Raman spectroscopy in a combined approach,” *J. Raman Spectrosc.*, vol. 49, no. 6, pp. 1023–1030, Jun. 2018, doi: 10.1002/jrs.5386.
- [50] L. Li, L. Wang, and R. Liu, “Effect of Ether-Based and Carbonate-Based Electrolytes on the Electrochemical Performance of Li-S Batteries,” *Arab. J. Sci. Eng.*, vol. 44, no. 7, pp. 6361–6371, Jul. 2019, doi: 10.1007/s13369-019-03760-7.
- [51] X. Ren *et al.*, “High-Concentration Ether Electrolytes for Stable High-Voltage Lithium Metal Batteries,” *ACS Energy Lett.*, vol. 4, no. 4, pp. 896–902, Apr. 2019, doi: 10.1021/acsenerylett.9b00381.
- [52] M. S. Park, S. B. Ma, D. J. Lee, D. Im, S.-G. Doo, and O. Yamamoto, “A Highly Reversible Lithium Metal Anode,” *Sci. Rep.*, vol. 4, no. 1, p. 3815, May 2015, doi: 10.1038/srep03815.

- [53] A. R. Septiana, W. Honggowiranto, Sudaryanto, E. Kartini, and R. Hidayat, "Comparative study on the ionic conductivities and redox properties of LiPF<sub>6</sub> and LiTFSI electrolytes and the characteristics of their rechargeable lithium ion batteries," *IOP Conf. Ser. Mater. Sci. Eng.*, vol. 432, p. 012061, Nov. 2018, doi: 10.1088/1757-899X/432/1/012061.
- [54] M. Dahbi, F. Ghamouss, F. Tran-Van, D. Lemordant, and M. Anouti, "Comparative study of EC/DMC LiTFSI and LiPF<sub>6</sub> electrolytes for electrochemical storage," *J. Power Sources*, vol. 196, no. 22, pp. 9743–9750, Nov. 2011, doi: 10.1016/j.jpowsour.2011.07.071.
- [55] R. Pathak *et al.*, "Fluorinated hybrid solid-electrolyte-interphase for dendrite-free lithium deposition," *Nat. Commun.*, vol. 11, no. 1, p. 93, Dec. 2020, doi: 10.1038/s41467-019-13774-2.
- [56] J. Lopez, A. Pei, J. Y. Oh, G.-J. N. Wang, Y. Cui, and Z. Bao, "Effects of Polymer Coatings on Electrodeposited Lithium Metal," *J. Am. Chem. Soc.*, vol. 140, no. 37, pp. 11735–11744, Sep. 2018, doi: 10.1021/jacs.8b06047.
- [57] M. Ender, J. Illig, and E. Ivers-Tiffée, "Three-Electrode Setups for Lithium-Ion Batteries," *J. Electrochem. Soc.*, vol. 164, no. 2, pp. A71–A79, 2016, doi: 10.1149/2.0231702jes.
- [58] A. V. Ruban, H. L. Skriver, and J. K. Nørskov, "Local equilibrium properties of metallic surface alloys," 2002, pp. 1–29.
- [59] Y. Yao *et al.*, "A compact inorganic layer for robust anode protection in lithium-sulfur batteries," *InfoMat*, vol. 2, no. 2, pp. 379–388, Mar. 2020, doi: 10.1002/inf2.12046.
- [60] K. Park and J. B. Goodenough, "Dendrite-Suppressed Lithium Plating from a Liquid Electrolyte via Wetting of Li<sub>3</sub>N," *Adv. Energy Mater.*, vol. 7, no. 19, p. 1700732, Oct. 2017, doi: 10.1002/aenm.201700732.
- [61] J. Drenth, *Principles of Protein X-Ray Crystallography*. Springer New York, 2007.
- [62] A. S. Cavanagh, Y. Lee, B. Yoon, and S. George, "Atomic Layer Deposition of LiOH and Li<sub>2</sub>CO<sub>3</sub> Using Lithium t-Butoxide as the Lithium Source," *ECS Trans.*, vol. 33, no. 2, pp. 223–229, Dec. 2019, doi: 10.1149/1.3485259.
- [63] Merck, "IR Spectrum Table & Chart." [Online]. Available: <https://www.sigmaaldrich.com/technical-documents/articles/biology/ir-spectrum-table.html>. [Accessed: 09-Dec-2020].
- [64] Y. Yuan *et al.*, "Regulating Li deposition by constructing LiF-rich host for dendrite-free lithium metal anode," *Energy Storage Mater.*, vol. 16, pp. 411–418, Jan. 2019, doi: 10.1016/j.ensm.2018.06.022.
- [65] G. Yang, Y. Li, S. Liu, S. Zhang, Z. Wang, and L. Chen, "LiFSI to improve lithium deposition in carbonate electrolyte," *Energy Storage Mater.*, vol. 23, pp. 350–357, Dec. 2019, doi: 10.1016/j.ensm.2019.04.041.



## 9 Appendix

Table 6: Maximum value of the overpotential at the first three cycles of different coated samples in the carbonate-based electrolyte.

<b>Carbonate electrolyte</b>				
<b>Sample No.</b>	<b>Max. overpotential before cycling [V]</b>	<b>Max. OP. Cycle 1 [V]</b>	<b>Max. OP. Cycle 2 [V]</b>	<b>Max. OP. Cycle 3 [V]</b>
<b>Pristine lithium</b>				
<b>S1</b>	0.158	0.119	0.132	0.146
<b>S2</b>	0.123	0.099	0.119	0.120
<b>S3</b>	0.135	0.101	0.110	0.112
<b>Average</b>	0.139	0.107	0.120	0.126
<b>Estimated error (%)</b>	<b>11</b>	<b>8</b>	<b>7</b>	<b>11</b>
<b>R-134a gas-phase coated lithium</b>				
<b>S1</b>	1.370	0.345	0.286	0.266
<b>S2</b>	1.170	0.320	0.284	0.258
<b>Average</b>	1.270	0.332	0.285	0.262
<b>Estimated error (%)</b>	<b>8</b>	<b>4</b>	<b>0</b>	<b>2</b>
<b>NH<sub>4</sub>HF<sub>2</sub> immersion-coated lithium</b>				
<b>S1</b>	0.392	0.292	0.206	0.159
<b>S2</b>	0.474	0.226	0.201	0.178
<b>S3</b>	0.666	0.322	0.298	0.277
<b>Average</b>	0.570	0.274	0.250	0.227
<b>Estimated error (%)</b>	<b>17</b>	<b>17</b>	<b>19</b>	<b>22</b>
<b>PVDF decomposition-coated lithium</b>				
<b>S1</b>	0.651	0.244	0.226	0.157
<b>S2</b>	0.631	0.215	0.153	0.155
<b>S3</b>	0.499	0.333	0.207	0.197
<b>Average</b>	0.565	0.274	0.180	0.176
<b>Estimated error (%)</b>	<b>12</b>	<b>21</b>	<b>15</b>	<b>12</b>

Table 7: Maximum value of the overpotential at the first three cycles of different coated samples in the ether-based electrolyte.

<b>Ether electrolyte</b>				
<b>Sample No.</b>	<b>Max. overpotential before cycling [V]</b>	<b>Max. OP. Cycle 1 [V]</b>	<b>Max. OP. Cycle 2 [V]</b>	<b>Max. OP. Cycle 3 [V]</b>
<b>Pristine lithium</b>				
<b>S1</b>	0.126	0.030	0.027	0.028
<b>S2</b>	0.138	0.029	0.029	0.029
<b>S3</b>	0.169	0.045	0.052	0.056
<b>Average</b>	0.144	0.035	0.036	0.037
<b>Estimated error (%)</b>	<b>13</b>	<b>21</b>	<b>31</b>	<b>35</b>
<b>R-134a gas-phase coated lithium</b>				
<b>S1</b>	0.782	0.043	0.034	0.031
<b>S2</b>	0.839	0.039	0.033	0.031
<b>Average</b>	0.810	0.041	0.033	0.031
<b>Estimated error (%)</b>	<b>3</b>	<b>5</b>	<b>2</b>	<b>1</b>
<b>NH<sub>4</sub>HF<sub>2</sub> immersion-coated lithium</b>				
<b>S1</b>	0.375	0.031	0.029	0.028
<b>S2</b>	0.305	0.044	0.041	0.033
<b>Average</b>	0.340	0.037	0.035	0.030
<b>Estimated error (%)</b>	<b>10</b>	<b>17</b>	<b>17</b>	<b>9</b>
<b>PVDF decomposition-coated lithium</b>				
<b>S1</b>	0.276	0.047	0.041	0.037
<b>S2</b>	0.380	0.039	0.036	0.036
<b>Average</b>	0.328	0.043	0.039	0.036
<b>Estimated error (%)</b>	<b>16</b>	<b>10</b>	<b>6</b>	<b>2</b>

The dissemination of this project, more precisely this Master Thesis was done at the Austrian Young Chemist Summit 2020 in Innsbruck (online). Therefore, a poster consisting of four A4 sheets was prepared. The poster is attached afterwards.

# Surface fluorination and electrochemical investigations of Li metal

*Michael Georg Stadt<sup>1</sup>, Alexander Beutl<sup>2</sup>*

<sup>1</sup> Faculty of Technical Chemistry, Vienna University of Technology, Vienna, Austria

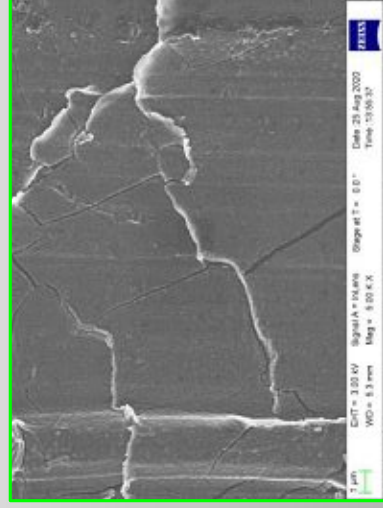
<sup>2</sup> Center for Low-Emission Transport – Electric Drive Technology, AIT Austrian Institute of Technology GmbH, Vienna, Austria

**Abbreviated abstract:** The usage of lithium metal as anode material promises increased energy densities in lithium ion batteries. However, severe dendrite formation and high volumetric changes upon charging/discharging lead to detrimental safety issues. A protective coating of LiF, which excels in electrochemical stability, but offers only poor ionic conductivity and mechanical properties, was suggested as a proper way to increase stability during operation.

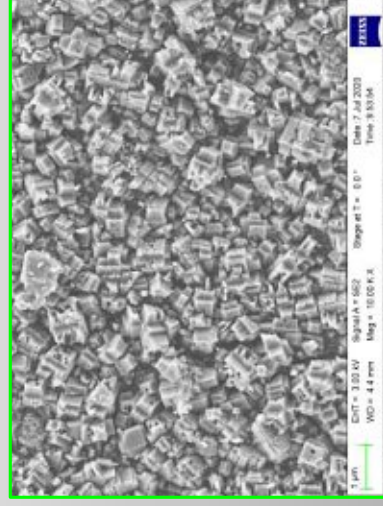
In this work, the effect of LiF coatings applied on metallic lithium were evaluated using different synthesis procedures (wet-chemically, gas-phase reaction, decomposition of fluorinated polymer).

# Motivation and Challenge

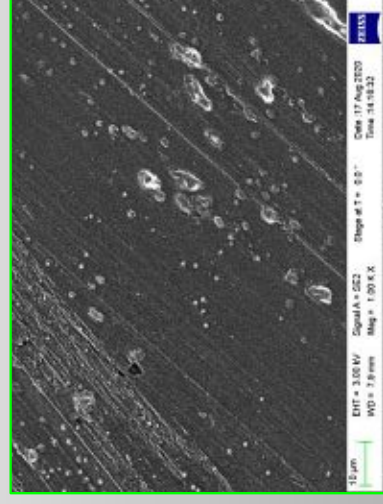
Contradicting findings on the „protectiveness“ of LiF-coatings have been reported (e.g. ref. 1,2) for lithium metal batteries. Different analytical methods and parameters used, however, do not allow for a direct comparison of these studies. Thus, three reported procedures for LiF-formation on lithium metal were reproduced in this study and directly compared with each other using different analytical methods (XRD, ATR-FTIR, galvanostatic cycling, electrochemical impedance,...)



LiF – reaction of Li with Freon 134a

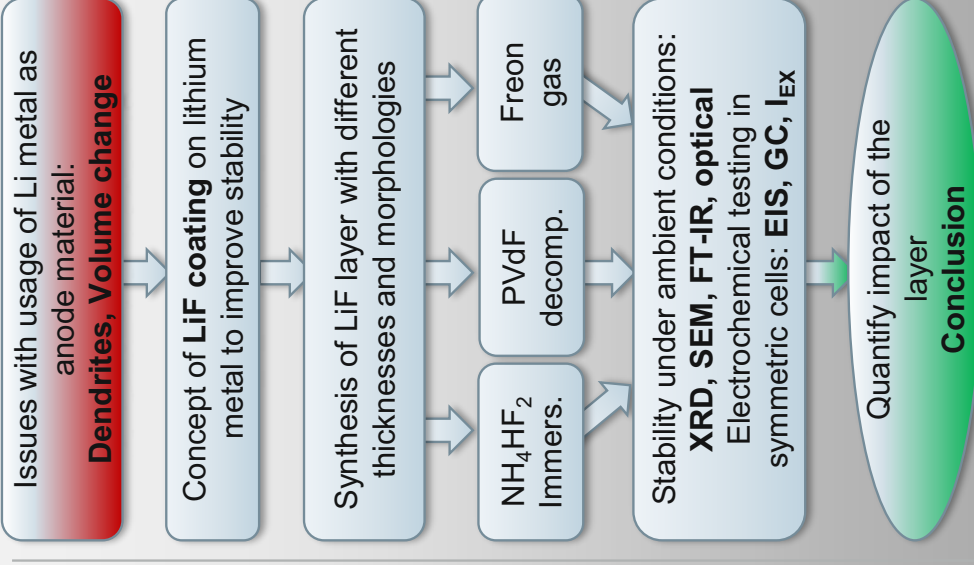


LiF – reaction of Li with NH<sub>4</sub>HF<sub>2</sub> in DMSO



LiF – decomposition of PVdF in DMF on Li surface

## Schematic



[1] Lin, D. et al. (2017). Conformal Lithium Fluoride Protection Layer on Three-Dimensional Lithium by Nonhazardous Gaseous Reagent Freon. *Nano Letters*, 17(6), 3731–3737.

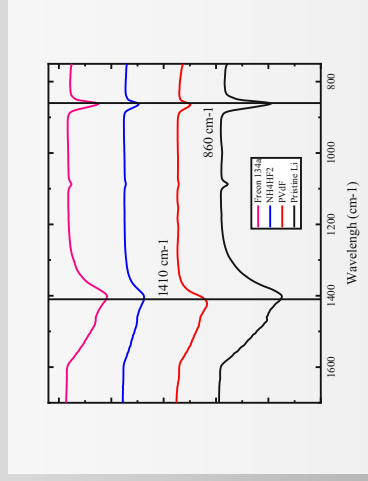
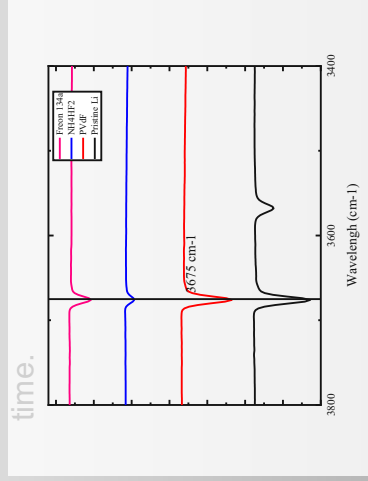
[2] He, M. et al. (2020). The intrinsic behavior of lithium fluoride in solid electrolyte interphases on lithium. *Proceedings of the National Academy of Sciences*, 117(1), 73–79.

# Results and Conclusions

## Chemical stability under ambient conditions

To estimate the stability against oxidation at ambient conditions of coated and uncoated Li-metal foils, FTIR, XRD and optical analysis was performed. Measurements were systematically done after 1, 5, 10 and 30 mins of exposure to ambient air (r.h. around 60%).

- **ATR FT-IR:** Analysis of the increase of LiOH and Li<sub>2</sub>CO<sub>3</sub> over time.



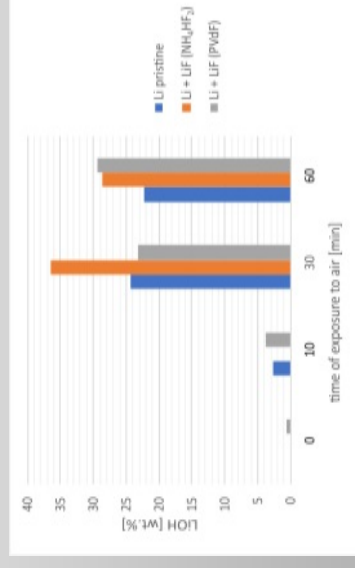
FTIR spectra of samples exposed to air for 10 mins show comparable amounts of the oxidation products LiOH and Li<sub>2</sub>CO<sub>3</sub>. (Pristine Li shows additional peak of LiOH\*H<sub>2</sub>O)

- **Photographs:**



Optical analysis indicated the apparent reaction rate of Li oxidation (from left to right: exposure to air for 0, 1, 5, 10, 30 mins)

- **XRD:**



XRD semi-quantitative analysis was conducted to determine the LiOH oxidation product after predefined timesteps. The relative LiOH content is comparable for all samples.

**A LiF layer on the lithium metal anode, seems to offer no proper protection against oxidation by exposure to air!**

# Results and Conclusions

## Electrochemical stability

during cycling

To estimate the electrochemical stability against dendrite formation and side reactions with the electrolyte, galvanostatic cycling and impedance measurements were conducted using a current density of 1 mA/cm<sup>2</sup> and capacities of 1 mAh/cm<sup>2</sup>.

- **Galvanostatic cycling:** Charge and discharge cycles with constant current applied.

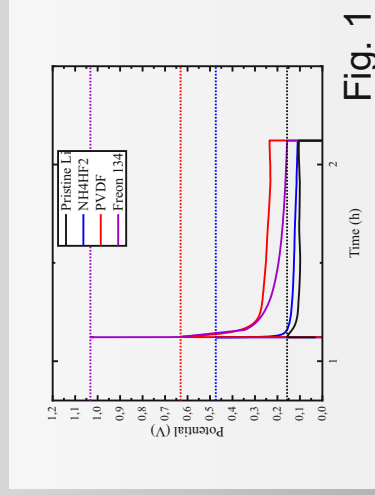


Fig. 1

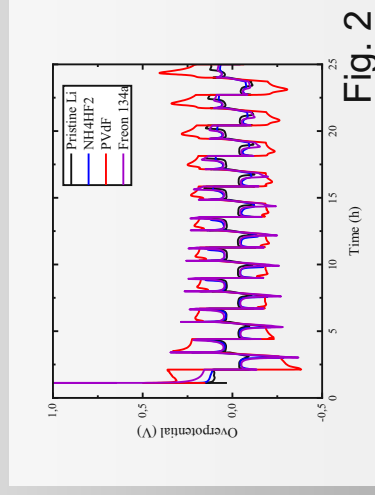
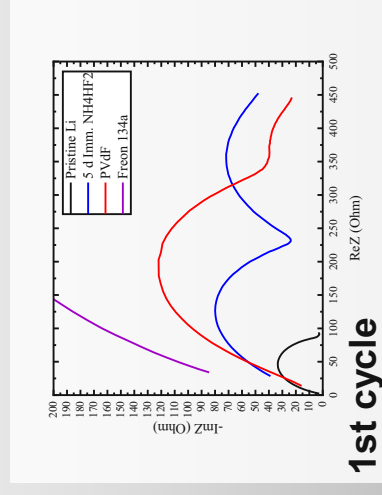


Fig. 2

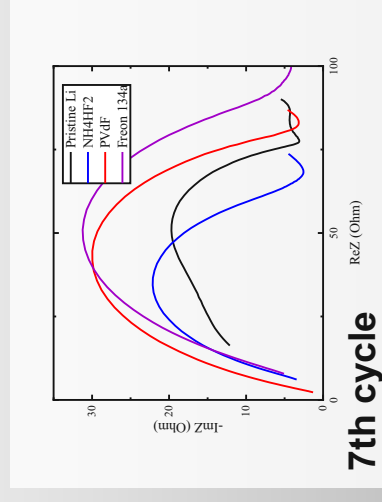
Fig. 1 shows the potential profiles of un-/coated Li metal foils. First anodic cycle shows higher overall resistance of coated samples compared to pristine Li.

Fig. 2: After several charging/discharging cycles the LiF layer breaks due to the mechanical stress evolving in the course of Li deposition/stripping, indicated by the increase in overpotential. After a few cycles the potential is assimilating.

- **Electrochemical impedance:** Measurement of the resistance as complex value during a potential sweep.



1st cycle



7th cycle

Impedance measurements verified the results from the potential profile analysis. Measurements of the as-prepared samples show higher resistance values for coated compared to uncoated Li. After 7 cycles though the impedances of uncoated and coated Li match.

The electrochemical data indicates the destruction of the layer in the first cycles, offering no protection whilst cycling!